minerals

Review

Natural Iron Silicides: A Systematic Review

Michael A. Rappenglück

Adult College and Observatory Gilching, 82205 Gilching, Germany; mr@infis.org

Abstract: This review systematically presents all finds of geogenic, impact-induced, and extraterrestrial iron silicide minerals known at the end of 2021. The respective morphological characteristics, composition, proven or reasonably suspected genesis, and possible correlations of different geneses are listed and supported by the available literature (2021). Artificially produced iron silicides are only dealt with insofar as the question of differentiation from natural minerals is concerned, especially regarding dating to pre-industrial and pretechnogenic times.

Keywords: minerals; fulgurites; planetary mantles and cores; terrestrial planets; moon; exoplanets; meteorites; ureilites; extraterrestrial dust; ejecta vapor; circumstellar envelops; interstellar matter; novae; supernovae; artificial

Citation: Rappenglück, M.A. Natural Iron Silicides: A Systematic Review. *Minerals* **2022**, *12*, 188. https://doi.org/10.3390/min12020188

Academic Editors: Roman Skála, Kord Ernstson, Pavel Svanda and Ioannis Baziotis

Received: 11 December 2021
Accepted: 27 January 2022
Published: 31 January 2022

1. Introduction

With the industrial production of iron silicides in the 20th century and parallel intensified research of versatile Fe-Si systems for high-tech applications, attention has been focused on rare natural iron silicides. In the last 20 years, more and more localities with different compositions of natural iron silicides have been discovered. The conditions and routes leading to the formation of mineral forms of these unusual compounds are numerous, e.g., the formation in the mantle and core of the Earth and the other terrestrial planets as well as of the Moon, through serpentinization, by impacts and lightning, during the entry of meteoroids into the atmosphere, during the recondensation of ejecta vapor, by space weathering, during the formation period of the solar planetary system, in the envelopes of S-stars, Luminous Blue Variables, classical novae, type II supernovae, and in certain nebulae. The compilation presented in this paper is intended to provide an overview of all natural iron silicide finds, as known to the author at the end of 2021. Such work has been lacking until now. The focus is on identifying the framework conditions and the different ways in which the formation, differentiation, mixing, persistence and decomposition of these rare mineral forms, as well as their association with paragenetic minerals, may be triggered. This synopsis can serve as a basis for further studies aimed at better distinguishing the formation of natural (geogenic-aerodynamic, exoplanetary, and cosmic) iron silicides from technogenic ones. Various disciplines are involved in this study, from geosciences to cosmochemistry, depending on each case. First, a brief outline of the early history of the artificial production of iron silicides is given. For some find situations, it is important to be aware of the history of the artificial synthesis of iron silicides in order to make an informed distinction between natural formation and artificial production. Iron silicides as minerals are the subject of the following section. Here, information on the mineralogical, chemical, and physical properties of iron silicides is given in the form of references to databases on the internet and some authoritative presentations in technical papers. This is followed by chapters on iron silicides as components of fulgurites, in planetary mantles and cores, in the core-mantle boundaries of Mercury, the Moon and super-Earths, in interplanetary dust, in meteorites, on the Moon, in association with a ureilite parent body (UPB), in rocks of unconfirmed status derived from extraterrestrial dust, as recondensation of ejecta vapor, in association with craters, as a component of circumstellar envelopes (CSE) and in interstellar matter (ISM), and in association with novae and supernovae. The conclusion consists of a brief synopsis.

2. Artificial Production of Iron Silicides

The first intentional artificial production of an iron silicide alloy with a silicon content of 9% was undertaken by Jöns Jakob Berzelius in 1810 [1,2]. In 1811, Friedrich Stromeyer (1776–1835) successfully repeated the experiment, which produced alloys with a silicon content of 2.2–9.3% [1]. In 1872, Valten reached 10–12% silicon content, and later, 20% [2]. In 1875, Alexandre Pourcel succeeded in producing iron silicide (10–18% silicon) in a blast furnace [1,2]. From this time onward, the production of iron silicides in blast furnaces became common. Starting in 1890, Ferdinand Frederic Henri Moissan also produced ferrosilicon with an electric arc furnace [2]. In 1899, Guillaume de Chalmot also used this technique to produce iron silicide (25–50%) [1,2]. This process became established worldwide on a large industrial scale for iron silicides with more than 20% silicon content. The blast furnace can be used only for iron silicides with a silicon content of 10–20% [2]. Usually, blast furnaces produce an iron silicide alloy with Si contents ranging from 10 to 15 % [2]. The commercial and industrial production of ferrosilicon, based on the use of electric furnaces, started in the USA in 1898 and in Europe (France) in 1899 [2].

FeSi was isolated and described by H. Hahn in 1864 [3], and later synthetically prepared by Edmond Frémy [2]. Artificially produced $(Fe,Mn)_3Si$, corresponding to Fe_3Si, was first documented in 1898 by Marie Adolphe Carnot and E. Goutal [2]. They also detected Fe_2Si, as did F. Osmond, Lebeau, Hahn, and Moissan between 1891 and 1912. In 1914, Fe_3Si_2 was found. $FeSi_2$ was studied by Hahn and Lebeau, and $FeSi_3$ by Carl Naske [2]. Artificially-produced Fe_xSi_y phases, with the exception of Fe_5Si_3, were described before 1934 [4,5]. However, the existence of $FeSi_2$, Fe_2Si_5, Fe_3Si, and Fe_3Si_2 was still uncertain at that time [6]. Fe_5Si_3 was identified in 1943 by A. R. Weill [7]. In 1939, as far as is known, the first Fe_2Si (denoted as $SiFe_2$), an unclear polymorph, was produced [8]. Since 1973/1974, trigonal (P3-m1), tetragonal (Pm3-m; CsCl), and hexagonal Fe_2Si (P3-m1; Ni2In) have been described [9–13].

Research shows that in blast furnaces, to a small extent, iron silicide phases (mainly Fe_3Si, but also Fe_5Si_3), together with SiC, form in the tuyere coke zone [14–17]. There are different types of deposits, i.e., droplets (spherules and semispherules) and irregular forms [15,16]. Carbon coats the droplets in a thin layer, and graphite crystals and flakes are inside them. Iron, silicon, and the coke matrix interact in varying degrees of penetration, saturation, and cooling. This process is reflected in the composition and shape of the droplets. It cannot be excluded that iron silicides were also produced as a byproduct, to a small extent, in some blast furnaces 2000–2500 years ago. In ancient China, blast furnaces existed in the Warring States Period (4th–3rd c. BC) [18]. In Jiudian (Xiping county, Henan province, China), a blast furnace was excavated, and its function was modelled. Close to the tuyère, 1800 K could be reached, while in the upper area, the temperature was still 700 K. In the center, the temperature was higher than in the upper and the outer area. In China, in the 9–8th c. BC, chimneys on ceramic furnaces, with which temperatures of up to 1473 K could be achieved, and blast furnaces with tuyères for copper smelting dating from the 7–5th c. BC, were precursors to the more mature technology of blast furnaces which were in use after the 4th–3rd c. BC. Around 300 AD, a process of preheating (up to 873 K) was used to generate temperatures of up to 2073 K in a tuyere-ventilated furnace at Early Iron Age sites at Kemondo Bay on Lake Victoria (Tanzania), in particular, at site KM3 [19–21].

3. Irons Silicides as Minerals

According to the Dana Classification, the minerals fersilicite/naquite (FeSi), ferdisilicite/linzhiite ($FeSi_2$), hapkeite (Fe_2Si), gupeiite Fe_3Si), luobusaite ($Fe_{0.84}Si_2$), xifengite (Fe_5Si_3), suessite (Fe,Ni_3Si), mavlyanovite (Mn_5Si_3), and brownleeite (MnSi) make up suessite group silicides [22,23]. The Nickel-Strunz Elements Classification lists $TiFeSi_2$, mavlyanovite (Mn_5Si_3), suessite ($(Fe,Ni)_3Si$), perryite ($(Ni,Fe)_8(Si,P)_3$), fersilicite (FeSi), ferdisilicite

($FeSi_2$), luobusaite ($Fe_{0.83}Si_2$), gupeiite (Fe_3Si), hapkeite (Fe_2Si), and xifengite (Fe_5Si_3) [24–35]. Other stoichiometries are known but have not been named. Natural iron silicides generally exist in orders of magnitude from a few μm to several nm [36]. They predominantly formed in extremely reducing environments under the highest temperatures and pressures. Iron silicides had been approved as minerals in the following order (IMA_Master_List_ 2021_09): suessite (Fe_3Si)—1979-056, xifengite (Fe_5Si_3)—1983-086, gupeiite (Fe_3Si)—1983-087, hapkeite (Fe_2Si) –2003-014, luobusaite ($Fe_{0.84}Si_2$)—2005-052a, and linzhiite ($FeSi_2$)—2010-011 [37]. In 1969, fersilicite (FeSi), described in 1930, was recognized as a mineral, but this was not accepted by the IMA. However, it was approved by the IMA under the new name 'naquite'—IMA 2010–010 [38,39]. Similarly, ferdisilicite ($FeSi_2$) was described in 1968, but first approved by the IMA under the new name 'linzhiite' (IMA 2010-011) [40,41]. Some studies summarize the physical and chemical data of Fe_xSi_y [42–44]. The long-term stability of Fe_xSi_y under the Earth's oxidizing atmosphere is still an open question. Theoretical considerations show that Fe-Si alloys at 298 K and 1 bar in air and water have a passivation film made of Fe_2O_3 and SiO_2 [45]. However, the resistance of artificial iron silicides in oxidizing atmospheres has been the subject of various experimental and theoretical studies against a background of possible industrial application. It is shown that iron silicides at temperatures between 673 K and 1273 K are involved in the formation of a very thin protective layer (SiO_2, Fe_2SiO_4) which significantly reduces corrosion [46]. Further studies examining natural iron silicides in this respect are needed.

The natural origin of fersilicites, reported as early as 1909/1910 in Ireland [47], and then in 1911 (Fe: 71.39%, Si: 20.03%, C: 8.14% from a kimberlite pipe's diamond mine, called Du Toit's Pan Mine, Kimberley, Sol Plaatje, Frances Baard, Northern Cape, South Africa, 28°45′49″ S, 24°47′28″ E) [48], 1924 (Fe: 65%, Si: 35%, British Guiana, unknown coordinates) [49], and 1926 (Renison Bell, Melba Flats, Tasmania, Australia, 41°48′ S, 145°25′ E) [50], and in Greece (unknown coordinates; FeSi, Fe_3Si, and $FeSi_2$, probably other phases, too; Ni: 0.10%)[49], which were termed "meteoritic ferrosilicine" (British Museum), has been questioned [47,49]. Now and then, the found material turns out to be of industrial origin [51,52]. However, some finds were hastily classified as terrestrial slag from industry, and a thorough analysis was not carried out. Although it is clear today that natural iron silicides exist terrestrially and extraterrestrially, as can be seen from the many examples below, it is still an important task to provide clear criteria for distinguishing between anthropogenic-industrial and natural origin. In the case of natural sources, it is necessary to improve the methods of determining which genesis is causal.

4. Fe_xSi_y as Components of Fulgurites

Lightning strikes can be powerful, with voltages >100 MV, amperages up to 10^5 A and more, energy of up to 1–10 GJ in the air, ~1 MJ on the ground, peak (1.5 μs) temperatures of up to ≃32,000 K, and sometimes exceeding 10^5 K, pressure/shock, according to modelling, of up to >7 Gpa (rock surfaces; focused on an altered area of radius ~9–11 cm) and sometimes >10 Gpa (soil) or even up to 25 GPa (neutron diffraction data) [53–58]. The discharge shock front propagates at more than 4 km/s. Temperatures drop quickly (some μs), but remain temporarily at around 15,000 K [59].

As such, lightning strikes produce fossilized traces in the ground, i.e., fulgurites (Figure 1). Fulgurites have been known since at least 1250 AD, e.g., from the Lapidario of King Alfonso X the Wise (1221–1284) [60–62]. However, the term 'fulgurite' was coined in 1790 by William Withering [63]. Fulgurites have been researched in depth, concerning their morphology, mineralogical composition, and origin [60,61,64–68].

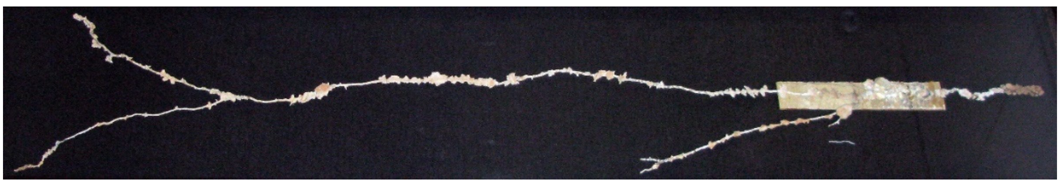

Figure 1. Fulgurite from Munkmarsch on the island of Sylt (Sylt community, Nordfriesland district, Schleswig-Holstein, Germany, 54°55′0″ N, 8°21′0″ E), University of Hamburg, Mathematicum. Source: Michael A. Rappenglück.

There are also studies on paleo-fulgurites, the oldest of which may be the Permian, i.e., from 250 Ma years ago [69–71]. In the Senckenberg Natural History Collections, Dresden, a 4.60-m long fulgurite is about 15 million years old [72]. Fulgurites are found in high mountains, e.g., the Black Forest (Germany) or the Alps [72–77]. Droplet fulgurites, produced by lightning strikes, are known from the archaeological site of the Roman settlement of Amallobriga, ca. 3rd c. AD, in Tiedra, province of Valladolid, Castile and León, Spain [45]. Different forms and compositions depend on the target ground. They also carry liquefied material into the air above the impact site, generating exogenic fulgurites [45]. An exogenic fulgurite cools down very quickly, deforms in the air like drops, solidifies, and falls back to the ground as a droplet fulgurite. These are characterised by the double process of ejection into the air and re-entry. There is a morphological classification of fulgurites (I-V) [78–80], comprising sand fulgurites (Type I), clay fulgurites (Type II), caliche fulgurites (Type III), rock fulgurites (Type IV), and droplet fulgurites (Type V) [78,80]. The energy of strikes required to produce fulgurites (Type I-IV) is between 1 and 30 MJ/m. The heating of the material is extremely fast, i.e., 1000 K/s. The lightning channel must be about 1mm thick. The exogenically produced droplets frequently appear vesicular and amorphous, caused by very fast cooling of liquefied material. Due to their low iron oxide content, the droplets are mostly dark green, in contrast to type I–IV fulgurites, which appear orange, reddish or brownish [45] and are coarse and granular; in contrast, type V fulgurites are smooth and glassy.

In any case, high temperatures (> 2000 K) and pressures (> 10 Gpa) are the most effective producers of fulgurites [81]. The transformation of matter is plasma-induced [82,83]. Shock effects (on Quartz) from 10 to 34 GPa can occasionally be detected in these materials [66,81,84,85], although these seem to be restricted to the outer zones [66]. Toasted quartz (22–30 GPa) and diaplectic glass were discovered in the Greensboro (North Carolina, USA) fulgurite, but no coesite or stishovite were identified, indicating a difference to a hypervelocity impact shock [85]. The fact that lightning strikes cause a change in the target soil's remanent magnetization is discussed based on findings in archaeological layers [86–88].

Analyses have shown that silicides with compositions ranging from Naquite (FeSi), Linzhiite ($FeSi_2$), Hapkeite (Fe_2Si), Gupeiite (Fe_3Si), Luobusaite (Fe_3Si_7), and Xifengite (Fe_5Si_3), but possibly also Fe_8Si_3 and Fe_7Si_3, as well as $FeTiSi_2$ or Fe-Si-Al alloys like $FeTi(Al,Si)_2$, $Fe(Al,Si)_3$, $Fe(Al,Si)_5$, or Fe_5AlSi_{10}, exist in fulgurites [62,78,80,89–94]. A lightning strike near Houghton Lake, Michigan hit unsorted glacial sediment and impact rocks. It produced a fulgurite (14 cm in diameter) which exhibited round drops (up to ~200 μm) in the vitrification, consisting of intergrown iron silicides naquite (FeSi) and linzhiite ($FeSi_2$) or xifengite (Fe_5Si_3), in the form of crystals up to 1 μm in size, with lesser amounts of native Si, Fe-Ti-Si, and other Ti-enrichments. Because of a lack of luobusaite (Fe_3Si_7), a low-temperature phase of Fe_xSi_y, which would indicate a very rapid cooling of the target soil, an artificial origin was excluded, and a lightning strike was assumed to be the cause [91]. Moreover, it was suggested (and contested) that the reduced mineral composition of some ophiolites may be the result of lightning strikes [82,83,95].

Thus, new studies have shown that lightning strikes, the conditions in the mantles and cores of terrestrial planets, and high-velocity impacts (in space and on Earth) produce convergent results in materials within a specific range. Certain shock features and highly reduced minerals, including various iron silicide phases (Fe_xSi_y), are present in fulgurites, ophiolites, meteorites, impact ejecta, and impact rocks [66,85,90,96–99]. However, it is essential to keep in mind the scale of the effects and the area, as well as the material penetration. Discussion is ongoing as to which criteria, taken together, allow distinctions to be made between terrestrial or impact-induced processes based only on the material in each case [47].

Fulgurites, impacts, and nuclear explosions belong to a common category regarding high temperatures, pressures, shock effects, extremely short-term heating and subsequent prolonged cooling, vitrification, and a highly reducing environment, although the differences cannot be overlooked. The nuclear explosions, e.g., at the Trinity site (near Socorro, New Mexico, July 16, 1945), exceeded 1773 K and reached pressures of at least 8 Gpa, causing planar deformation features (PDF) [100], but nonetheless being at the lower end of the value scale for fulgurites and high-velocity impacts [81,101].

5. Iron Silicides within Planetary Mantles and Cores

The Earth's lowermost mantle and core conditions are characterized by high temperatures and pressures as well as an extremely reducing environment. The entire mantle's oxygen fugacity (fO2) is discussed intensively in [102–109]. These publications show that heterogeneity and the development of the mantle across eras play a significant role. Some studies see Fe_xSi_y as an indicator for the mineral composition of the Earth's mantle [110]. From the decrease in seismic velocity, it is inferred that a small amount of B2-type FeSi phase is probably responsible for the ultralow velocity zone at the base of the lower mantle, that is, the core-mantle boundary zone (CMB) [18]. This is because only B2-FeSi is stable at the very high temperatures that prevail there, in contrast to other iron silicides [111]. With the high pressures and temperatures which prevail in the CMB, the silicate mantle, consisting mainly of perovskite $(Mg,Fe)SiO_3$, reacts with the liquid iron in the core [112,113]. This leads to the formation of FeO and naquite (FeSi) at 140 GPa, as well as the silicates stishovite (SiO_2) and perovskite ($MgSiO_3$) that make up the "D" layer, the lowermost, very mixed 200–300 km of the Earth's mantle. These processes, accumulating a large quantity of B2-FeSi, which is stable at high pressures, explain the unusually high electrical conductivity and can influence the terrestrial magnetic field on the surface [114–116]. Some iron silicides are related to the Earth's mantle (Figure 2).

Kimberlites come from the Earth's upper mantle. They form there at depths of 150-450 km. They rise very quickly to the earth's surface in the form of violent vertical eruptions (kimberlite pipes), or horizontally as tabular sheet intrusions (sills) or magmatic flow filling up fractures in existing rock (dykes). While α-SiC and β-SiC crystals can be embedded in diamonds, SiC grains themselves often contain inclusions of Fe_xSi_y, SiO and nanodiamonds [112,117–119] (Xu et al., 2008).

Ferdisilicite $(Fe,Ti,Mn,Cr,Ni)Si_2$, corresponding to $FeSi_2$, is found trapped in natural moissanite (SiC) grains from the Mir kimberlite pipe sites in Yakutia (Udachnaya, Daldyn, Mirninsky District, Sakha Republic, Russia, 66°25′59″ N, 112°19′0″ E) and limestones in north-western Bulgaria, attributed to the Triassic (251.902 ± 0.024–201.36 ± 0.17 mya) [120,121]. The grains have sizes of between 1 mm (NW Bulgaria) and 100 microns (Mir, Yakutia). In one SiC grain of Udachnaya, an iron silicide was detected which was close to $(Fe,Ti)Si_3$ [120]. In the $FeSi_2$ inclusions, light rare elements (LREE) are significantly more enriched than heavy rare earths (HREE) [120], i.e., there are negative anomalies in Eu, Sm and Yb, as well as a substantial Zr content.

Iron silicide (Fe_3Si_7) was found to be embedded in 0.5–1 mm-sized SiC crystals (hexagonal α-SiC 6H, trigonal 33R and 15R, cubic β-SiC polytypes) from the Sakha Republic (Yakutia), Russia, kimberlite pipes, Mir (Mirny, Mirninsky District, Sakha Republic, Russia 62°31′45.92″ N, 113°59′36.74″ E), nine crystals, and from Aikhal (65°59′56″ N, 111°13′57″ E), 14 crystals [117,122–124]. Si, Fe-Ti silicides, Rare Earth Elements silicate, sinoite (Si_2N_{20}), Fe, and traces of Al, Ca, V, Cr, and Mn were admixed [117]. Ferdisilicite ($FeSi_2$) was also found [120,124]. Several hypotheses about the origins of these compounds have been put forward, but from detailed research, it was concluded that the SiC and the embedded iron silicides originated by the metamorphism of reduced carbonaceous sediments due to subduction. Irons silicides in moissanite are also present in the Sytykanskaya (Alakit field, Yakutia, Russia) kimberlite pipe [122,125].

Figure 2. Iron silicides in terrestrial rocks associated with the Earth's mantle: (1) Avachinksy stratovolcano, (2) Aikhal, (3) Udachnaya, (4) Mount Carmel, (5) Yizre'el Valley of the Kishon, (6) Is River, (7) Luobusha mining district, (8) Dalihu, (9) Manitanyrd Ridge of the Ray-Iz massif, (10) Near Izmir, (11) Yimeng Mountains, (12) Donghai Co., (13) Shandong Gold Province, (14) Longquan, (15) Ir-Tash Stream Basin, (16) Targhasa reef massif, (17) Kurama Ridge, (18) Crimea, (19) Volcano Chinarsay, (20 Carpathian mountains, (21) Hodruša Intrusive Complex, (22) Spiš-Gemer Ore Mountains, (23) Chusovaiā̆river, Kamen Omut, (24) Krasnovishersky district, (25) Cherdynskiy district, (26) Gornozavodsky district, (27) Alexandrovsky district, (28) Bobruisk Ring Structure, (29) Tolbachik volcanic complex, (30) Kazachyn, (31) Putritsi, (32) Ternava, (33) Chernihiv, (34) Shunga, (35) Lebeshchina, (36) Tim-Yastrebovskaya structure, (37) Du Toit's Pan Mine, (38) Renison Bell, (39) Ireland, unknown coordinates, (40) Guyana, unknown coordinates, (41) Greece, unknown coordinates. Source: Michael A. Rappenglück, based on Google My Maps.

Peridotite xenoliths collected at the still active Avachinksy stratovolcano (Kamchatka Peninsula, Russia; 53°15′18″ N, 158°49′48″ E; altitude: 2741 m) were attributed to upper mantle material. Native Ni, Fe, and possible Ti, as well as Fe silicides (Fe-Si-Ti, Fe-Ni-Si, $Fe_{55}Si_{40}Ti_6$, luobusaite/FeSi, Fe_3Si_7) and Fe-Ni-Ti, were found [126]. It is suggested that H_2O (supercritical) fluids, which are carried by the subducting plate (oceanic lithosphere) moving through the peridotite layer within the mantle wedge, which is situated below the overriding plate (continental lithosphere) with the volcanic front to the cool forearc, reacted with it (serpentinization). The volcanic arc source depth is between 70 and 170 km [113]. H_2- and CH_4- fluids are produced and rise from the subducting plate to the overriding mantle wedge. H_2 reduces the peridotite, thereby triggering the precipitation of metals, including iron silicides.

Xenocrysts of corundum (Al_2O_3), moissanite (SiC) crystals (≤4.14 mm), native iron (Fe), and some other minerals, as well as partially extremely reduced matter, including iron silicides (Fe_xSi_y), were found in pyroclastic ejecta of Late Cretaceous (Cenomanian/Turonian stage, 98–94 mya) volcanoes, Mount Carmel (northern Israel, southern Galilee, Haifa District, Israel, 32°44′ N, 35°3′ E); these are associated with alluvial deposits in the Kishon River area [114,115]. The so-called 'Carmel Sapphire' nongem corundum contains melting nests which may be differentiated into four types (S, A, N, and DF). Type A melts consist of Fe-Ti-Si-C-P alloys which have crystallized to phases including gupeiite (Fe_3Si), FeTi(Si,P), FeTiSi, FeTi, and TiC (khamrabaevite). The iron silicides are gupeiite (Fe_3Si), xifengite (Fe_5Si_3), naquite (FeSi), hapkeite (Fe_2Si), and (unnamed) Fe_5Si, either pure or in combination with Ti and P [114,116,127,128]. However, these findings are disputed and the materials in question are considered by some to be industry-generated (abrasives) [129,130]. Nonetheless, there are also good arguments for a natural origin [115,131,132].

At a location in the Yizre'el Valley of the Kishon River (Israel; 32°40′20″ N, 35°17′22″ E), close to Mt. Carmel, moissanite (SiC) crystals (3–4 mm) with metal-silicide and silicon inclusions in situ from tuff, dated to the Miocene (23.03–5.332 Ma), were discovered [112]. Zangboite ($FeSi_2Ti$) and ferdisilicite/linzhiite ($FeSi_2$) could be identified based on the crystal structure. The analysis and comparison with findings at other locations suggest that high temperature and highly reduced conditions, but not necessarily high pressure, were needed for their formation [116,133]. It was suggested that the matter formed at a depth of 60–100 km at ca. 2 Gpa and at ≥1273–1423 K to ≤1683–1933 K.

At the old platinum mining area at Is River (Nizhnyaya Tura, Sverdlovsk Oblast, Russia; 58°46′59″ N, 59°40′0″ E), naquite/fersilicite (FeSi), gupeiite (Fe_3Si), and xifengite (Fe_5Si_3) were discovered [25,26,38,134].

During a collision of the oceanic lithosphere (especially of an atypical ocean crust) and, partially, the underlying upper mantle with the continental lithosphere, components, especially basic and ultrabasic rocks, rise and are emplaced (obduction) onto the continental crust [135]. Thus, ophiolites are parts of the oceanic crust and old continental margins and the Earth's lithospheric upper mantle, whose typification depends on the extent of partial melting [135]. Ophiolites occur mostly in sutures; they are associated with the suprasubduction zone (SSZ), which is caused by a very rapid expansion of the fore-arc crust at the beginning of subduction. In any case, ophiolites provide insights into the asthenosphere, lithosphere and melting and cooling processes, as well as into continental drift [135] (Figure 3).

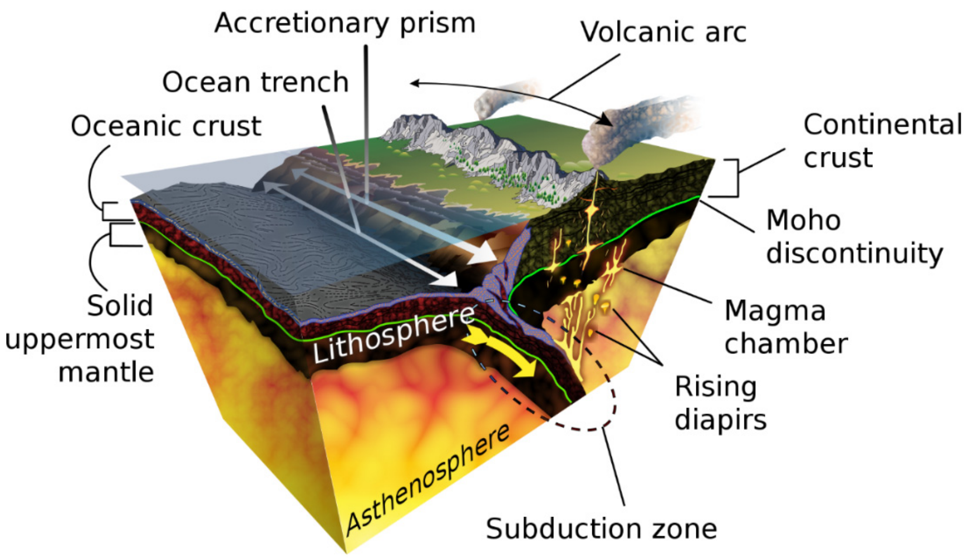

Figure 3. Formation of iron silicides related to the Earth's lithosphere (continental and oceanic crust) and asthenosphere. Source: K. D. Schroeder, Subduction-en.svg from Wikimedia Commons. License: Creative Commons Attribution-Share Alike 4.0.

Fe_xSi_y were detected in chromitites of the Luobusa ultramafic massif (southern Tibet, China), belonging to the Indus-Yarlung Zangbo suture [136]. They were attributed to a midocean ridge which probably existed ca. 177 mya ago and, around 126 mya, was changed by mafic extrusive rock melts (Boninite), extending over an intraoceanic subduction [137,138]. In the Luobusha mining district (Qusum Co. [Qusong Co.], Shannan Prefecture [Lhokha Prefecture; Lhoka Prefecture], Tibet, China; 29°13′52″ N, 92°11′25″ E), fersilicite/naquite (FeSi) [38,138,139], ferdisilicite/linzhiite ($FeSi_2$; $Fe0.{}_{84}Si_{2.00}$) [41,139–143], β-$FeSi_2$ [139] irregular grains (0.1–0.2 mm) of Luobusaite (Fe_3Si_7; empirical $Fe_{0.83}Si_2$) [33,142,144], Fe_7Si_3, Fe_6Si_4, and $Fe_4Ti_3Si_2P$ [143] as well as zangboite ($TiFeSi_2$) [145] or zhiqinite ($TiSi_2$) [132,146] were verified. The Fe_xSi_y in Luobusa ophiolites are likely to have been created in an extremely reducing environment at high pressures [135,138–

140,143,147]. The evidence of diamonds and coesite suggests that the material was formed at a depth of more than 300 km and under more than 10 Gpa pressure, and thus, must be assigned to the lower part of the upper mantle or even the lower mantle [147,148]. From the deeper zones, this material was transported to the lower ones by a rising plume and then embedded as xenocrysts [140,142,149]. However, this analysis is not without controversy. Instead of being attributed to the Earth's mantle, some have associated these materials with fulgurites, triggered by plasmas, i.e., by lightning strikes [82,95,150]. Native Fe_xSi_y was detected in ultramafic and metamorphic rocks and granite at other places in China [151].

At Dalihu (Inner Mongolia, China, 48°17″18.5′ N,106°57″12.8′ E) within Neogene (23.03 ± 0.3–2.588 ± 0.04 mya) basalt, situated in the inner Mongolia Daxing'anling Orogenic Belt (Daxing'anling Prefecture), carbonaceous xenoliths found in situ mostly contained SiC (20–50 mm) with TiC, Si, Fe, Ni, Fe-Cr, and Fe_xSi_y [152,153]. Polytopes of SiC occur in descending order of degree: β-SiC (3C), 4H, 15R, and 6H (C: cubic; H: hexagonal; R: rhombohedral). The iron silicides comprised samples DLH06112-3 $(Fe,Ni)_2Si$ (empirical: $Fe_{1.56}Ni_{0.49}Si_{1.00}$), corresponding to hapkeite (Fe_2Si), DLH0601-2 $(Fe,Ni)_3Si$ (empirical: $Fe_{2.92}Ni_{0.02}Cr_{0.01}Si_{1.08}$) corresponding to suessite, and DLH06112-5 $(Fe,Ti,Ni)_3Si_7$ (empirical: $Fe_{2.86}Ti_{0.19}Ni_{0.16}Al_{0.11}Si_{7.00}$). Native carbon in the xenoliths exists as graphite (10–70 nm) and diamond (around 20 nm). These minerals are considered typical examples of upper mantle material recycling. Volcanic activity began about 15 mya ago and continued until 0.16–0.19 mya.

The sandstone beds of the Manitanyrd Ridge of the Ray-Iz massif, Polar Urals (Russia, 66°55′ N, 65°25′ E), contain moissanite (SiC) in two different forms (crystals, 0.2–0.4 mm and grains), together with native Si and Fe_xSi_y [137,154,155]. The grains contain minute (3–100 μm) [156] inclusions of (unnamed) Fe_3Si_7 (empirical: $Fe_{2.3–3.7}Si_{6.3–7.7}$) and Fe_3Si_4, Fe_6Si_4 (empirical: $Fe_{6.4}Si_{3.6}$), as well as Si and SiO_2. The Ray-Iz material, mainly peridotite and chromitites, belongs to the Voikar-Syninsk ophiolite belt and probably originates from the upper mantle (top of the transition zone [410–660 km depth]: >300 km depth) [137]. Besides SiC, diamonds were also found in this material [154]. Indeed, more than 60 minerals were discovered in these samples [154]. The chronology is early Ordovician (Tremadocian: 485.4 ± 1.9–477.7 ± 1.4 to 485.4 ± 1.9 mya) to late Cambrian (Furongian:497 ± 1.0 to 485.4 ± 1.7 mya) [137].

On a beach on the Turkish coast of the Mediterranean Sea, ca. 150 km north-west of Izmir, a special rock was found [119]. Though it was a pick-up find, analysis favors a natural source. Possibly, it was formed through tertiary (66.0–2.6 mya) volcanism. It was shown to contain Fe_xSi_y, especially the (unnamed) phase Fe_3Si_7, as exsolution areas within the Si or showing up at the Si-/SiC- boundaries. An origin from the Earth's mantle was assumed.

Naquite (FeSi) was discovered in kimberlites dykes from the Yimeng Mountains (Yimeng Shan, Linyi, Shandong, China; 35°40′ N, 117°47′ E) [157]. There are several locations in China where ferdisilicite/linzhiite ($FeSi_2$) have been found: Tibet, Xinjiang, Anhui, Liaoing, Jiangsu, Hebei, and Zhejiang [158–160]. The rocks containing iron silicides were magmatic, sedimentary, or metamorphic (mafic, ultramafic) and chronically belong to a time of Archean (4000–2500 mya) until today.

Some Fe_xSi_y minerals are thought to have originated in the Earth's mantle (kimberlites of Tieling and Fu county, Liaoning province or Mengyin county, Shandong) [158]. Ferdisilicite/linzhiite ($FeSi_2$) may be found in ultrabasic rocks and chromite of the northern Jiangsu province (Donghai Co., Lianyungang, China; 34°N, 118°E) [159]. Its formation is probably related to the collision of oceanic crust and underlying oceanic upper mantle with the continental crust and the underlying upper mantle, as well as the obduction of the former with the latter two, as evidenced by harzburgite and lherzolite rocks. Ferdisilicite/linzhiite ($FeSi_2$), together with natural silica in gneisses connected with gold ores, was found in the Shandong Gold Province (eastern Laizhou Bay, Shandong Peninsula, Shandong Province, China; 37.47°N, 119.43°E) [161]. The chronology is the Early Cretaceous to Pleistocene (123 ± 4.2 mya to 0.3 mya).

At Longquan (Lishui, Zhejiang, China; 28°04′ N 119°08′ E), there are naquite (FeSi), linzhiite ($FeSi_2$), xifengite (Fe_5Si_3) as well as Fe_2Si_3 and Fe_5Si_2 as irregular grains (1.5 mm) in rocks from the Proterozoic (2500–541.0 ± 1.0 mya) [162]. The grains contain trace elements, i.e., Mn, Al, Ce, Eu, Ti. It has been suggested that the fersilicites found widely in the southern Zhejiang metamorphic area may be related to a sizeable Archean meteorite event, which is thought to have triggered the recondensation of ejecta vapor. Though such meteorite falls of the Archean are, in general, topics of recent research work and discussion [163–166], the justifications (formation conditions of xifengite, secondary enrichment) are not very convincing and leave the genesis open.

The Ir-Tash Stream Basin (Arashan Mountain, Chatkal-Kuraminskii Range, Tashkent, Uzbekistan; 41°23′59′ N, 70°30′0″ E). Amygdules of basaltic porphyrite (≈100 μm) contains calcite ($CaCO_3$), khamrabaevite ((Ti,V,Fe)C, type locality) [167,168], suessite $(Fe,Ni)_3Si$), gupeiite (Fe_3Si; empirical: Fe 84.3 wt.%, Si 13.8 wt%; $Fe_{3.02}Si_{0.98}$) and is covered with thin graphite (C) rims. The suessite accumulates in ellipsoidal and mostly spherical shapes, with a minimum of 0.25 mm but a maximum of up to 4 cm in diameter. Within the suessite enrichments, there are graphite and cubic crystals of TiC, preferentially at the rims. Moreover, there are tiny inclusions of feldspar (K, Na), lepidocrocite, quartz, and octahedral mica. The chronology is assigned to be the Early Permian (298.9 ±0.15 to 254.14 ±0.07 mya).

Suessite-like mineral $(Cr,Fe)_3Si$ and native chromium (Cr 92.2 wt%, Fe 5.7 wt%, Ti 1.4 wt%, Ni 0.2 wt%, Co 0.1 wt%, V 0.1 wt%) were found in dykes of gabbro diabase in the Kurama Ridge (Gava-sai; Chatkal-Kurama ridge, Middle Tien Shan, Uzbekistan, 40°50′00.0″ N, 71°07′00.0″ E) volcanic area [168–170]. The mineral is included in the core of amygdales (0.05–0.8 mm, 0.2 mm on average), which are embedded alkali basalt porphyry. The globules are polymineralic and zoned. Chromium containing suessite surrounds the nucleus and is also found in the interstices of the matrix. The outer shell of the tiny globes consists of cohenite. In between, there is $(Cr, Fe, Ti)_3Si$ with the empirical formula Fe 21.8, Cr 55.2, Ti 7.1, Ni 0.2, Cu 0.1, Si 15.2 intermediate. The mineral is assigned to the Early Triassic (251.902 ± 0.024–247.2 mya).

From the Targhasa reef massif (Eastern Sayan mountains, Krasnoyarsk Krai, Russia; 55°56′40.7″ N, 92°51′11.4″ E), along the river Kaltat (Bazaikha), at a depth of 330 m, limestones were collected in a sequence of bedrock exposures [171–175]. The repeated detection of iron silicides in different layers provides evidence for a nonanthropogenic origin. The first sample was taken from red sandy limestones in the lower part of the section and the second from reef limestones in the upper part. The carbonate rocks were assigned to the Early Cambrian (541 ± 1.0 to 509 ± 1.7 mya). There are iron silicides grains (≤1 mm) in large amounts, i.e., naquite (FeSi), ferdisilicite/linzhiite ($FeSi_2$), hapkeite (Fe_2Si), xifengite (Fe_5Si_3), (unnamed) $FeSi_9$, (unnamed) Fe_3Si_2, and (unnamed) Fe_4Si_9 were found in two samples (371-1 and 373-16) from exposures opposite the mouth of the Kaltat [176]. Glass accompanies the iron silicides. There is much moissanite (α-SiC) and occasional native Si in the fine intergrowths of the Fe_xSi_y. A principal-component factor analysis was made concerning the distribution of trace elements in meteorites of different types, terrestrial rocks, and the samples of the river Kaltat [173]. The composition of the material from different phases of iron silicides and moissanite (α-SiC, β-SiC), the quantities of Cr, Co, Ni, Cu, Ga, As, Au, W, and the presence of fused particles resembling cosmic dust suggest a proximity to the iron and stony meteorites and ultrabasic rocks, as well as the influence of high temperatures and pressures [173].

Naquite (FeSi) and ferdisilicite/linzhiite ($FeSi_2$), intertwined with grains up to 120 μm, isolated grains (≥100 μm) luobusaite ($Fe_{0.84}Si_2$), and zangboite ($TiFeSi_2$) as grains (≤0.15 mm) associated with linzhiite, as well as single grains of SiO_2 were discovered in Late Sarmatian limestones of Crimea (Kamenolomnya, Eupatoria, Saksky district, 45°14′52″ N, 33°25′3″ E) at a depth of 64 m [177,178]. Admixed were moissanite (SiC) with inclusions of iron silicides and native Si, cohenite (Fe_3C) and other minerals, still not identified. The chronology is the Lower Miocene (23.03 ± 0.05 mya to 15.97 ± 0.05 mya). The present researchers propose the following hypothesis to explain the origin of iron silicides: The source is associated with the rapid upwelling and intrusion of superdeep and super-compressed high-temperature fluids from the asthenosphere. Local areas were created, in which mineral-forming solutions could have a highly reducing effect, possibly with present-day methane-processing through the involvement of bacteria, thus triggering the formation of iron silicides.

Suessite $(Fe,Ni)_3Si$ with empirical formula $(Fe_{3,05}Mn_{0,02})_{3,07}Si_{0,97}$ and $(Fe_{3,13}Mn_{0,02})_{3,15}Si_{0,84}$ was discovered in the ore-bearing perlite rhyolite deposits of the submarine paleo volcano Chinarsay (Hissar range, Tian Shan mountain ranges, Uzbekistan, 38°55′ N 68°15′ E) [179]. Accompanying minerals were ferrian kinds and a new mineral Cr_3Si, which is an analogue to gupeiite. The suessite concentrates in oval accumulations (≤65 × 100 µm). It is thought that the outflow of acidic lava of the submarine volcano produced a reducing environment. A rapid decrease in temperature and pressure led to the formation of suessite, which formed with manganese-wüstite (FeO with Mn 11.2 wt%) and spherular Fe_3C. The chronology is the Mississippium (358.9–323.2 mya).

Iron silicides Fe_xSi_y are known from Paleogene (66.0–23.03 mya) sediments of the Carpathian mountains (47°00′ N, 25°30′ E) too [180].

In rhyolites from the Hodruša Intrusive Complex, Banská Štiavnica (Banská Štiavnica district, Banská Bystrica region, Slovakia, 48°27′29″ N 18°53′47″ E), the heavy fraction exhibited FeSi grey spherules (0.09–0.12 mm) [181]. The Hodruša Intrusive Complex is a subvolcanic intrusion in the middle of the Banská Štiavnica stratovolcano, belonging to the Central Slovakian volcanic field. The chronology is the Neogene (14.5–11.5 mya or 12.7 ± 0.4 to 11.4 ± 1.2 mya) [182]. The Khodrus intrusion, Klotilda vein, comprises rocks bearing iron silicides. There are different spherules in terms of size, shape, color, and composition. Grey spherules consist of FeSi, and blackish brown ones of Fe. The crust of the grey spherules shows a polygonal fragmentation which can be attributed to the fact that FeSi was heated to about 12,000 K and then rapidly cooled by water. This was associated with an immediate volume compression and a pressure drop. The impact of extraterrestrial bodies or terrestrial phenomena, e.g., volcanism, could have been responsible for such a process. Significant in this context are also spherules (90–120 µm) from the granitoid-metamorphic rock of the Spiš-Gemer Ore Mountains (Hnilec, Spišská Nová Ves district, Košice region, Carpathian Mountains, Slovakia, 48°50′30″ N, 20°30′10″ E), which contain Fe_xSi_y [183,184]. The chronology is Mesozoic (251.902 ± 0.024–66.0 mya).

Iron silicides, fersilicite/naquite (FeSi) and ferdisilicite/linzhiite ($FeSi_2$), as well as probably α-Fe, have been discovered in quartzite-sandstone deposits on the left bank of the Chusovaiā̆river, Kamen Omut (Omutnaya) cliff in the Middle Urals (Visimo-Utkinsk, Sverdlovsk Oblast, Russia, Perm Krai, Russia, 57°39′50″ N, 58°55′32″ E) [172,174]. The chronology could be Devonian (419.2 ± 3.2–358.9 ± 0.4 mya).

Iron silicides were also found in pyroclastic sediments, with diamondiferous intrusions, located at different sites in north-western Ural (Russia), i.e., the Krasnovishersky district (Perm oblast, 60°43′1.2″ N, 55°45′21.6″ E), the Cherdynskiy district (Perm oblast, 60°49′48″ N, 56°28′58.8″ E), the Gornozavodsky district (Perm oblast, 58°35′2.4″ N, 57°32″42″ E), and the Alexandrovsky district (Tomsk oblast, 60°26′0″ N, 77°54′0″ E) [185]. The chronology is the Palaeozoic (541.0 ± 1.0–251.902 ± 0.024 mya). Many minerals have been detected which formed in a high explosive eruption of quickly decompressed and boiled magma which was very enriched with water. This process occurred under high heat (1473–2773 K). Planar defects in xenocrystic quartz grains evidence shock pressure. The evaporation and condensation of the matter led to the separation and formation of various materials. Iron silicides formed from the gas phase at 1473–1673 K. In the rocks, moissanite (SiC) and corundum (Al_2O_3) grains had inclusions of native silicon (Si), fersilicite/naquite (FeSi), ferdisilicite ($FeSi_2$), gupeiite (Fe_3Si), and other unnamed Fe_xSi_y phases

($FeSi_5$, Fe_5Si), Fe-Ni-silicides, (Fe,Ti)Si. palladium silicide (Pd_3Si). Khamrabaevite ((Ti,V,Fe)C) was also present.

The occurrences of Fe_xSi_y in the Tolbachik volcanic complex (Kamchatka Peninsula, Russia, 55°49′51″ N, 160°19′33″ E) [186,187]) are doubted [129,188]. Instead, because of the comparability of a few indicators in the micro-inclusions of natural with industrially-produced corundum grains, anindustrial genesis (e.g., abrasive materials, steel production) is suggested [188]. According to the authors, the questionable mineral inclusions include carmeltazite ($ZrAl_2Ti_4O_{11}$), tistarite (Ti_2O_3), titanium nitride (TiN), titanium carbide (TiC), iron silicides (Fe_xSi_y), Fe-Si-Ti alloys, hibonite ($(Ca,Ce)(Al,Ti,Mg)_{12}O_{19}$), grossite ($CaAl_4O_7$), anorthite ($CaAl_2Si_2O_8$), residual feldspathic ($((Ba,Ca,Na,K,NH_4)(Al,B,Si)_4O_8)$) glass, and even diamonds. The researchers, questioning the findings so far, call for criteria to distinguish between natural and industrial generation. However, there are arguments in favor of natural origin concerning the apparent differences between the natural minerals and artificial substances [132,135,189].

Xifengite (Fe_5Si_3), empirical Fe (68–69%), Si (24–25%), Ni (5.2%), and Cr (0.7–0.8%), was found alongside around 80 other rare minerals, e.g., moissanite (SiC), as well as native elements, metallic alloys, etc., associated with the Bobruisk Ring Structure (Babruysk District, Mogilev Region, Belarus; 52°58′56″ N, 28°59′49″ E) [190], which is a multiringed basin. The inner ring, which shows significant anomalies, measures 28–32 km across. The outer ring has a diameter of 40–48 km. The structure is estimated to belong to the Paleoproterozoic (1.8–1.9 Ga) and to have formed by mantle plumes fluids.

Iron silicides were detected either completely or partially in material found at different locations in Ukraine, e.g., aluminum-bearing deposits near the ultrabasic intrusion of Kazachyn (Kirovogradskaya region, Golovanivsky district, Ukraine, 48°16′27″ N, 29°56′37″ E), Putritsi (Khmelnytskyi region, Shepetivsky district, Ukraine, 50°08′58″ N, 26°49′14″ E), Ternava, Dobromil region, Sambirskiy district, Ukraine, 49°34′14″ N, 22°47′22″ E), as well as the diamondiferous sediments of the Bilokorovitsky structure (2–6 km width, 22 km length), 1.98–1.80 bya old (Ukrainian Shield). In material from the Bilokorovitsky structure, there were fersilicite/naquite (FeSi) and ferdisilicite/linzhiite ($FeSi_2$), diamond (C), moissanite (SiC), coesite (SiO_2), cogenite (Fe_3C), kusongite (WC), kyanite ($Al_2[O|SiO_4]$,), pyrope ($Mg_3Al_2[SiO_4]_3$), pyro ilmenite ($FeTiO_3$), chromium spinels, gold (Au), native metals (Zn, Sn, As, Sb, Fe, Pb, Cu, Ni, Cr, Ag), and their intermetallic alloys, e.g., metal alloys of the Cu-Zn system. In grains of corundum (Al_2O_3), inclusions of Fe_xSi_y, native Fe and amorphous oxide and metal phases of the solid solution of the Zr-Ti-Al-Fe-Sc-TR system phases of various metals (Zr, Ti, Sc, Mg, Ca, Al, Si) were found. These high-pressure minerals attest to an origin in the Earth's mantle.

A metallic piece (65 mm × 22 mm × 10 mm), embedded in a mineral carbonate silicide rock, was discovered at a depth of 1 m on the property of the Ancient Chernihiv National Architectural and Historical Reserve in Chernihiv (Chernihiv district and region, Ukraine, 51°29′20.13″ N, 31°18′22.97″ E) [110,191]. It was found in a layer from sandy loam and pieces of brick, dated to the early 19th century. It is not anthropogenic. The piece has two areas: an outer fine-grained zone composed of graphite (C), khamrabaevite (Ti,V,Fe)C [167] with empirical formula $(Ti_{0.7}V_{0.3})C$ and suessite $(Fe,Ni)_3Si)$, and an inner lamellar-crystalline zone composed of suessite with moissanite (SiC). Moreover, other polymorphs of carbon, probably carbines, seem to be present. There are also detectable admixtures of K, Na, Ca. The piece is thought to have originated in the northern part of the Ukrainian Shield, as material from it was used to construct buildings in the Ancient Chernihiv National Architectural and Historical Reserve site. Its production is probably related to a mantle plume. The caldera of the paleo volcano of Chernihiv (Late Devonian 382.7 ± 2.8–358.9 ± 2.5 mya) is located at a great depth below the site.

Crystalline and microcrystalline inclusions of suessite have been reported in veins of the mineraloid shungite (elementary noncrystalline carbon), which appears as migrated shungite, in Shunga (Zaonezhie peninsula, Lake Putkozero, Karelia, Russia, 62°35′33″ N 34°56′14″ E), as well as in shungite basalts near Lebeshchina (Karelia, Russia, 62°31′55″ N, 35°20′38″ E) [110,192]. These are very similar to meteoritic suessite, and chronology dates them to the Lower Proterozoic.

Likewise, a natural terrestrial origin is assumed for the suessite in the magmatic norite breccias of the Tim-Yastrebovskaya structure, Oskol Ore province, crystalline Voronezh massif/Voronezh Anteclise (Voronezh Oblast, Russia, 51°40′18″ N, 39°12′38 E), as part of the East European Craton, which were unearthed from a depth of 320–446 m (borehole 22) [110,193]. The mineral is found together with native gold, chromium, iron, and bismuth, with alloys of gold-cadmium and natural zinc-copper, graphite, chromium nitride as micro-inclusions in native chromium, tungsten carbide, and moissanite (α-SiC). The chronology (Rb-Sr dating) is 1985 ± 8 and 1972 ± 19 Ma (Orosirian Period of the Paleoproterozoic). The origin of the material is attributed to paleo-volcanism.

In the Fore-Sudetic Monocline, appearing in the Polkowice-Sieroszowice and Rudna copper mines (Gmina Nowa Ruda, Lower Silesian Voivodeship, Kłodzko County, Poland; 50°33′2″ N, 16°31′16″ E), Fe_xSi_y exists in the phases of fersilicite/naquite (FeSi), xifengite (Fe_5Si_3), Fe_2Si_3, and Fe_4Si_9 [178], shaped as spherules with different structures and mixtures. They are mainly composed of Fe_5Si_3 (xifengite), with some P, Ti, Cr, and Mn. Slight traces of very native Si and Ti, rare in nature, were detected. The chronology of the material is the Permian age (red-shale, Rotliegend-Ludwikowice, 301.2–298.9 mya). At present, it is not possible to make a clear statement about the origin of the spherules; they may have formed of ultramafic magnetic material collected from neighboring areas in sediments, or may have originated from extraterrestrial dust, as suggested by the author.

In the suessite group, there are other silicides which are structurally like the iron silicides brownleeite (MnSi), mavlyanovite (Mn_5Si_3), zangboite ($TiFeSi_2$), or perryite ($(Ni,Fe)_8(Si,P)_3$)). These are associated with volcanism, but are also in meteorites and even in comets [194,195]. Similar to iron silicides, there is often an association with moissanite (SiC) and graphite (C) [196]. Cubic brownleeite (Mn,Fe,Cr)Si, with the empirical formula $(Mn_{0.77}Fe_{0.18}Cr_{0.05})Si_{1.00}$, was found in the dust stream of short periodic (5 a 38 d) comet 26P/Grigg-Skjellerup (diameter: 2.6 km) in three grains (100, 250, and 600 nm). Comets are the types of locality for this mineral [194,197]. Hexagonal mavlyanovite (Mn_5Si_3) grains (≤1–2 mm) with empirical formula ($(Mn_{4.66}Fe_{0.40})_{5.06}(Si_{2.91}Ti_{0.01}P_{0.02})_{2.94}$) were detected in a lamproite diatreme (Koshmansay River, Chatkal-Kuraminskii Range, Tashkent, Uzbekistan, ca. 40°45′ N, 70°10′ E) [198]. Mavlyanovite is the analogue of xifengite Fe_5Si_3 with the substitution of Fe by Mn. The accompanying minerals are suessite ($(Fe,Ni)_3Si$), moissanite (SiC), khamrabaevite ((Ti,V,Fe)C), native Iron (Fe), diamond (C), chromite ($Fe^{2+}Cr^{3+}{}_2O_4$), and alabandite (MnS). The mineral is believed to be from the Upper Mantle. It was also found in the Volnovakha River basin (Eastern Azov area, Azov Sea Region, Donetsk Oblast, Ukraine, ca. 47°N, 37°E) [196]. Here, the accompanying minerals are alabandite, graphite, khamrabaevite, and moissanite, i.e., nearly the same as in the previous example, but with an additional, unnamed mineral which is a manganese-iron silicide $(Mn,Fe)_7Si_2$ [199]. The type locality of zangboite ($TiFeSi_2$) is Orebody 31 (Chromite deposit 31) of the Luobusha Mine (see above), Qusum Co. (Shannan Prefecture, Tibet, 29°13′52″ N, 92°11′25″ E). This mineral belongs to the Luobusha ophiolites. Zangboite, together with the iron silicides fersilicite/naquite (FeSi), ferdisilicite/linzhiite ($FeSi_2$) and luobusaite ($Fe_{0.84}Si_2$), also exist in the Sarmatian limestones in Crimea (see above) [141]. Trigonal perryite ($(Ni,Fe)_8(Si,P)_3$)) has only been found in meteorites to date (as of 2021: 27 meteorites) [30,200]. The type locality is the Horse Creek meteorite (Baca County, Colorado, USA, 37°35′ N, 102°46′ W) [200,201]. Finally, grains (diameter 0.7–39.1 mm) of a palladosilicide (Pd_2Si) were found in the Kabanga and Kapalagulu Intrusion in the mafic and ultramafic layers (Lake Tanganyika, Kigoma Region, Tanzania, 5°53′16″ S, 30°03′51″ E and 5°54′26″ S, 30°05′37″ E) and in the Bushveld Complex (UG-2 Reef, Bojanala Platinum District Municipality, North West, South Africa, ca. 25°S, 27°E) [202].

The Earth's core is thought to consist of an Fe-Ni alloy and additional components of light elements, because of the measured core density, density variations, and sound speeds [111,203]. The composition of the light elements in the core is important for planetary formation, differentiation, motion conditions, material reactions, temperature course, and changes in the geodynamo in the core [203]. From experimental studies and modelling dedicated to the understanding of the Fe-Si system (phases at high pressure and temperature, melting curves) and focused on iron silicides Fe-16wt%Si, Fe-17wt%Si, Fe-18wt%Si, Fe-5wt%Ni-15wt%Si close to Fe_3Si (gupeiite, suessite), it was determined that a certain amount (~6 wt%?) of Si must be dissolved in the Fe-Ni alloy of the Earth's core [204–206]. However, Fe-Si-H alloys ($Fe_{0.88}Si_{0.12}H_{0.17}$) were also suggested to fit seismological data for the outer core [207]. A Fe–5 wt%Ni–4 wt%Si alloy was studied to create a temperature-pressure phase diagram of the Earth's core [208]. Similar research was done concerning the Fe–S–Si immiscible system [206,209]. Si could be a main alloy component in the Earth's outer core. Fe_xSi_y can exist at the core-mantle boundary (CMB) at 4000 K, 136 Gpa conditions [210–216]. Thus, experimental research in the lab, supported by geophysical and geochemical data as well as modelling, was and is important to assess the structural properties, interrelationships of the phases, behavior of iron silicides ($FeSi_2$, $FeSi_3$, Fe_2Si, Fe_3Si, Fe_5Si, Fe_5Si_3, $Fe_{11}Si_5$), chemical equilibria, flows at the highest pressures and temperatures, and to derive conclusions for their existence and the reaction processes at the core-mantle boundary [43,111,203,205,213,217–224]. However, research shows that oxygen in higher amounts, in addition to Fe, Ni, and Si, plays a nonnegligible role in the outer core [208,225]. It has been proposed that the outer core contains a (Fe–Ni)–O–Si system, e.g., Fe-5.8(0.6) wt%Si–0.8(0.6) wt%O [208]. The inner core could consist of a Fe–Ni–Si [214,215] mixture, e.g., Fe–5wt%Ni–4wt%Si (B2 and hexagonal packed [hcp]) [214]. The outer core could have Si: 1.2–3.6% and O. While FeSi could be stable at the lowermost part of the mantle (the D″ layer), stability is discussed for the inner core [219]. It seems, however, that the high-pressure phase of iron silicide FeSi with a CsCl (B2) crystal structure is a stable candidate (the only one) at up to 400 GPa for a phase at the inner core boundary (ICB) at around 5000 K [205,210–216,220,222,223,226–228].

6. Iron Silicides in the Core-Mantle Boundaries of Mercury, the Moon, and Super Earths

The existence and significance of iron silicides in the cores of terrestrial planets is a matter of debate, especially concerning the characteristics of the Fe-S-Si ternary system [216] (see Figure 4). The Fe-Ni-Si system was also studied in detail regarding the possible composition of terrestrial planets [229]. Moreover, some models calculate hydrogenation of FeSi ($FeSiH_x$) in the innermost region of planetary cores (>10 Gpa) [230].

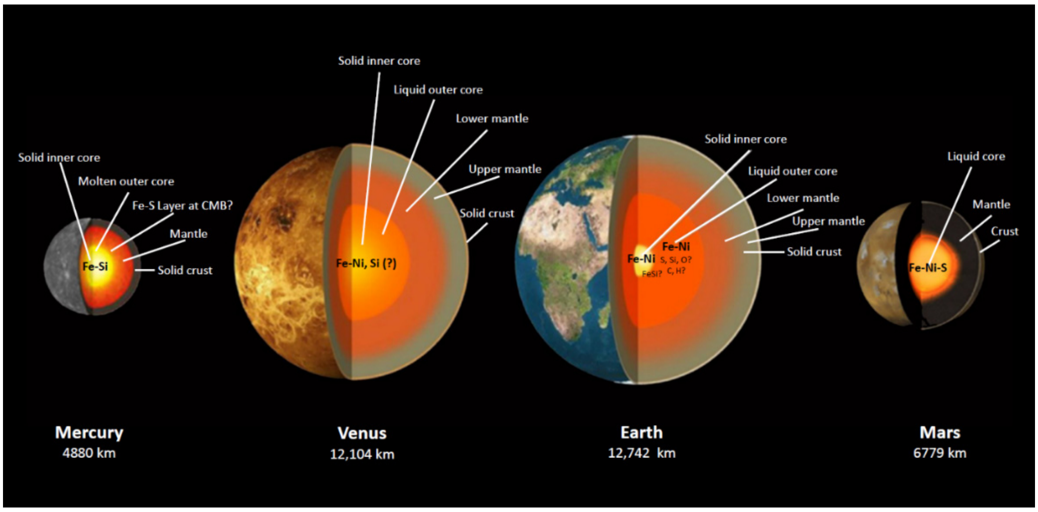

Figure 4. The structure of the terrestrial planets in the solar planetary system: Mercury, Venus, Earth, and Mars. Source: Michael A. Rappenglück.

Iron silicides are thought to be essential in Mercury's core–mantle boundary (CMB), though NiSi may also be important in that case [216,231]. Mercury could have an extraordinarily Fe-rich inner solid core and a liquid outer core based on measurement data from the Messenger spacecraft, cosmochemistry, and modelling. Above this would be a solid outer core layer of iron sulfide (Fe-S), then a solid mantle and a solid silicate crust [115]. At the core–mantle boundary (CMB) at 1900 K and 5 Gpa, there would be an Fe-Si/S alloy (Si: 8.5–33.5 wt%, S: 0–36.5 wt% on average) [216,232,233]. An Fe-Si alloy (Si: 0–25%) is proposed to exist in both the outer and inner core, or a core consisting of Fe-S-Si, where molten Fe-Si and Fe-S alloys form two layers inside, surrounded by a more solid Fe-S layer [234,235].

From models of the Martian core, a Fe-S core is suggested with a large amount of S (16–20 wt%), little O (<1 wt%) and negligible Si [216,236]. Too little data are available for Venus at present. However, the data and modelling suggest that despite the presumed Earth-like inner structure, there are likely few, if any, light elements, i.e., also Si, in the core [237]. Concerning the interior of more minor planets, NiSi at 13 GPa and 1000 K could be more significant than FeSi [115].

The moon's (Figure 5) lunar seismic profiles, sound wave velocity measurements, and modelling indicate a division into a liquid outer core and solid inner core. S, C, Ni, Si, and P had been suggested to make up the light elements in the core. However, the P content seems to be negligible. A pure Fe core has also been proposed; however, it is very probable that at the CMB, Fe-Si alloys (Si: 2–17 wt%) exist at 1600 K and 5–7 Gpa [216,238].

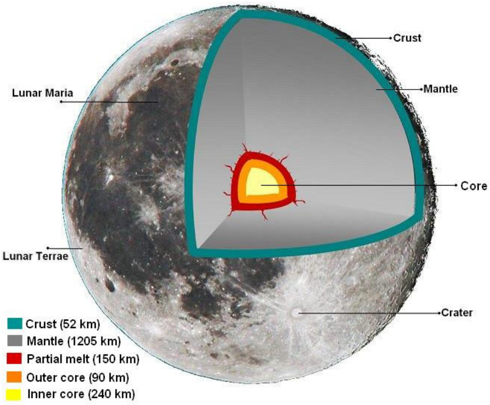

Figure 5. Internal Structure of the Moon. Source: IqbalMahmud, Internal_Structure_of_the_Moon.JPG from Wikimedia Commons. License: Creative Commons Attribution-Share Alike 4.0 International.

For Jupiter's Ganymede, the largest moon in the solar system, modelling shows that Fe-S alloys predominate at the core-mantle boundary (CMB) and within the inner-core boundary (ICB). There is (probably) no Si present [216].

Recent studies have dealt with the Fe/Si ratios in super-Earth type exoplanets (~1.3 $R_{\oplus}$[Earth's radius]) [239–241]. Pressure experiments and modelling, regarding crystal structures and densities, show that the hcp- (Fe-7Si) and bcc-phase (Fe-15Si) are stable up to 1314 Gpa, with the former in a hexagonal and the latter in a cubic structure. Thus, such Fe-Si alloys could be essential components of super-Earth cores of ~3 $R_{\oplus}$.

7. Iron Silicide in Interplanetary Dust

In an interplanetary dust particle (IDP), L2055I3, with a diameter of ~4 μm, three grains (100, 250, and 600 nm) of Brownleeite ($Mn_{0.77}Fe_{0.18}Cr_{0.05}$)Si were discovered [194,242]. The IDP was collected during the Earth's passage through the dusty tail of the short periodic comet 26P/Grigg-Skjellerup (size: 2.6 km; aphelion: 4.9332 AU; perihelion: 1.1168 AU; eccentricity: 0.6631; orbital period: 5.31 a; orbital velocity at perihelion: 38.48 km/s; Inclination: 22.36°), which triggers the meteor stream pi Puppids. Therefore, an origin from that comet is very probable. However, this could also have been associated with matter condensing in the early solar system, with circumstellar envelopes or supernova remains. Brownleeite (Mn, Fe, Cr)Si belongs to the fersilicite group and, according to the Dana classification, to the Suessite Group of silicides (01.01.23) [195,197].

The Stardust mission to comet 81P/Wild 2 (size: 5.5 km × 4.0 km × 3.3 km; density: 0.6 g/cm^3; mass: 2.3 × 10^{13} kg) provided evidence of iron silicides, but these are very likely to be secondarily produced. In aerogel track #44 within three grains (C2004,1,44,1,0, C2004,1,44,2,0, and C2004,1,44,3,0 all approximately 15 µm × 20 µm sized), Fe-Si phases (~100 nm, quenched-melt spheres) Fe_2Si (hapkeite), Fe_3Si (suessite), up to (Fe,Ni,Cr)Si alloy ($Fe_{3.35}Ni_{0.13}Cr_{0.05}$)$(Si)_{1.0}$, corresponding a Fe_7Si_2 (unnamed), were detected [243]. Suessite was also found in 16 grains of track #35 [244]. These iron silicides are thought to have been produced by a hypervelocity impact of (Fe,Ni)-S particles, leading to a temperature above 1400 K, heating the aerogel substrate (containing Si), melting it and mixing matter from the particle and the aerogel (SiO_2), followed by rapid cooling.

In this context, the discovery is significant of a meteorite which was assigned to the meteor shower of the Leonids (Comet of origin is 55P/Tempel-Tuttle). In 1998, a slaggy rock found at El Aybal (near Salta, Department of La Paz, Catamarca Province, Argentina; 24°52′ S, 65°29′ W) contained wüstite and the iron silicides gupeiite (Fe_3Si), xifengite (Fe_5Si_3), fersilicite (FeSi) and ferdisilicite ($FeSi_2$), in addition to native Cu, Fe und Si [245,246]. The detected spherules were highly magnetic. A connection with the meteor shower of the Leonids (Comet of origin is 55P/Tempel–Tuttle), which occurred on the day of the find (17 November 1998) in the La Puna area, is suspected. The find is recognized as a meteorite and was included in the Catalogue of Meteorites from South America. However, it is not officially listed in the Meteoritical Bulletin Database [246].

In a dust particle (4 µm) associated with the comet Grigg-Skjellerup, free tiny grains (≤600 nm) of Brownleeite (MnSi) were detected [194]. Brownleeite is structuraly similar to fersilicite/naquite (FeSi) and is in the suessite group (see above).

From these research results and data on meteorites, iron silicides in nebulae, as well as the envelops of novae and supernovae type II remains (see below), it is concluded that fersilicite/naquite (FeSi), ferdisilicite/linzhiite ($FeSi_2$), hapkeite (Fe_2Si), suessite ($(Fe,Ni)_3Si$), gupeiite (Fe_3Si), luobusaite ($Fe_{0.84}Si_2$), xifengite (Fe_5Si_3), and zangboite ($TiFeSi_2$) may be attributed to the high pressure impact phase during the formation and differentiation process of the planetary system, also caused by impacts, and thus, to the original mineral of the primeval Earth's Hadean eon surface (~4600–4000 mya) [247,248].

It has been experimentally shown that, under cooling and reduction conditions, iron silicides are produced as grains (10 nm) from kamacite and taenite. Iron silicides fersilicite (FeSi), gupeiite (Fe_3Si) and xifengite (Fe_5Si_3) form in grains with sizes of 30–100 nm, via the melt condensation of high temperature gases [249]. Native Fe and iron sulfides are embedded in amorphous silicate grains with sizes of some hundred nanometres. The experimentally produced matter is very similar to the natural one found in interplanetary dust. It is believed to be part of the building blocks of the solar planetary system. The material could form in the region of a protosolar disk, i.e., in the early stages of planetary systems, or in the envelopes of stars in the final stages of their evolution (AGB stars, supernovae type II-P, i.e., the core collapse supernova of a star with more than eight solar masses).

8. Iron Silicides in Meteorites

In 1859, a phase of iron silicide (Fe: 87.279%, Si: 11.008%, P: 1.312%, C: 0.400%, Mg: traces) was found in a rock (≈ 8 cm × 7 cm × 5 cm) near Rutherfordton (Rutherford County, North Carolina, USA) by C. U. Shepard, named 'ferrosilicine' [2,49,250,251]. However, the assessment of this sample as being of natural origin and meteoritic was questioned by some researchers, and industrial production was hypothesized [49]. Again and again, some finds are initially considered meteoritic, but then a terrestrial or anthropogenic (industrial) origin is found to be more likely upon closer analysis [52,250]. However, there is also clear evidence for the existence of iron silicides in various types of meteorites.

8.1. Iron Silicides on the Moon

Over aeons, a process known as 'space weathering' shapes the surface of airless (near-vacuum) bodies (planets, dwarf planets, moons, planetoids, comets) in planetary systems. Significant impacts, the effect of a steady flow of micrometeorites, the solar wind and cosmic rays continuously forms and reshapes the soil and regolith on these bodies if they hold only a sporadically forming atmosphere of trace gases and solid particles, or if they are directly surrounded by the vacuum of space [36,252–265].

According to several studies, there were tetragonal Fe_2Si, named Hapkeite-1C (c for cubic), naquite (FeSi), linzhiite ($FeSi_2$), and $(Fe_{2.9}Ni_{0.1})_3Si_{1.1}$ close to gupeiite (Fe_3Si)/suessite, $(Fe_{4.33}Cr_{0.67})_5(Si_{3.04}P_{0.07})_{3.11}$ close to xifengite (Fe_5Si_3), and $(Fe_{2.89}Mn_{0.04}Cr_{0.03}Ti_{0.04})_{3.0}Si_{7.09}$ close to (unnamed) Fe_3Si_7, in the lunar meteorite Dhofar 280 (Dh 280; Dhofar, AI Janubiyah Province, Oman, 19°19′36″ N, 54°47′0″ E)[266–270]. Hapkeite exists as a relatively large metallic grain, i.e., ~35 μm. Dhofar-280 is an impact melt breccia of anorthosite type, containing inclusions of Si grains and Fe_xSi_y droplets (2–30 μm) that are oxygen-depleted. There are some minor elements in the ferroan anorthosite matrix [267]: Al, Ca, Co, Cu, Mn, Ni, Mg, P, S as well as trace amounts (if any) of Na, K, T, and Cr. In addition to the iron silicides, there are $CrSi_2$, $TiSi_2$, and Fe-Ni phosphides. The melt consists of SiO_2, Al_2O_3, FeO, MgO, CaO, Na_2O, and K_2O and, to a small extent, Ni, N, and Ti. Space weathering by micrometeorite impact melting and vaporizing lunar soil are the favored explanations for these [266,267,269,270]. It is, however, thought that a giant impactor was primarily or secondarily responsible for the very high temperatures (~1500° C), leading to the necessary reducing conditions for the iron silicides [267]. A candidate for that huge impact is the same as that which created the South Pole-Aitken Basin (53°S 169°W; diameter: ca. 2500 km, depth: 6.2–8.2 km) on the Moon's far side, one of the largest impact craters in the Solar System [271]. There is growing evidence that the basin was caused by a low-velocity projectile (about 200 km) that hit the lunar surface at an angle of about 30° or less [272]. The impact that created the Copernicus crater about 800 Ma years has also been suggested as a possible primary triggering event [271]. In any case, the impact likely happened ≤ 1 Ma ago [271]. Moreover, the meteorite experienced three more impact events [271]. High shock, caused by impacts, is indicated by maskelynite glass [270,273].

Hapkeite (Fe_2Si) was also discovered, together with inclusions of troilite (FeS), in one of the samples from crater ejecta blanket at the Mare Crisium landing site (12°14′16″ N, 62°11′56″ E), returned by the Luna-24 mission (22 August 1976) [274,275]. Luna-24 made a core drilling in the Mare's lunar soil.

Moreover, an Apollo 16 regolith sample (# 61,500, subsample 61,501,22; A6–8, A6–7), from Flag Crater (8.97° S, 15.45° E; diameter: ca. 40 m, depth: >20 m) in the Descartes Highlands contained FeSi ($Fe_{44}Si_{56}$), Suessite $(Fe,Ni)_3Si$, Linzhiite $FeSi_2$ ($Fe_{32}P0_2Si_{66}$), and Luobusaite Fe_3Si_7, ($Fe_{28}Si_{71}$) as 0.1–2 μm-sized inclusions, as well as Si metal (< 1 μm) embedded in a plagioclase matrix [276–280].

8.2. Iron Silicides and an Ureilite Parent Body (UPB)

It is notable that iron silicides occur frequently in urelite meteorites [281] (Figure 6). It is suggested that some iron silicides are the remains of an ureilite parent body (UPB), disrupted by different impactors, which re-accreted, forming the regolith of the UPB, mixed up with the core and the mantle, as evidenced by polymict ureilite meteorites [281–294]. The parent body could have been a protoplanet in the size range between Mercury and Mars [289]. There is still disagreement about whether ureilites originate from different parent bodies or other areas of a single object. It is also unclear whether ureilitic meteorites are the remains of undissolved material from the time when the solar system was formed, or building blocks that were left over after more volatile components had melted away during specific processes of heating. Finally, ureilites could also represent a mixture of carbonaceous chondrite and molten basaltic rocks. There are indications that the inner and outer solar system material was mixed [295].

Figure 6. Iron silicides in meteorites: (1) DaG 1000, (2) DaG 1023, (3) DaD 999, (4) DaG 319, (5) DaG 1047, (6) DaG 1054, (7) DaG 1066, (8) EET 83,309, (9) EET 87,720, (10) North Haig, (11) Nilpena, (12) FRO 90,036, (13) FRO 90,054, (14) FRO 90,168, (15) FRO 90,233, (16) FRO 90,228, (17) FRO 93,008, (18) 2008 TC3 Almaha Sitta, (19) Goalpara, (20) Novo Urei, (21) Dingo Pup Donga, (22) Kenna, (23) Dho 837, (24) SaU, (25) Asuka 881,020, (26) Khatyrka, (27) Allende, (28) Kyker and Zelenoye Ozero, (29) Dho 280, (30) El Aybal (?), and (31) Chernivtsi. Source: Michael A. Rappenglück, based on Google My Maps.

Suessite $(Fe,Ni)_3Si$ is found in polymict meteorites DaG 1000 (Dar al Gani, Libya; 27°00.81′ N, 16°21.95′ E) [296,297], heavily shocked DaG 1023 (Dar al Gani, Libya; 27°1′ 33″ N, 16°23′16″ E) [296,297], and DaG 999 (Dar al Gani, Libya; 27°1′33″ N, 16°21′57″ E) [296,297].

In the polymict ureilite DaG 319 (Dar al Gani, Libya; 27°1′41″ N, 16°21′31″ E), suessite (Fe_3Si) and perryite (Fe_5Si_2) has been identified. The highly shocked polymict ureilite DaG 1047 (Dar al Gani, Libya; 27°2′9″ N, 16°23′7″ E) has feldspars, olivine, pyroxenes, and troilite. Moreover, it shows suessite $(Fe,Ni)_3Si$ and kamacite (Fe,Ni) with up to 27.6wt% Ni [298–300].

The polymict ureilite DaG 1054 (Dar al Gani, Libya; 27°25′40″ N, 16°9′56″ E) is highly shocked. It consists of mainly olivine (≤30 μm), few orthopyroxenes, rare grains of sulfide (mainly troilite), carbon including tiny diamonds at the grain boundaries, and suessite [$(Fe,Ni)_3Si$], with fractions of Cr and Ni, grains (≤100 μm) or metal veins [301].

Suessite (Fe_3Si), hapkeite (Fe_2Si), and naquite (FeSi) are present in the barely weathered polymict meteorite, DAG 1066 (Dar al Gani, Libya; 27°9′7″ N, 16°16′12″ E) [302–304]. The meteorite shows signs of being highly shocked (S3). The iron silicides indicate a formation under significantly reducing conditions [304]. They are embedded as minute spots in a matrix largely consisting of olivine crystals (0.2–1.5 mm) and, to a lesser extent, pyroxene and feldspar, on the edge of the olivine grains and graphite. Other inclusions are pentlandite $(Fe,Ni)_9S_8$ and FeNi. An analysis showed that the embeddings are partially ureilitic, carbonaceous chondrites (CC), or chondrules rich of forsterite and enstatite. The meteorite is assumed to be of ureilite origin based on the present investigation.

The polymict ureilite EET 83,309 (Elephant Moraine, Antarctica; 76°18′52″ S, 157°13′11″ E) [297] consists of olivine, pyroxene, and plagioclase in one grain (0.6 mm), as well as suessite (Fe_3Si) and many fragments (>300 μm) of opal ($SiO_2{\cdot}nH_2O$), which, as a 10 μm thick skin, completely envelopes the suessite (Fe_3Si) grains [305–307]. In EET 87,720

(Elephant Moraine, Antarctica; 76°11′ S, 157°10′ E) [297], the (unconfirmed) detection of a hapkeite (Fe_2Si) grain was reported [291].

In the North Haig polymict ureilite (Sleeper Camp, North Haig, Western Australia, 30°13′ S, 126°13′ E), section B (WAM12,809 'B′), mainly suessite $(Fe,Ni)_3Si$, filling cracks and appearing as blebs (1 μm) or grains (30 μm × 150 μm), and one grain xifengite (Fe_5Si_3), were found, while in section 'A′, a (hitherto unnamed) phase $(Fe,Ni)_4Si$ was detected [282,308,309]. There is also a magnetic signal indicating suessite [288]. The meteorite gives the type specification for suessite $(Fe, Ni)_3Si$ [309]. Previously, the existence of suessite had been doubted [190]. Probably paired with the North Haig is the polymict ureilite Nilpena (Hundred of Nilpena, County Taunton, Australia; 31°5′ S, 138°18′ E) [282], which also contains suessite $(Fe,Ni)_3Si$, with a different percentage of Si (North Haig: 10–16.7%, Nilpena: 11.8 -17.1% [308,310,311].

Paired meteorites from Frontier Mountain [312], Antarctica (FRO 90,036 [72°57′12″ S, 160°26′22″ E], FRO 90,054 [72°57′21″ S, 160°26′19″ E], FRO 90,168 [72°57′18″ S, 160°26′46″ E], FRO 90,233 [72°57′22″ S, 160°26′18″ E], FRO 90,228 [72°57′ S, 160°26′ E], and FRO 93,008 [72°57′16″ S, 160°26′16″ E], found between 1990 and 1993) [312–319] have been found to contain Fe_xSi_y. In all of them, the unnamed phase $(Fe,Ni)_9Si$ was identified [281]. FRO 90,168 and 93,008 contain suessite $(Fe,Ni)_3Si$ in the veins, produced by high degrees of shock (as mosaic olivine) [291,320]. A grain of Fe_2Si, probably hapkeite, was detected in FRO 90,228 dimict ureilite [291]. Remarkably, suessite $(Fe,Ni)_3Si$ and hapkeite (Fe_2Si) were discovered in the veins of dimict ureilites, indicating their origin as impact-induced melt [291].

The monomict ureilite NWA 1241 (north-western Africa, unknown coordinates) consists of silicates (olivine, pigeonite), carbonaceous material, nanodiamonds, and, as the main abundant metallic phase, suessite [288,297,321,322]. From the mineralogy of NWA 1241, it is assumed that due to an impact on the ureilite parent body (UPB), suessite was produced by olivine and kamacite at ca. 1400–1500 K and very high fugacity of oxygen.

The highly shock-melted and recrystallized ureilite NWA 14,274 (north-western Africa, unknown coordinates) is composed of olivine (a dunite >90 vol.%), pigeonite, orthopyroxene, kamacite, graphite, secondary calcite and gypsum, as well as glasses enriched in Si, NaMgAlSi, and FeSi [323].

In addition to olivine, pigeonite, clinopyroxene, graphite, troilite, pentlandite, sub calcic augite, and kamacite (Ni: 3.4%, Si: 3.8%), the ureilite meteorite NEA 027 (Northeast Africa, unknown coordinates), which was shock recrystallized, also contains suessite [324].

The superbolide 2008 TC3 Almaha Sitta (Nahr an Nil, Nubian Desert, Sudan, 20°44′45″ N, 32°24′46″ E) was the first planetoid whose entry into the Earth's atmosphere on 7 October 2008 over the Nubian Desert could be accurately predicted. It was 3–4 m in size (Apollo type) and disintegrated at an altitude of about 37 km [325]. This superbolide belongs to the F-type of planetoids [325]. It consists of more than 30 individual components with 20 different compositions, including sections of 18 different amino acids and polycyclic aromatic hydrocarbons (PAHs). It may be associated with the main belt, in particular, the planetoids of the Nysa-Polana family [326]. Recent research suggests a Ceres-sized (ca 640–1800 km) planetoid as the water-rich parent body [327]. All ureilitic fragments of 2008 TC3 showed various mixtures of kamacite with very low nickel content, suessite (Fe_3Si), schreibersite $(Fe,Ni)_3P$, troilite (FeS), and daubréelite ($FeCr_2S_4$)–heideite $(Fe,Cr)_{1.15}(Ti,Fe)_2S_4$ in grains of olivine close to the veins, which were enriched in C [328,329]. The magnetism was attributed to these components and an extraterrestrial origin was assumed [288,322]. The exact contribution of suessite (Curie-temperature: 823–873 K) to magnetisation is the subject of further investigation [288].

Moreover, the ureilite meteorites Goalpara (Assam, India; 26°10′ N, 90°36′ E) [330], Novo Urei (Respublika Mordoviya, Russia; 54°49′ N, 46°0′ E) [330], and Dingo Pup Donga (Western Australia, Australia; 30°26′ S, 126°6′ E) [330] as well as NWA 766 (Northwest Africa; unknown coordinates) [331], Kenna (New Mexico, USA; 33°54′0″ N, 103°33′12″ W)

[330], and Dho 837 (Zufar, Oman; 18°18′21″ N, 54°8′59″ E) [296] all show magnetic signals of suessite [288,332].

8.3. Iron Silicides in other Types of Meteorites

The EH3 chondrite Northwest Africa 8789 (coordinates unknown) contains suessite $(Fe,Ni)_3Si$ (Ni 80.7 wt.%, Si 14.8 wt.%, Fe 4.1 wt.%, Co <0.1 wt.%) as well as several other minerals within chondrules (0.6 ± 0.4 mm, one 2.1 mm, in a red-brown matrix [333,334]. An analysis concluded that the EH and the EL type were once exposed to powerful shocks at their location in the planetary system [333]. In addition, the enstatite chondrites EH3 Qingzhen and MacAlpine Hills (MAC) 88,136 (EU) contain perryite $(Ni,Fe)_8(Si,P)_3$ [335]. The meteorite NWA 13,108 (unknown coordinates) is classified as an enstatite chondrite (EL6). It consists of many other minerals and iron silicide without Ni, probably naquite (FeSi) [336].

Based on spectral analyses, the Main Belt planetoids (21) Lutetia and (97) Klotho could be associated with the parent body of enstatites (M type; size: 121 ± 1 × 101 ± 1 × 75 ± 13 km; density: 3.4 ± 0.3 g/cm³) [337]. Lutetia seems to consist partially of enstatite material (E-type chondrite) and carbonaceous chondrites of CB, VH, or CR [338]. However, based on the densities of the two classes of meteorites and (21) Lutetia, it can be concluded that a differentiated core exists [338]. (12) Lutetia could be a primordial planetesimal [338,339]. Another planetoid, (97) Klotho (M type; size: 100.717 km; density: 4.16 ± 0.62 g/cm³), is also seen as a possible candidate for the enstatite parent body [337].

The carbonaceous CH3 chondrites SaU (Sayh al Uhaymi) 290 (Al Wusta, Oman; 21°4′32″ N, 57°8′49″ E) [340] and Asuka 881,020 (Antarctica; 72° S, 26° E) [330] contain suessite $(Fe,Ni)_3Si$, fersilicite (FeSi), and perryite ($(Ni,Fe)_8(Si,P)_3$), in addition to barringerite, andreyivanovite, troilite, daubreelite, pyrrhotite, pentlandite, and magnetite. There are places that are free of silicon and others where silicon is enriched [341]. Based on spectral analyses, planetoid 21 Lutetia is proposed for the CH3 meteorites, as is the case for the enstatites listed above [342].

Iron silicides occur in grain 126 of the carbonaceous chondrite Khatyrka CV3 meteorite (Listvenovyi stream, Koryak Mountains; Chukotka Autonomous Okrug, Russia; 62°39′11″ N, 174°30′2″ E) [343–346]. The meteorite is believed to be one of the solar system's building blocks, created some 4.5 billion years ago. It is rich in Al, Ni, and Cu, e.g., $Al_{0.97}Cu_{0.03}$, $Ni_{0.91}Fe_{0.05}Cu_{0.04}$, $Cu_{0.96}Fe_{0.04}$, or unnamed $Al_{78}Cu_{15}Fe_7$ beads of Fe (<10 nm to ~5 μm) were found. These include iron silicides Naquite (FeSi), suessite (Fe_3Si), xifengite (Fe_5Si_3), but less Ni (<0.1 wt%) [345]. There are many other minerals in that meteorite, e.g., hercynite, chromite, magnetite, corundum, iron, taenite, hollisterite (Al_3Fe), kryachkoite $(Al,Cu)_6(Fe,Cu)$, stolperite (AlCu), steinhardtite ($Al_{0.38}Ni_{0.32}Fe_{0.30}$) [345,347–349]; it is an unusual mix. Moreover, icosahedrite ($Al_{63}Cu_{24}Fe_{13}$ and $Al_{62}Cu_{31}Fe_7$), as well as decagonite ($Al_{71}Ni_{24}Fe_5$; ≤60 μm), the first natural quasicrystals [350], were detected [351–355]. It was assumed that these were formed by shock synthesis when planetoids collided [356,357]. Khatyrka experienced at least one high-velocity impact event.

The CV3 carbonaceous chondrite Allende (Pueblito de Allende, Chihuahua, Mexico; 26°58′ N, 105°19′ W) contains many different minerals, CAIs, graphite, nanodiamonds, alkane, amino acids, and hemolithin [358]. Moreover, a xifengite (Fe_5Si_3) grain was detected [359]. Kaitianite, $Ti^{3+}_2Ti^{4+}O_5$ tistarite (Ti_2O_3), rutile (TiO_2), corundum (Al_2O_3), mullite ($Al_6Si_2O_{13}$), osbornite (TiN), and a Ti,Al,Zr-oxide were present in this area. The meteorite is thought to be 4.567 billion years old.

The achondrite NWA 8014 (Northwest Africa; unknown coordinates) also contains suessite $(Fe,Ni)_3Si$.

A special find, that was identified as meteoritic, was made around the Kyker and Zelenoye Ozero villages (Tungokochenskii district, Transbaikalia Krai, Zabaikalsky region, Russia; 53°19′ N, 116°19′ E) which was named after the nearby Ilekta creek river [51,360]. The high nonuniform magnetic boulder (15 cm × 9 cm × 1–8 cm; 12 kg) is rounded, appears shiny metallic with an oxidized surface. On it and parts of the interior, traces of melting and boiling are visible. The stone shows plastic deformations and brittleness, depending on the heating and cooling it experienced. Moreover, the boulder is dotted with sprinkles in the holes. The surface is covered on one side with an oxide crust (1–4 mm thick) caused by the prolonged period of time it spent on the bottom of a river terrace, where the surface was exposed on one side. Basically, however, the block is unoxidized due to the high content of iron silicide. The boulder consists mainly of gupeiite (Fe_3Si; empirical formula: Fe 81.60–86.87%, Si 14.63–15.54%, Mn 1.06–1.23%, T: 1.13–1.25%, P 0.30–0.42%), with trapezoidal crystalline inclusions of TiC (Ti 47.48–68.5%) and schreibersite ($(Fe,Ni)_3P$; empirical formula: Fe 73.53–75.65%) P 13.79–15.27 %, Mn 5.00–5.28, Si 6.62–7.29%, Ti 0.58–1.79%, Cr 0.36–0.51%), with the latter shaped as needle-like crystals. It is assumed that the block is extraterrestrial, as there is no evidence of anthropogenic production; there has never been any industrialisation in this area, and other findings support this. A terrestrial origin has not been evidenced so far.

A conspicuous lump of magnetic rock (16 cm × 12 cm × 8 cm, 5934 kg) with a molten surface was found in a suburb of the city of Chernivtsi (Ukraine; 48°17.4′ N; 25°52′ E) at a depth of about 16.0 m [361]. The chronology is Serravalian (13.82–11.63 mya; Dashavian Miocene, N1ds). Two samples were taken for examination. The matrix (> 90 %) consisted of $(Fe_{3.04}Mn_{0.03}Cr_{0.01})_{3.08}(Si_{0.9}Ti_{0.02}V_{0.01})_{0.93}$, corresponding to gupeiite (Fe_3Si). In the second sample, there was a small amount of Ni (0.01vol%). There were rectangular, trapezoidal, tandem, isometric, and irregular within inclusions (0.01–0.5 mm) of titanium carbide (TiC; empirical formula: $(Ti_{0,98}V_{0,05})_{1,03}C_{0,96}$). An extraterrestrial origin is suggested.

9. Iron Silicides Deriving from Extraterrestrial Dust

The irregularly shaped particle L 2009 I14 (33 μm × 22 μm) was collected during a flight with NASA ER-2 in several successive ascents to 20 km altitude in the stratosphere. If the system had been near equilibrium, it would have contained SiO_2, pyroxene (enstatite), cordierite, pentlandite $(Fe_{0.65}Ni_{0.35})_9S_8$ and iron silicide hapkeite (Fe_2Si). There were also more minor traces of Mg, S and Ni and much smaller indications of Al and Cr. NASA classified the particle as cosmic dust (type "C") [362]. On Earth, iron silicides can be found in so-called extraterrestrial dust (Figure 7).

Figure 7. Iron silicides in extraterrestrial dust: (1) Polkowice-Sieroszowice and Rudna copper mines, (2) Ferghana Valley, (3) Poltava series (4) Yan mountains, (5) Üveghuta, (6) An Carnach and Broadford, Strathaird Peninsula, (7) Peter's Pond (?), (8) Hogden Lane, and (9) Belo Horizonte Source: Michael A. Rappenglück, based on Google My Maps.

In the Ferghana Valley (Isfara river, Uzbekistan, 40°44′24″ N, 72°37′48″ E), naquite (FeSi), gupeiite (Fe_3Si) and xifengite (Fe_5Si_3) spherules (<2 mm), together with moissanite (SiC) spheric nodules, were discovered. The moissanite globules consisted of SiC in the nucleus, a mantle of C, and an envelope of Fe_3C. Two of the Ferghana samples had Si 10–15wt%, Fe > 30 wt%, Ca 3 wt%, Na 1 wt%, Ni 0.1–0.2 wt%, Mo up to 0.1 wt%. The dispersed iron silicides area is like a strewn field, roughly 50 km width. The chronology, ~145.0–66.0 mya, is derived from the Cretaceous sedimentary of the Isfara river [156,172,363].

Cubic fersilicite/naquite cubic (FeSi), tetragonal ferdisilicite/linzhiite ($FeSi_2$), Fe_2Si_3, gupeiite (Fe_3Si), xifengite (Fe_5Si_3), intertwined, were found in placers and drill-core sandstones at the Poltava series (Zachativsk station, near Vysoke, Donetsk, Donetsk Oblast, Ukraine; 48°N, 38°E), Konksko-Yalynskaya depression, North Azov [156,173,176,364–368]. Initially, the minerals FeSi and $FeSi_2$ were not approved by the CNMMN, but in 2012, they were approved and named naquite and linzhiite [38,41,138,140]. Besides iron silicides, wüstite (FeO) together with silicate glass, was also found. Native Si, magnetite (Fe_3O_4), kamacite (α-(Fe,Ni)), moissanite (α-SiC), barringerite ($(Fe,Ni)_2P$), schreibersite (Fe_3P) and cohenite ($(Fe,Ni,Co)_3C$)) were identified. Magnetic rims also showed up in the material. Grains ranged from 0.05 to 7 mm, with those over 0.5 mm predominating. A pronounced groove can be seen on some, especially on the large grains, of the iron silicides. The ferrosilicon is irregularly formed (tetrahedral, prismatic, lanceolate, toothed, dendritic, globular, etc.). An opaque, dark, grey coloured film covers the grains. Only spalling and fractures show the characteristic strong lustre of the mineral. The heavy and bright mineral is found in quantities averaging 3–5 kg/m^3, and, in some places up to 250 kg/m^3, in an elliptical field (4 km × 1.8 km), 5–90 m deep. The amount of material decreases toward the periphery of the elliptical field. The Poltava series was dated to the Oligocene-Miocene (28.1–11.62 mya). The origin of the material is considered to be anthropogenic, tectonic, or meteoritic, but it may also be meteoritic. Mineralogical, morphological, and structural features indicate a cosmogenic origin for all these minerals, i.e., either cometary material or another source [173]. Barringerite so far is usually (14 times) discovered in meteorites, and at only nine terrestrial sites [369].

Gupeiite (Fe_3Si; empirical formula: $Fe_{2.971}Ni_{0.027}Mn_{0.023}Si_{0.979}$) and xifengite ($Fe_5Si_3$; empirical formula: $Fe_{4.905}Ni_{0.018}Mn_{0.015}Si_{3.062}$) inclusions were discovered in the cores of spherules (0.1–0.5 mm) embedded in in placers in the Yan Mountains (Yan Shan, Chengde prefecture, Hebei province, China, 41°N, 117°E) [370–372]. The placers have chromite, copper, gold, graphite, titanium carbide, ilmenite. It is the type of locality for gupeiite and xifengite. The spherules consist of magnetite, wüstite, and maghemite, forming a mantle. Then follows an inner shell made up of kamacite and taenite, and inside, there is a core of gupeiite and xifengite. TiC is often in the nucleus, too. The surface characteristics, which indicate flight through the atmosphere, and the minerals present, indicate the spheres to be extraterrestrial in origin.

Hapkeite (Fe_2Si) was reported for magnetic spherules (100–200 μm) from Üveghuta, Lower Carboniferous Mórágy Granite Complex (Tolna County, Southern Transdanubia, Hungary, 46°11′51.9″ N, 18°35′25.7″ E) and from the Mesozoic Gemeric Granite Complex, too. This could be related to extraterrestrial dust or a meteorite impact [183,373]. Besides hapkeite, moissanite (SiC), metallic (Fe) silicate spherules, and minor amounts of Al, Si, P (few wt%), S, K, Ca, Ti, V, Cr, Mn, and Ni were also discovered. Spherules and lamellae produce magnetism. Shocked metamorphic quartz was also identified [183], indicating the effects of high pressure, initially high temperatures (>1473 K) and then very rapid cooling.

In the late Danian (66.0–61.6 mya)/early Selandian (61.6–59.2 mya), an impact ejecta layer was found at two locations on the Isle of Sky (An Carnach and Broadford, Strathaird Peninsula, Scotland, UK; 57°15′ N, 5°55′ W) Fe(Si) [374]. The age is between 61.54 ± 0.42 and 60.00 ± 0.23 mya. At location 1, the impact ejecta layer (≥95 vol% matrix, 47 wt% SiO_2, high Al_2O_3 and FeO) is 0.9 m; at location 2, it is 2.1 m thick. The analysis of a Fe(Si) grain from site 2 shows the inclusion of vanadium-rich osbornite (TiVN), barringerite

[(Fe,Ni)$_2$P], and native Fe(Si) metal. A spherule (≈107 μm) from the exact location shows a ferro silicate glass with vesicles which encloses a spherical core (≈45 μm) of highly reduced native Fe(Si). The material contains unmolten vanadium-rich osbornite (TiVN), niobium-rich osbornite (TiNbN), high-pressure zircon polymorph reidite ($ZrSiO_4$), barringerite [(Fe,Ni)$_2$P], baddeleyite (ZrO_2), alabandite (MnS), carbon-bearing native iron (Fe) spherules, graphite (C) trails, FeO, and Si, Ni, and Cu in traces. The crystallisation of the spherules occurred extremely quickly. Reidite in single zircons mostly shows distinct shock lamellae. PDF and diaplectic glass in quartz imply pressures ≥30 Gpa at both locations. All this evidence together makes it clear that an impact created the deposits. TiVN and TiNbN are thought to be the remains of an extraterrestrial body.

Some 200 rock pieces (in total 200 kg) were discovered, conspicuously scattered and embedded in an area of ca. 10,000 m^2 of a partially eroded colluvial fan, about 50 km north of Belo Horizonte (Minas Gerais, Brazil, 19°55′0″ S, 43°56′0″ W) [375,376]. Whether industrial, natural (terrestrial or even extraterrestrial), the assignment of the locality remains unclear. Most of the pieces show strong magnetism. Less than 5% are slightly to moderately oxidised. There are different mineralogical groupings: the main group (>90%) consists mostly of corundum (Al_2O_3) and a minor spinel ($MgAl_2O_4$) matrix that contains internally highly crystalline structured polymetallic nodules. Most are spherules (<1 mm), some of which are perfectly rounded. However, oval-shaped nodules (>10 cm) were also observed. Minerals of the Melilite group ((Ca,Na)$_2$(Al,Mg,Fe^{2+})[(Al,Si)SiO$_7$]), e.g., gehlenite ((Ca$_2$Al[AlSiO$_7$])) are present. The material is unusually enriched in Zr and depleted in Al. Grossite ($CaAl_4O_7$) was also identified. Cu-Ni-Sn, Fe-Ni-Cu, Fe-Ni-Cu-Sn, Fe-Si-Ti, Fe-Si-Cr, Fe-Si-Ti-Al alloys are present in small quantities in all nodules. Kamacite (a(Fe,Ni)], xifengite (Fe_5Si_3), gupeiite (Fe_3Si)] and spherulite (Zn,Fe)S were also detected, as well as sulfides and phosphides. W, Pb, Zr exist in trace amounts. Some findings seem to indicate a meteoritic origin of the material, i.e., certain meteoritic shapes, regmaglypts, fusion crusts, Ca-Al-rich inclusions, enigmatic triangular crystallization structure like Widmanstätten pattern, and Grossite. The latter is known from only four locations on Earth (Hatrurim Formation, Israel; Kishon Mid Reach zone 2, Kishon river, Israel; Rakefet magmatic complex, Israel; Dellagiustaite type locality, Sierra de Comechingones, San Luis Province, Argentina), but from 17 meteorites. Thus, in principle, the material could be terrestrial, including industrial production, but is more likely meteoritic. In any case, extremely reducing conditions needed to be in place in either case.

Unusual glassy melt spherules (≤ 700 mm in diameter) were found at Peter's Pond (Blacksville SC, Carolina Bay, South Carolina, USA, 41°41′30.82″ N, 70°28′49.08″ E) [377]. Additionally, highly heated and partially melted clay clast was observed. The material showed numerous vesicles. There were three types of spherules. Mullite ($Al_6Si_2O_{13}$), corundum (Al_2O_3), and aluminosilicate were evidenced in glasses and spherules. The mullite cores were partially surrounded by incompletely dissolved kaolin clay balls, which had been slightly heated. Needles of mullite had grown through the boundary layer between clay and glass. Spherules with Mullite of the most common type typically contain a few corundum crystals. Interspersed spherules of gupeiite (Fe_3Si) occurred between the mullite-enriched glass and the layer of heat-decomposed black clay. It is suggested that the Fe_3Si was produced by the reduction of FeO in the glass. This was caused by the carbon content in the black clay, which was exposed to very high temperatures. Cohenite (Fe_3C) globules (10–20 μm), which have very small inclusions of steadite (90.71 % Fe + 6.89 % P + 2.4 % C at 950 °C, and 1.10 wt % Ni, 0.78 wt % Co), were found in the reduced regions of the spherules. These also occur in irregular areas (10–20 μm) within highly oxidised aluminium hematite. The delineation of the fusion exhibits crystals of aluminous hematite quenched in both rich and poor Fe glasses. Moreover, Ir (15 ± 7 ppb), Ni (395 ± 40 ppm), Cr (574 ± 57 ppm) was detected. It is suggested that the melt glasses originated from the kaolinite clays, which contained smaller quantities of iron oxides and illite. The unusual melting material requires high temperatures and extreme reducing processes. The genesis of iron silicides is unclear.

Different spherule types (wüstite, magnetite, iron silicide, chondritic silicate), which show characteristic textures, were discovered at 7 m depth in the chalk of Hogden Lane (North Downs, Ranmore Common, Surrey, UK, 51°15′18.4″ N, 0°23′32.0″ W). The iron silicide type (50–150 μm) contained Fe_3Si (empirical formula: $Fe_{2.89}Si_{1.11}$), without any Ni and with small amounts of O_2 (<1.21wt%,), Cr (<1wt%), and Mn (0.3–0.7wt%) [378]. The chronology is Coniacian (87 ± 1 mya). The iron silicide spherules were identified as original cosmic ones of the iron-type (I-type) that had been diagenetically modified.

10. Iron Silicides as Recondensation of Ejecta Vapour

It has been suggested that many of the spherules thought to be of extraterrestrial origin are, in fact, the result of processing through the recondensation of ejecta vapour [156]. (Figure 8).

A greyish-black rock block (60 cm × 80 cm × 13–15 cm) from Koshava gypsum deposit (Moesia region, Danube River, Northwest Bulgaria; 44°3″8.748′ N, 22°59″35.311′ E), discovered at a depth of 290 m, contained gupeiite (Fe_3Si), hapkeite (Fe_2Si) and probably naquite (or fersilicite) FeSi embedded in petrified organic matter (showing a wooden texture) [379–381]. There were also other stoichiometries of Fe_xSi_y (Si: 3.57 wt% to 9.08 wt%). One grain of Suessite $(Fe, Ni)_3Si$ was also verifiable. At first, the find was identified as a meteorite, but since then, it has been been reclassified as impact ejecta. Evidence of extensive high-temperature melting is given by melted quartz rosettes, ballen structures in quartz, melted wood relicts, regmaglypts on the surface crust, lechatelierite (SiO_2), iron silicides (Fe_xSi_y), moissanite (SiC), melted spherules. High shock impact is indicated by coesite (>2.5–3 Gpa and >973 K), mineraloid lechatelierite (SiO_2; >1973 K, 85 GPa), strongly broken quartz, deformation lamellae, and high $\delta^{18}O$ values of quartz. It is suggested that the Ries-Steinheim impact event (Middle Miocene, Langhian, 14.37 ± 0.30 [0.32] mya [2σ]) ejected the block [382]. However, the Koshava gypsum deposit is located ~1100 km to the southeast from that impact site. Such a distance weakens this hypothesis significantly.

Figure 8. Iron silicides as recondensation of ejecta vapor: (1) Chiemgau impact crater strewn field, (2) Koshava gypsum deposit, (3) Blackville, (4) Tell Abu Hureyra 1, (5) Alatau and Kalu ranges, (6) Laurel Hills, Holmdel. Source: Michael A. Rappenglück, based on Google My Maps.

In Blackville (South Carolina, USA, 33°21′25″ N, 81°16′22″ W), suessite $(Fe,Ni)_3Si$ was found in molten siliceous glass (420–2700 μm) situated in layers at a depth of 1.75–1.9 m, [383]. Moreover, glassy spherules (15–1940 μm) were also present. The suessite appeared together with globules of native Fe, quenched grains of corundum (Al_2O_3) and different stoichiometric mullite ($2Al_2O_3{\cdot}SiO_2$ and $3Al_2O_3{\cdot}2SiO_2$), Fe_3C spherules including ferro phosphorus (Fe_2P, Fe_3P). The glass also contains the mineraloid lechatelierite (SiO_2). At Melrose (Pennsylvania), molten siliceous glass spherules (2–5 mm) were found which contained the same minerals and mineraloids as well as molten magnetite [383,384]. The presence of mullite, suessite and lechatelierite in particular, testifies to high temperatures and pressures [383,384]. Suessite forms at 2273–2573 K [383,384]. Lechatelierite in granite needs 85 Gpa to emerge [385]. Thus, it is suggested that the material formed during an impact which melted the silicates. The chronology is the onset of the Younger Dryas, which is believed by research teams to have occurred 12,800 ± 300 cal BP with 2σ (95%) probability (calibrated BP: calendar years before 1950) [383,386]. This dating, however, remains contestable [387–390]. The onset of the Younger Dryas Event also corresponds to the date of a third site with iron silicides, which is an archaeological settlement, i.e., Tell Abu Hureyra 1 (now submerged in the Lake Assad, Raqqa Governorate, Syria, 35°51′57.6″ N, 38°24′0″ E). The Epipaleolithic or Natufian settlement was founded c. 13,500 years ago, was inhabited for approximately 1000 years, and then abandoned around 12,200 years ago [391]. Excavations have revealed layers rich in charcoal, with molten glass, molten Fe, Si and C spherules, magnetic spherules, nanodiamonds, platinum, lechatelierite, and plant imprints [392]. Molten glass on the surfaces of spherules and in vesicles reveals the enrichment of Fe, FeO and iron silicides [392]. Globules (1–22 μm) of fersilicite/naquite (FeSi), hapkeite (Fe_2Si) with empirical formula ($(Fe_{1.9}\ Ni_{0.8}Cr_{0.2})_2\ (Si_{0.9}P_{0.1})$), and gupeiite ($Fe_3Si$) were found in the inner walls of vesicles. There, and on the outer surfaces of the glass, native Si was embedded. Temperatures between 1773–2473 K (e.g., suessite, molten magnetite), shock pressure (e.g., lechatelierite), and the effects (e.g., iron silicides, native Fe and Si) of extreme reducing environments only suggest a high-energy event. This could have been the impact of an extraterrestrial body, i.e., a planetoid or a comet, in parts or en bloc, which struck the atmosphere at Mach 8.8, triggering an airburst and cascading into fragments which subsequently hit the ground. The rapidly ignited biomass and the fused soil, both evaporating, account for the reducing carbon. Rapid cooling followed. Because the Younger Dryas event was associated by the research teams with a global effective impact, a cascading impactor (multiple impacts) was also assumed. There are a number of criticisms of the assessment of an impact with global implications and their relation to the origin of the Younger Dryas period. The anomalies could be attributed to volcanism, the Plinian eruption of the Laacher See volcano (Ahrweiler, Rhineland-Palatinate Germany, 50°25′ N, 7°16′ E), the supernova Vela XYZ, a super-sized solar proton event, or a massive melting of the ice sheets during the preceding warm period of the Allerød oscillation (c.13,900–12,900 BP, uncalibrated), resulting in considerable disturbance of the North Atlantic Current and associated cooling (Heinrich Event H0) due to heavy snowfall [390,393–399]. A combination of different causes cannot be ruled out either.

From an area between the Alatau and Kalu ranges, close to the abandoned settlement of Utar-Yurt (Southern Urals, Ishimbayskiy rayon, Republic of Bashkortostan, Russia, 53°46′0″ N, 56°51′0″ E), natural silicides (0.05–8 mm, irregular to spherical shaped ≤2.7 cm) have been reported in the streambed of a tributary to the Sheshenyak Minor river [156,400,401]. The spherules (5.1 kg) were found scattered or clustered (1 m × 1 m to 2 m × 5 m, partially washed up) over an area of 300 m radius in the streambed, in outcrops on the bank (depth 0.5–1.5 m). The area is difficult to access and is uninhabited. An industrial origin of the iron silicides has been excluded. Most silicides (>98%) appear to be ferromagnetic or paramagnetic. The chronology is Pleistocene (from sediments). The main matrix components are intertwined iron silicides like gupeiite (Fe_3Si) and xifengite (Fe_5Si_3), partially fersilicite/naquite (FeSi) and hapkeite (Fe_2Si), and other phases (Fe_7Si_2, Fe_3Si_2) or $(Fe,Ti)_4Si_5$, $(Fe,Ca,Ti)_5Si_4$, and $(Fe,Ca,Ti)_4Si_7$. There are inclusions (3–10 μm) of fersilicite/naquite (FeSi), linzhiite ($FeSi_2$), hapkeite (Fe_2Si), titanium carbide (TiC), moissanite (SiC), cohenite (Fe_3C), khamrabaevite (T,V,Fe)C), graphite (C), magnetite (Fe_3O_4) and wüstite (FeO) typical on rims (1–3 μm), zirconium silicide carbide (Zr-Si-C), and unnamed (Fe,Al,U)Si, $(Fe,U,Al)_2Si$, $(Fe,U,Zr)_5(SiP)_2$, and $(Fe,U)_4(SiP)$,$(Fe,U)_5Si$, as well as $(Fe,U,Al,Zr)_5Si_3$. Smaller areas (<30 μm) contain C, Al, Ti enrichments. Depending on the size of the spherules, the composition and proportion of different iron silicide phases vary. Limonite nodules (20–30 mm) are paragenetic and contain tiny spherules of iron silicides (Fe_xSi_y), spinel ($MgAl_2O_4$), clay and silicate glass. The matrix of limonite shows signs of shock metamorphism. An isotopic ($^{87}Rb/^{86}Sr$, $^{87}Sr/^{86}Sr$, $^{3}He/^{4}He$, $^{40}Ar/^{36}Ar$, $^{143}Nd/^{144}Nd$, $^{147}Sm/^{144}Nd$) analysis showed certain deviations from terrestrial values. There was no cosmogenic ^{3}He, ^{21}Ne, and ^{38}Al or radiogenic ^{40}Al. The elemental ratios of AI, Kr, and Xe evidence terrestrial sediments. Ni is below 0.1 %. There is probably no Ir or Os. All this supports sediments of the upper crust of the Alatau and Kalu ranges as the origin of the material. Their chronology is Chibanian/Middle Pleistocene (314–121 ka).

There are similar findings of iron silicides in terms of morphology and composition distributed in an area of 25 m × 5 m, 2.5 m deep, at Laurel Hills, Holmdel (New Jersey, USA, 39°56′56″ N, 74°54′1″ W) [156]. The 75 magnetic pieces are slightly smaller (0.05–4 mm). They were discovered in the Wenonah formation. The chronology is Upper Cretaceous (100.5–66 mya). From the findings, it was deduced that the material was terrestrial. It is thought that the iron silicide spherules were produced secondarily from terrestrial material following an impact [156]. The morphology of the spherules at both sites gives clear evidence that they were intensely heated (>3700° C) during flight through the atmosphere, before quickly slowing and cooling down in the process. They show characteristics of aerodynamic stress, ablation, quenching, and extremely high temperatures >2100 K (SiC TiC, Fe_xSi_y) during two heating events, as well as shock. A mixing with primary extraterrestrial material cannot be excluded [156]. It is thought that the spherules were produced as ejecta by an impact event and the subsequent hypervelocity crash back to the ground. The researchers argue that the uranium iron silicides and aluminium and zirconium carbides, within the iron silicides, were not formed in any technological process.

The closest and only third hitherto known association of uranium and fersilicites, moissanite, titanium carbide, graphite, and the special khamrabaevite, was found in the uraniferous iron silicides of the Chiemgau Impact site (see below).

11. Iron Silicides Associated with Craters

In a few cases, iron silicides may be associated with individual craters or crater fields (Figure 9). The Haughton impact crater (Devon Island, Territory of Nunavut, Canadian Arctic, 75°22′ N, 89°41′ W), 23–24 km in diameter, contains iron silicides together with moissanite (SiC, native Si, and other silicides of Al, Ni, Ba, Ti, and V (here VSi_2). The hexagonal crystals comprise vanadium silicide (VSi_2) with minor Ti and Ba substitutions for V within silicate glass produced by the impact event [402,403]. The impact is dated to the Eocene, 39 mya ago.

Figure 9. Iron silicides associated with craters: (1) Houghton impact crater (2) Chiemgau impact crater strewn field. Source: Michael A. Rappenglück, based on Google My Maps.

A comprehensive relation of iron silicides in craters in an extensive strewn field may be undertaken using material from the Chiemgau Impact site. The crater strewn field of the "Chiemgau impact" is evidence of a large meteorite impact that occurred in prehistoric times in the foothills of the Bavarian Alps [404–406]. The area extends roughly elliptically over an area of about 60 km × 30 km (c. 1800 km^2, 47.8°- 48.4° N, 12.3°- 13.0°E) between Altötting, Lake Chiemsee and the Alps, Bavaria, Germany. Nearly 80 craters have been documented. The impactor that caused the event is likely to have been a relatively porous object consisting of various components that broke apart in the atmosphere. The analysis of the composition of an impact rock showing the shock metamorphoses typical for an impact and, at the same time, fusing with the metallic components (high lead bronze and iron) of artefacts from the archaeological layer, makes it possible to date the Chiemgau impact to ca. 900–600 BC [407,408]. The published research results evidence an impact event based on the relevant criteria and methodology required in the scientific community. However, the relationship of the geological and archaeological structures and material findings to an impact event has been questioned [409–413] and debated [404,408,414–422].

In the crater strewn field, a total of 2–3 kg of particles, hardly corroded or not corroded at all and showing a metallic sheen, were found distributed over hundreds of square kilometres. They were often are shaped in aerodynamic forms such as ellipsoids, spheres, buttons and drops, but also as splinters and pieces (from 1 mm up to 6 cm and 167 g), or even an 8 kg lump in the subsoil down to the substratum (≈ 30–40 cm) in a glacially formed layer [404,405]. A smoothed convex face and a flat irregularly shaped reverse were frequently observed. The material is tough and magnetic [414,423]. Some specimens show a remaglyptic surface. There is also accretionary lapilli with magnetic xifengite cores. Iron silicide splinters also occurred in foamy-porous carbonate matrices, presumably recrystallised carbonate melt. Big sparkling crystals (moissanite) protruding from the metallic matrix are visible to the naked eye. Fersilicite/naquite (FeSi), ferdisilicite/linzhiite ($FeSi_2$), hapkeite (Fe_2Si) as cubic (hapkeite-1C) and trigonal (hapkeite-1T), gupeiite (Fe_3Si), suessite $(Fe,Ni)_3Si$, xifengite (Fe_5Si_3), and in traces suessite $(Fe,Ni)_3Si$ were detected [404,424–427]. Fe_xSi_y appeared as irregular, round blebs (5–40 μm) and pyramid-shaped formations (≈600 μm) in the microstructure. The intergrown iron silicides formed a matrix for various mineral inclusions. Among them were cubic moissanite ([β]3C-SiC) and titanium carbide (TiC) crystals (≈ 40 μm × 80 μm) of extreme purity, as well as $TiC_{0.63}$. Khamrabaevite ((Ti,V,Fe)C) was frequently present. There was zirconium carbide (ZrC), possibly baddeleyite (ZrO_2) and uranium carbide (UC). Zircon $Zr[SiO_4]$ crystals (3–10 μm) and uranium (U) as caps were recognisable. Sometimes, SiC appeared peppered with U blobs. Moreover, calcium-aluminium-rich matter, like the calcium aluminate/krotite ($CaAl_2O_4$) and dicalcium dialuminate ($Ca_2Al_2O_5$) [426], was identified in the material. There were also graphite and nanodiamonds (C). Ni (≈ 0.8wt%) was present in the suessite $(Fe,N)_3Si$. The amount of Cr was ≈ 0.5wt%. In addition to the main component, i.e., Fe_xSi_y, more than 40 other chemical elements, including uranium and REE (e.g., Y, Ce, La, Pr, Nd, Gd, Yb) have been detected so far. In one sample Th was marginally detectable, and in another, a trace of Po was found. Lead was completely absent. Previous individual findings of a different nature could not be confirmed [409,410]. Although uranium was present in spectra in clear quantities, there was no evidence of daughter nuclides, grandchild nuclides, etc.

The microstructure of the material showed clear signs of very intense mechanical overload, which, in principle, could have been caused by high shock effects (pressure, dynamic spallation, and thermal). This caused deformation lamellae and various crack features, e.g., tensile open fractures and groups of subparallel open fissures in Fe_xSi_y, TiC crystal, and multiple sets of planar features (PF), kink bands, planar deformation features

(PDF) in SiC crystal. The Fe_xSi_y matrix was littered with rimmed microcraters (10–20 μm), sometimes showing "ring walls", probably from the impacts of microparticles. The fersilicites regularly occurred near rimmed nanometre craters. Detailed images showed that zircon crystals struck the plastically deformed or even liquefied matrix of iron silicides. It is assumed that disturbance waves ran through the material and suddenly stopped, so that the matrix froze.

The mixture of minerals in the iron silicide matrix was unusual; they were distributed in it with low/high pressure and/or low/high temperature. There was monoclinic high temperature (>1773 K), low-pressure dimorph of $CaAl_2O_4$ [419,426], known as krotite. As a natural mineral, it has been identified in meteorites NWA 1934 [428] and in the basic/ultrabasic basaltic volcano complex of Mt. Carmel (Rakefet magmatic complex, Mount Carmel, Haifa District, Israel, 32°43′59″ N, 35°2′59″ E; see above), dated to the Late Cretaceous (96.7 ± 0.5 Ma) and assigned to kimberlites [429]. At the latter site, orthorhombic dicalcium dialuminate ($Ca_2Al_2O_5$), was found, i.e., unnamed UM1977-08-O:AlCaH [430], a high-pressure phase (>2.5 Gpa) [431] with the brownmillerite-type structure. This was also identified in the iron silicide matrix of the Chiemgau impact [419,426]. That phase can also be produced at ambient pressure but under quite high temperatures [431]. Moreover, in the large area of the Hatrurim Formation (Israel, 31°N, 35°E), where the rocks, consisting of chalk, limestones, marl, enriched with bituminous compounds, have been intensely heated and metamorphosed, $Ca_2Al_2O_5$ was also detected [432,433]. The chronology there is Late Cretaceous/Early Eocene (66.0–47.8 mya). $Ca_2Al_2O_5$ was also detected in the xenoliths of the Ettringer Bellerberg volcanic system (Ettringen, Mayen-Koblenz, Rhineland-Palatinate, Germany, 50°21′0.88″ N, 7°13′41.65″ E), dated c. 0.215 ± 0.004 to 0.190 ± 0.004 mya [434]. In addition, the iron silicide suessite $(Fe,Ni)_3Si$ formed from the matrix at more than 2000 K, and cubic moissanite ([β]3C-SiC) as well as nanodiamonds indicated high shock pressure [243]. Xifengite (Fe_5Si_3) and carbon spherules within amorphous carbon were found in the glazed enamel skin of a pebble from crater #004 in the field. High temperatures (thermal shock), >1773 K and pressures, as well as a magnetic anomaly, have been documented for the rocks in that crater [417,435]. Finally, an iron silicide lump (c. 16 cm × 11 cm × 5 cm, 8 kg), found approximately 30 years ago near Grabenstätt at Lake Chiemsee, is reported to contain cubic hapkeite (Fe_2Si, cubic and trigonal polymorph), gupeiite (Fe_3Si), xifengite (Fe_5Si_3), titanium carbide (TiC)/khamrabaevite ((Ti,V,Fe)C), moissanite (cubic SiC), zirconium carbide (ZrC), graphite and graphene [424,426]. When writing this review, the block is the largest known example containing natural cubic and trigonal Fe_2Si.

Collectively, the iron silicides hapkeite (Fe_2Si), suessite $(Fe,Ni)_3Si$ and xifengite (Fe_5Si_3) in the matrix, the mixture of mineral inclusions, which prove the effects of high but also low temperatures and pressures, the large-scale distribution, the association with craters in a strewn field, the finds in proven old layers of the Middle Ages from below a medieval hoard of coins and a castle, in peat mires and on the heights (>1000 m) of the neighbouring Alps exclude an anthropogenic-industrial origin (including bombing) [410] of these materials [404,405,414,435]. A geogenic source is also not plausible [414,435]. A primary extraterrestrial, including perhaps already a mixture in space or a secondary terrestrial (ejecta) source, is suggested [404–406]. The high degree of similarity among the finds from the Chiemgau impact with those from the Alatau and Kalu ranges (Southern Urals, Ishimbayskiy rayon, Republic of Bashkortostan, Russia Ural, Russia) and Laurel Hills, Holmdel (New Jersey, USA) is striking (see above). The findings on the association of uranium and fersilicites, moissanite, titanium carbide, graphite, and the special khamrabaevite are particularly significant. Thus, the iron silicides of the Chiemgau impact can, in principle, also be classified as (distal) impact ejecta. However, in contrast to, and as an extension of, the Alatau and Kalu as well as the Laurel Hills findings, there is a vast crater-strewn field which is genetically associated with the iron silicides, and within the iron silicide matrix are rare krotite ($CaAl_2O_4$) and dicalcium dialuminate ($Ca_2Al_2O_5$). Although Fe_xSi_y can be anthropogenic in origin, it is usually not comparable to the iron silicides and associated material found in the Chiemgau strewn field. Given that the known occurrences of Fe_xSi_y include several examples of extraterrestrial origin, such an origin is plausible unless a separate, nonimpact origin for Fe_xSi_y can be clearly demonstrated.

An additional, still unknown process or a mixture with the extraterrestrial material of the impactor is assumed here.

12. Other Iron Silicide Findings

There are very few iron silicides with other formation geneses (Figure 10). Amorphous Fe-Si mineral in a turbidite was dragged up from the Nares's abyssal plain (western North Atlantic; 23°30′ N 63°0′ W) [436]. It is thought to have been produced as precipitate by the mixture of diffusing dissolved iron and silica. A piece from ferromanganese crust (7,5 cm thick layer) from a guyot in 2486 m depth, Mid-Pacific Rise, Pacific Ocean (19°37′59″ N, 175°48′0″ W) revealed various minerals like apatite, goethite, barite, and rustenburgite [437,438]. Grains (<3 μm) of Cu-silicides $(Cu,Pt)_4Si$, $(Cu,Pt)_5Si$, Fe-silicides (Fe_2Si), (Fe_3Si), and Fe_5Si_3 as well as platinum group elements (PGE) were found [437,438]. The formation of metal silicides in the ocean floor, which was almost completely sediment-free, is here attributed to highly reducing fluids in the context of basalt formation. Still, an artificial origin cannot be excluded concerning the tetracopper silicide (Cu_4Si).

In a heap of the dormant Piast coal mine in Nowa Ruda (Kłodzko County, Lower Silesian Voivodeship, Poland; 50°35′3″ N, 16°31′6″ E) native iron (Fe), possible gupeiite (Fe_3Si) / schreibersite ($(Fe,Ni)_3P$), (unnamed) $Fe_7(P,Si)3$ and (unnamed) $Fe_5(P,Si)_3$ has been found [439]. The natural process of self-heating, set in motion anthropogenically by waste rock piles, induced pyrometamorphism. Among them, iron silicides may form during the spontaneous combustion of coal [439,440]. In comparable burning heaps at other locations, barringerite $(Fe,Ni)_2P$ [369], cohenite (Fe_3C), and oldhamite $(Ca,Mg)S$ [441] have been identified [439]. This moves the generation form of these pyrometamorphic rocks into a certain proximity to meteoritic material [442]. In the latter case, however, there would also have been considerable changes due to shock effects, and many other general conditions would have to be considered.

Figure 10. Iron silicides with other formation genesis: (1) Nares abyssal plain, (2) Mid Pacific Rice, and (3) Nowa Ruda coal mine heap Source: Michael A. Rappenglück, based on Google My Maps.

13. Iron Silicides as a Component of Circumstellar Envelops (CSE) and in Interstellar Matter (ISM)

Iron silicides/Iron-Nickel silicides, typically with sizes of tens of nm and with an abundance of >> 1 ppm, evidenced only as inclusions in other presolar phases, are among the presolar grain types associated with AGB stars and supernovae (SNe) [443].

Theoretical considerations and modelling [444–448] show that in circumstellar envelops (CSE) of certain so-called AGB (Asymptotic Giant Branch) stars, during the final phase of their evolution, if C/O > 1, phases of iron silicide (Fe_xSi_y) can condense into small grains. These seem to be a component of the dust envelops related to S-type stars and Luminous Blue Variables (LBVs). Depending on the proportion, C/O S-type stars with C/O ≈ 1 (± 0.25) are classified between carbon stars with C/O > 1 (spectrum dominated by TiO bands) and M-type AGB stars (normal giants) with C/O < 1 (spectrum dominated by ZrO bands) [449,450]. A stellar superwind forms the circumstellar envelopes (gas, dust) during the last phase of the star's existence, slowly enriching the interstellar matter. There is not enough oxygen in S stars to form oxides and too little carbon to form soot (C/O~1). S-stars mark the transition from M-stars (main sequence stars) to C-stars (carbon stars) on the Asymptotic Giant Branch (AGB) (Figure 11). As such, unusual native Fe (α-Fe) and rare iron silicides FeSi are expected in the dust, along with other silicides and nitrides [445,447,448]. FeSi can be more stable than Fe at a critical carbon content limit. In the dust envelopes of S-stars, SiC (moissanite), TiC (titanium carbide), and $Mg_2[SiO_4]$ (forsterite) also condensate.

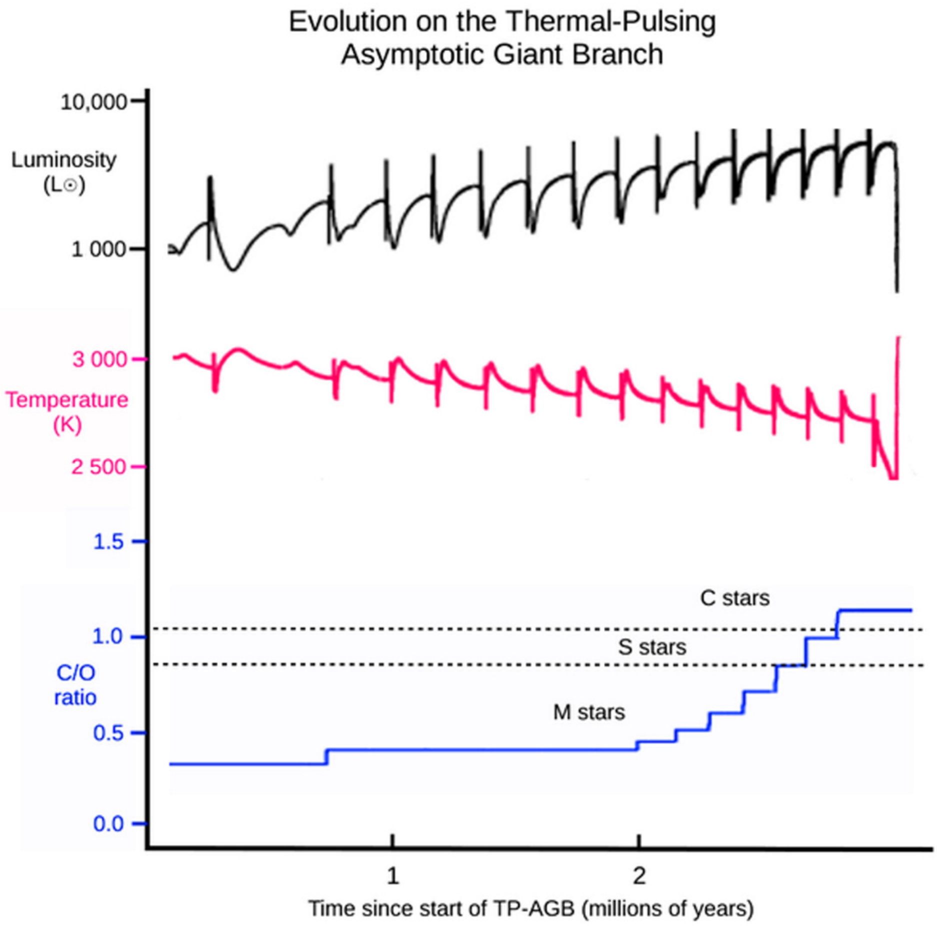

Figure 11. Diagrams showing the change in properties of a Template Solar mass solar-metallicity star as it evolves along the Thermally Pulsing Asymptotic Giant Branch. Source: Lithopsian, Evolution_on_the_TP-AGB.png. License: Creative Commons Attribution-Share Alike 4.0 International.

Luminous Blue Variables (LBVs; S Doradus variables or Hubble-Sandage variables) are extremely variable supergiants or even hypergiants, which, besides some periodic outbursts, undergo powerful eruptions. LBVs can have between 10 and 100 $M_\odot$. Their luminosity is between 0.25 and 1×10^6 $L_\odot$ [451]. LBVs represent the final stage in the evolution of such massive star types. Random violent mass ejections lead to the shedding of shells with a mass loss of 7×10^{-7} to 6.6×10^{-4} $M_\odot/yr^{-1}$ [452]. According to modelling [448] for a sample LBV star (parameters: T_{eff} = 7500 K, outburst mass loss rate: 0.3 $M_\odot/yr^{-1}$referring to η Car, mass: 100 $M_\odot$, luminance: 2×10^7 $L_\odot$), the LBVs dust ejecta are dominated by metallic Fe, FeSi, forsterite (Mg_2SiO_4). Sic is also produced. It has been proposed that TiC is a supporting grain for dust building.

There is some evidence for iron disilicide (β $FeSi_2$) in the so-called "Iris Nebula" (LBN487) in the Cepheus constellation [453,454](Figure 12). It is a reflection nebula (Figure x), ca. 1300 ly away. It measures six light-years in diameter. SAO 19,158, also known as HD 200,775 (Herbig Ae/Be star), is a very bright and hot star (spectral class B2Ve), having ten times the sun's mass. It is in a formative stage of evolution and illuminates the dust surrounding it. In the case of LBN487, a specific strong emission at 1.5 μm in the northwestern, but not in the southern filament, indicates the existence of low-temperature, amorphous $FeSi_2$ particles of ca. 100 nm size.

Figure 12. There is some evidence for iron disilicide (β FeSi2) in the so-called "Iris Nebula" (LBN487) in the Cepheus constellation. It is a reflection nebula, ca. 1300 ly away. It measures 6 light-years in diameter. Source: Observatory vhs Gilching, Germany, Michael A. Rappenglück.

There is spectral evidence of iron silicides (FeSi) in the expanding (≈ 30–40 km s^{-1}) dust shell (≈ diameter 8″/2 × 10^{12} km) around the spectroscopic binary star, AFGL 4106

[444,455,456], 10.764 ly away. The 47.5 μm and somewhat less clear 45 μm emission band is interpreted as indicating the presence of FeSi [444]. The findings suggest that there may be grains with a radius of 0.1μm and a temperature of 120 K. The expansion age of the envelope is 3.7×10^3 yr. Both agglutinated dust and ionized gas form the shell. The binary star consists of an F- classed post red supergiant (≈7250 ± 250 K) evolving towards a Wolf Rayet (WR) star and an M-classed member (≈ 3750 ± 250 K), a red supergiant, of nearly equal luminosity (7.4×10^4 L⊙ and 1.3×10^5 L⊙), both having masses 15–20 times that of the sun (M⊙) [455–457]. The stars are separated from each other by 0.3″.

14. Iron Silicides Related to Novae and Supernovae

A classical nova is a close binary star system in which one component has evolved from a progenitor red giant to a white dwarf. The other component may be a main sequence, subgiant, or red giant star [458]. The white dwarf, due to its extraordinary gravitational pull, accretes material from the other orbiting approaching component. It may also be that the other component expands beyond its Roche limit and starts the process. The matter from that component, mostly hydrogen, produces a dense but thin atmosphere around the white dwarf. The thermal heating of that accretion disk by the white dwarf ignites a very powerful thermonuclear runaway that appears as a Nova outburst. It may be potent (i.e., very short-lived temperatures of up to $2–3 \times 10^8$ K, expansion speeds of up to some thousand km, 50,000–100,000 times the solar luminosity, gammy rays >100 MeV [459]), triggered by a thermonuclear runaway. That causes them to eject shells of matter (10^{-4}–10^{-5} M⊙) into the interstellar medium.

For type II supernovae, modelling predicted the condensation of iron silicides in the C-He, Si-S, and Fe-Ni zones (Figure 13). In the Fe-Ni zone, Ti_5Si_3 (an analogue to Fe_5Si_3) condensates at 1622 K, (Fe,Ni)Si [fersilicite/naquite] at 1528 K, $(Fe,Ni)_3Si$ [suessite] at 1561 K. In the Si-S zone, Ti_5Si_3 condensate at 1641 K, TiSi at 1609 K, (Fe, Ni)Si at 1546, and $(Fe,Ni)_3Si$ at 1461 K. In the C-He zone, $(Fe,Ni)_3Si$ condensates at 1176 K [460]. Modelling a supernova with 21 M⊙ shows that FeSi condenses at the bottom of the O/Si zone at 1060 K, in the Si/S zone between 1405 K and 1200 K, and at the top of the Ni zone at 1400 K [461].

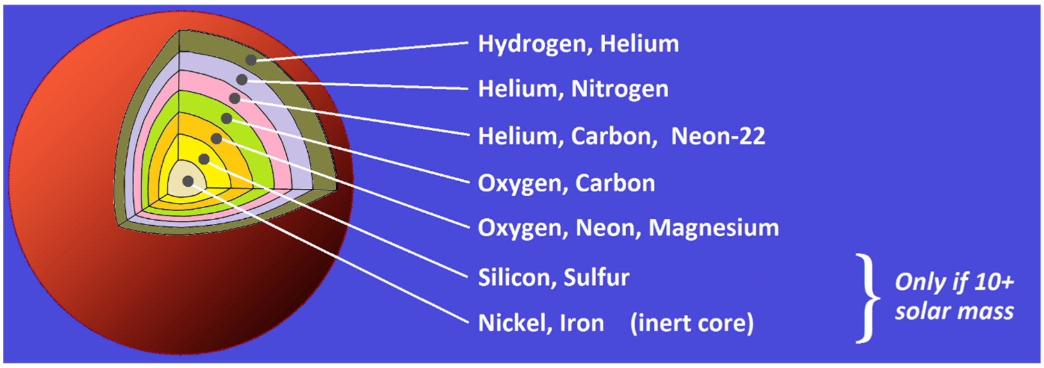

Figure 13. Shell of a massive star (>10 M⊙). License: Creative Commons CC0 1.0 Universal Public Domain Dedication.

According to another model [462], condensation occurs in zone M6, counted from the outer edge of the star towards the core [463], which is enriched in S and Si, dominated by a 50/50 Fe-Si alloy, condensing at 1670 K, with trace amounts of TiC appearing at 1560 K and TiN at 1510 K. The stable alloy is likely to be iron silicide (FeSi), for which we do not have thermodynamic data. In zone M7 (enriched in Si, Ca, Ti, Cr, Fe, Co, Ni), TiC appears at 1570 K, and TiN at 1540 K, containing all the C and N, respectively. Abundant metallic Ti appears at 1460 K, and $Fe_{0.65}Si_{0.35}$ alloy appears at 1430 K, incorporating 30% Co by 1330 K.

The presolar SiC grain M2-A1-G674 contains FeSi within subgrains 6 and 8 [464]. Subgrains (11 to 45 nm) of presolar SiC X grain KJG-N2-129-1 from the Murchison CM2 meteorite, a carbonaceous chondrite, selected for the grain type (X), contain iron, nickel silicides $(Fe,Ni)_xSi_y$ [465,466]. However, these research results are not yet recognised as sufficient by some scholars [467]. The findings could be explained by the iron silicides $(Fe,Ni)_3Si$, $(Fe,Ni)_2Si$. X grains originate from the supernova type II stage of massive stars ($8\ M_\odot \geq M < 40–50\ M_\odot$). The Murchison CM2 meteorite is approximately 7×10^9 years old [468]. From modelling, it was derived that FeSi alloy condensed at 1670 K in the M6 zone of the supernova shell, and that $Fe_{0.65}Si_{0.35}$ alloy was generated in the M7 zone at 1430 K [462]. However, a secondary formation at the interfaces between SiC domains appears to be more probable than direct condensation from the gas [468].

An analysis of a very tiny piece (7 μm diameter) of graphite (OR1d3m-18) of the Orgueil meteorite, for which the origin from a supernova (SN) could be determined (C, O, N, and Si isotopes), showed grains with unusual enrichments of $Fe_xNi_ySi_z$ ($Fe_{64}Ni_{14}Si_{21}$, $Fe_{67}Ni_7Si_{27}$ and $Fe_{68}Ni_9Si_{23}$), sometimes associated with TiC. However, notably, there were also spots of cubic Fe_2Si [469]. From the composition analysis and the correlation of the components, the pathway of the condensation of the stellar material can be deduced: $TiC \rightarrow Ni_2Si \rightarrow \alpha$-(Fe,Ni), enriched in Si/$Fe_2Si \rightarrow SiC \rightarrow C$ (graphite). This is consistent with the modelling, except that graphite should condense at the beginning. There is more Si enrichment from the Si/S zone of the star.

15. Discussion

The findings to date lead to some fundamental conclusions for the differentiation and methodological determination of the genesis and origin of natural iron silicides, as well as their differentiation from technogenically-synthesized ones.

Natural iron silicides in general form in highly reducing environments and at high temperatures. These conditions exist during lightning strikes, in the mantle and core of the Earth and in other terrestrial planets as well as the Moon, in the primordial period of the solar planetary system during the formation of protoplanets and proto-moons from impacts of planetesimals and cometesimals, during impacts on the Earth or terrestrial planets, during the entry of meteoroids into the atmosphere, during recondensation of ejecta vapour, and nuclear detonations. Similar conditions are given for the condensation of iron silicides in the envelopes of S-stars, Luminous Blue Variables, classical novae, supernovae of type II, and in certain nebulae. In some cases, permanent high pressures are significant (e.g., in the cores of terrestrial planets). High shock pressures are relevant in the rapid formation of iron silicides, e.g., during impact events.

There are a few examples of the generation of iron silicides as pyrometamorphic rocks without thermal shock or shock pressure, e.g., in the natural process of self-heating in coal heaps, mostly anthropogenically generated or in turbidites of the abyssal ocean floor, by highly fluids during basalt formation. In addition, apart from significant impacts, iron silicides on the surfaces of airless bodies (planets, dwarf planets, moons, planetoids, comets) in the planetary system are produced by 'space weathering', that is by the effect of a steady flow of micrometeorites, solar wind and cosmic rays.

According to their origin, a classification of iron silicides has been proposed on various occasions [156,179,361]. However, the following typification from the above examples seems appropriate: technogenic, geogenic, aerodynamic, exoplanetary, and cosmic. The clearest possible allocation to the respective categories must be based on a sufficient variety of methods. The exact specification of all setting conditions is of the utmost importance, to distinguish technogenic from geogenic-aerodynamic samples, and these, in turn, from exoplanetary and cosmic natural iron silicides.

There are some more detailed considerations od the chemical-physical processes of the genesis of natural iron silicides and the transitional stages, as well as the end products formed by their thermal decomposition. However, some aspects are not yet fully understood [96,156,172,174,185,191,260,270,378,439,442,446,447,461,462,470–473].

Finally, the analysis of paragenetic minerals, focusing on unusual conditions of formation, special mixing ratios, contradictions of associations, and signatures of origin, is essential.

Research into natural iron silicides has aroused great interest for decades, and remains an important and exciting task for the future.

Funding: This research received no external funding.

Data Availability Statement: Not applicable.

Acknowledgments: The author expressly thanks the reviewers for their valuable advice on optimising this extensive study.

Conflicts of Interest: The authors declare no conflict of interest.

References

1. Kaess, F. Die technische Herstellung des Ferrosiliziums. In *Elektrothermie: Die Elektrische Erzeugung und Technische Anwendung hoher Temperaturen, Zweite völlig Neubearbeitete und Erweiterte Auflage*; Breil, G., Dawihl, W., Hänlein, W., Kaess, F., Koenig, P., Pirani, M., Ragoss, A., Reidt, E., Rummel, T., Schaidhauf, M., et al., Eds.; Springer: Berlin/Heidelberg, Germany, 1960; pp. 205–215, ISBN 978-3-642-92779-9.
2. Lyon, D.A.; Keeney, R.M.; Cullen, J.F. *The Electric Furnace in Metallurgical Work*; Department of the Interior Bureau of Mines: Washington, DC, USA, 1914; pp. 1–216.
3. Hahn, H. Chemische Untersuchung der beim Lösen des Roheisens entstehenden Producte. *Eur. J. Org. Chem.* **1864**, *129*, 57–77. https://doi.org/10.1002/jlac.18641290108.
4. Hanson, D.; West, E.G. The Constitution of Copper-Iron-Silicon Alloys. *Mon. J. Inst. Met. Metall. Abstr.* **1934**, *1*, 95–116.
5. Guertler, W.; Tammann, G. Über die Verbindungen des Eisens mit Silicium. XVII. *Z. Anorg. Chem.* **1905**, *47*, 163–179. https://doi.org/10.1002/zaac.19050470112.
6. Yap, C.-P. A Critical Study of Some Iron-rich Iron-Silicon Alloys. *J. Phys. Chem.* **1933**, *37*, 951–967. https://doi.org/10.1021/j150349a011.
7. Weill, A.R. Structure of the Eta Phase of the Iron-Silicon System. *Nature* **1943**, *152*, 413–413. https://doi.org/10.1038/152413a0.
8. Dodero, M. Sur l'électrolyse de mélanges fondus de fluosilicates alcalist et de fluorures ou d'oxydes. *C. R. Acad. Sci. Paris* **1939**, *208*, 799–801.
9. Khalaff, K.; Schubert, K. Kristallstruktur von Fe2Si(h). *J. Less Common Met.* **1974**, *35*, 341–345. https://doi.org/10.1016/0022-5088(74)90247-1.
10. Kudielka Heinz. Die Kristallstruktur von Fe2Si, ihre Verwandtschaft zu den Ordnungsstrukturen des α-(Fe, Si)-Mischkristalls und zur Fe5Si3-Struktur. *Z. Krist.-Cryst. Mater.* **1977**, *145*, 177–189.
11. Rix, W. Über Eisensilizide: Züchtung von ß-FeSi2-Einkristallen durch Chemischen Transport, Strukturelle und Physikalische Charakterisierung. Ph.D. Thesis, Albert-Ludwigs-Universität, Freiburg im Breisgau, Germany, 2001.
12. Tang, C.P.; Tam, K.V.; Xiong, S.J.; Cao, J.; Zhang, X. The structure and electronic properties of hexagonal Fe2Si. *AIP Adv.* **2016**, *6*, 65317. https://doi.org/10.1063/1.4954667.
13. Tang, C.P.; Tam, K.V. The Study of Hexagonal Fe2Si: In Terms of Its Structure and Electronic Properties. In *21st Century Nanoscience—A Handbook*, Sattler, K.D., Ed.; CRC Press: Boca Raton, FL, USA, 2020; pp. 20–21. https://doi.org/10.1201/9780429347313-20.
14. Ye, Z.; Gupta, S.; Kerkkonen, O.; Kanniala, R.; Sahajwalla, V. SiC and Ferro-silicides Formation in Tuyere Cokes. *ISIJ Int.* **2013**, *53*, 181–183. https://doi.org/10.2355/isijinternational.53.181.
15. Gornostayev, S.S.; Heikkinen, E.-P.; Heino, J.J.; Fabritius, T.M.J. Fe-Si particles on the surface of blast furnace coke. *Int. J. Miner. Met. Mater.* **2015**, *22*, 697–703. https://doi.org/10.1007/s12613-015-1124-9.
16. Gornostayev, S.S.; Fabritius, T.M.J.; Kerkkonen, O.; Härkki, J.J. Fe-Si droplets associated with graphite on blast furnace coke. *Int. J. Miner. Met. Mater.* **2012**, *19*, 478–482. https://doi.org/10.1007/s12613-012-0583-5.
17. Li, K.; Zhang, J.; Liu, Z.; Barati, M.; Zhong, J.; Wei, M.; Wang, G.; Jiao, K.; Yang, T. Interfaces Between Coke, Slag, and Metal in the Tuyere Level of a Blast Furnace. *Met. Mater. Trans. A* **2015**, *46*, 1104–1111. https://doi.org/10.1007/s11663-015-0335-9.
18. Qian, W.; Huang, X. Invention of cast iron smelting in early China: Archaeological survey and numerical simulation. *Adv. Archaeomater.* **2021**, *2*, 4–14. https://doi.org/10.1016/j.aia.2021.04.001.
19. Schmidt, P.R. Science in Africa: A History of Ingenuity and Invention in African Iron Technology. In *A Companion to African History*, 1st ed.; Worger, W.H., Ambler, C.H., Achebe, N., Eds.; Wiley Blackwell: Hoboken, NJ, USA, 2018; pp. 267–288, ISBN 9781119063575.
20. Schmidt, P.; Avery, D.H. Complex Iron Smelting and Prehistoric Culture in Tanzania. *Science* **1978**, *201*, 1085–1089. https://doi.org/10.1126/science.201.4361.1085.
21. Schmidt, P.R. Resisting homogenization and recovering variation and innovation in African iron smelting. *Mediterr. Archaeol.* **2001**, *14*, 219–227.

22. Mineralogy Database. Minerals Arranged by the New Dana Classification: 01.01.23 Suessite Group Silicides. Available online: http://webmineral.com/dana/dana.php?class=01&subclass=01&group=23 (accessed on 19 October 2021).
23. Anthony, J.W.; Bideaux, R.A.; Bladh, K.W.; Nichols, M.C. Handbook of Mineralogy. Available online: http://www.handbookofmineralogy.org/ (accessed on 23 November 2021).
24. Mineralogy Database. Minerals Arranged by Nickel-Strunz (Version 10) Classification: 01.BB Silicides. Available online: http://webmineral.com/strunz/strunz.php?class=01&subclass=01.B&group=01.BB (accessed on 31 October 2021).
25. mindat.org. Xifengite. Available online: https://www.mindat.org/min-4335.html (accessed on 31 October 2021).
26. mindat.org. Gupeiite. Available online: https://www.mindat.org/min-1780.html (accessed on 31 October 2021).
27. mindat.org. Hapkeite. Available online: https://www.mindat.org/min-26419.html (accessed on 31 October 2021).
28. mindat.org. Suessite. Available online: https://www.mindat.org/min-3821.html (accessed on 31 October 2021).
29. mindat.org. Luobusaite. Available online: https://www.mindat.org/min-7677.html (accessed on 31 October 2021).
30. Wasson, J.; Wai, C.M. Composition of the metal, schreibersite and perryite of enstatite achondrites and the origin of enstatite chondrites and achondrites. *Geochim. Cosmochim. Acta* **1970**, *34*, 169–184. https://doi.org/10.1016/0016-7037(70)90004-9.
31. Mineralogy Database. Gupeiite Mineral Data. Available online: http://webmineral.com/data/Gupeiite.shtml (accessed on 31 October 2021).
32. Mineralogy Database. Hapkeite Mineral Data. Available online: http://webmineral.com/data/Hapkeite.shtml (accessed on 31 October 2021).
33. Mineralogy Database. Luobusaite Mineral Data. Available online: http://webmineral.com/data/Luobusaite.shtml (accessed on 31 October 2021).
34. Mineralogy Database. Suessite Mineral Data. Available online: http://webmineral.com/data/Suessite.shtml (accessed on 31 October 2021).
35. Mineralogy Database. Xifengite Mineral Data. Available online: http://webmineral.com/data/Xifengite.shtml (accessed on 31 October 2021).
36. Gopon, P.; Fournelle, J.; Sobol, P.E.; Llovet, X. Low-Voltage Electron-Probe Microanalysis of Fe–Si Compounds Using Soft X-Rays. *Microsc. Microanal.* **2013**, *19*, 1698–1708. https://doi.org/10.1017/s1431927613012695.
37. International Mineralogical Association. Commission on New Minerals, Nomeclature and Classification: The official IMA-CNMNC List of Mineral Names. Updated List of IMA-Approved Minerals. September 2021. Available online: http://cnmnc.main.jp/IMA_Master_List_%282021-09%29.pdf (accessed on 31 October 2021).
38. mindat.org. Fersilicite Mineral Data: Naquite. Available online: https://www.mindat.org/min-40148.html (accessed on 31 October 2021).
39. Mineralogy Database. Fersilicite Mineral Data. Available online: http://webmineral.com/data/Fersilicite.shtml (accessed on 31 October 2021).
40. Mineralogy Database. Ferdisilicite Mineral Data. Available online: http://webmineral.com/data/Ferdisilicite.shtml (accessed on 31 October 2021).
41. mindat.org. Linzhiite. Available online: https://www.mindat.org/min-40150.html (accessed on 31 October 2021).
42. Yang, Z.; Wu, S.; Zhao, X.; Nguyen, M.C.; Yu, S.; Wen, T.; Tang, L.; Li, F.; Ho, K.-M.; Wang, C.-Z. Structures and magnetic properties of iron silicide from adaptive genetic algorithm and first-principles calculations. *J. Appl. Phys.* **2018**, *124*, 073901. https://doi.org/10.1063/1.5036992.
43. Wang, G.-M.; Zeng, W.; Xu, X.; Liu, W.-H.; Tang, B.; Fan, D.-H.; Liu, Q.-J.; Chang, X.-H.; Zhong, M. Effects of Pressure on Structural, Mechanical, and Electronic Properties and Stability of Fe x Si y Compounds. *Phys. Status Solidi B* **2020**, *257*. https://doi.org/10.1002/pssb.202000083.
44. Macías Hemer, P.A. *Estudio de Aleaciones de Fe1-xSx y Fe1-xSix a Condiciones del Núcleo Interno Terrestre. Tesis o trabajo de Investigación Presentada(o) como Requisito Parcial para optar al título de*; Universidad del Norte: Barranquilla, Colombia, 2020.
45. Nikolaychuk, P.A.; Tyurin, A.G. The estimation of Fe-Si system oxidation at 298 K in air and water environments. In *Proceedings of the 11th International Conference on Fundamental and Applied Aspects of Physical Chemistry*; Anić, S., Draganić, I.G., Eds.; Society of Physical Chemists of Serbia: Belgrade, Serbia, 2012; pp. 37–39, ISBN 9788682475279.
46. Atkinson, A. A theoretical analysis of the oxidation of Fe Si alloys. *Corros. Sci.* **1982**, *22*, 87–102. https://doi.org/10.1016/0010-938x(82)90071-3.
47. Moss, R.J.; Seymour, H.J. A Supposed New Mineral. *Nature* **1909**, *81*, 518. https://doi.org/10.1038/081518a0.
48. Sutton, J.R. A new mineral? *Nature* **1911**, *87*, 314.
49. Spencer, L.J. Fictitious occurrences of iron silicide (ferrosilicon). *Miner. Mag. J. Miner. Soc.* **1935**, *24*, 160–164. https://doi.org/10.1180/minmag.1935.24.150.03.
50. Conder, H. Geological pitfalls. *Ind. Aust. Min. Stand.* **1926**, *76*, 6.
51. Minyuk, P.S.; Savva, N.E.; Subbotnikova, T.V. Magnetic Property of Exotic Iron Silicides. In *Proceedings of the International Conference on Paleomagnetism and Rock Magnetism*, Kazan, Russia, 2–7 October 2017; Fattakhova, L.A., Kuzina, D.M., Eds.; KFU Publishing House: Kazan, Russia, 2017; p. 64.
52. Stępniewski. Marian; Borucki, J. Pseudometeorite from Łapino (Pomerania, North Poland) Marian. *Geol. Q.* **2001**, *45*, 343–345.
53. Kieu, N.; Gordillo-Vázquez, F.J.; Passas, M.; Sánchez, J.; Pérez-Invernón, F.J.; Luque, A.; Montanyá, J.; Christian, H. Submicrosecond Spectroscopy of Lightning-Like Discharges: Exploring New Time Regimes. *Geophys. Res. Lett.* **2020**, *47*. https://doi.org/10.1029/2020gl088755.

54. Walker, T.D.; Christian, H.J. Triggered Lightning Spectroscopy: 2. A Quantitative Analysis. *J. Geophys. Res. Atmos.* **2019**, *124*, 3930–3942. https://doi.org/10.1029/2018jd029901.
55. Kenny, G.G.; Pasek, M.A. The response of zircon to the extreme pressures and temperatures of a lightning strike. *Sci. Rep.* **2021**, *11*, 1560. https://doi.org/10.1038/s41598-021-81043-8.
56. Chen, J.; Elmi, C.; Goldsby, D.; Gieré, R. Generation of shock lamellae and melting in rocks by lightning-induced shock waves and electrical heating. *Geophys. Res. Lett.* **2017**, *44*, 8757–8768. https://doi.org/10.1002/2017gl073843.
57. Collins, S.; Melosh, H.J.; Pasek, M.A. Can Lightning Strikes Produce Shocked Quarz? In *Proceedings of the 43rd Lunar and Planetary Science Conference*, The Woodlands, TX, USA, 19–23 March 2012.
58. Carter, E.A.; Hargreaves, M.D.; Kee, T.P.; Pasek, M.; Edwards, H.G.M. A Raman spectroscopic study of a fulgurite. *Philos. Trans. R. Soc. A Math. Phys. Eng. Sci.* **2010**, *368*, 3087–3097. https://doi.org/10.1098/rsta.2010.0022.
59. Walker, T.D.; Christian, H.J. Triggered lightning spectroscopy: Part 1. A qualitative analysis. *J. Geophys. Res. Atmos.* **2017**, *122*, 8000–8011. https://doi.org/10.1002/2016jd026419.
60. Gilbert, L. Noch einiges von den Blitzröhren. *Ann. Phys.* **1819**, *61*, 249–262.
61. Merrill, G.P. *On Fulgurites*; United States National Museum: New York, NY, USA, 1886; pp. 83–91.
62. García-Guinea, J.; Furió, M.; Fernandez-Hernan, M.; Bustillo, M.; Crespo-Feo, E.; Correcher, V.; Sánchez-Muñoz, L.; Matesanz, E. *The Quartzofeldspathic Fulgurite of Bustarviejo (Madrid): Glassy Matrix and Silicon Phases*; Universidad Complutense de Madrid: Madrid, Spain, 2009.
63. Withering, W. On Fulgurites. *Trans. Philos. Soc. Lond.* **1790**, *29*, 3.
64. Julien, A.A. A Study of the Structure of Fulgurites. *J. Geol.* **1901**, *9*, 673–693. https://doi.org/10.1086/620966.
65. Fiedler, K.G. Ueber die Blitzröhren und ihre Entstehung. *Ann. Phys.* **1817**, *55*, 121–164. https://doi.org/10.1002/andp.18170550202.
66. Ende, M.; Schorr, S.; Kloess, G.; Franz, A.; Tovar, M. Shocked quartz in Sahara fulgurite. *Eur. J. Miner.* **2012**, *24*, 499–507. https://doi.org/10.1127/0935-1221/2012/0024-2188.
67. Pye, K. Sem Observations on Some Sand Fulgurites from Northern Australia. *J. Sediment. Res.* **1982**, *52*. https://doi.org/10.1306/212f80a8-2b24-11d7-8648000102c1865d.
68. Feng, T.; Abbatiello, J.; Omran, A.; Mehta, C.; Pasek, M.A. Iron Silicides in Fulgurites. *Minerals* **2021**, *11*, 1394. https://doi.org/10.3390/min11121394.
69. Harland, W.B.; Hacker, J. 'Fossil' lightning strikes 250 million years ago. *Adv. Sci.* **1966**, *22*, 663–671.
70. Sponholz, B.; Baumhauer, R.; Felix-Hennignsen, P. Fulgurites in the southern central Sahara, Republic of Niger and their palaeoenvironmental significance. *Holcene* **1993**, *3*, 97–104. https://doi.org/10.1177/095968369300300201.
71. Navarro-González, R.; Mahan, S.A.; Singhvi, A.K.; Navarro-Aceves, R.; Rajot, J.-L.; McKay, C.P.; Coll, P.; Raulin, F. Paleoecology reconstruction from trapped gases in a fulgurite from the late Pleistocene of the Libyan Desert. *Geology* **2007**, *35*, 171. https://doi.org/10.1130/g23246a.1.
72. Thalheim, K. Die Bltzröhre im Staatlichen Museum für Mineralogie und Geologie zu Dresden. *Lapis* **1992**, *17*, 66–68.
73. Wimmenauer, W. Vorkommen und Strukturen von Fulguriten im Schwarzwald. *Aufschluss* **2006**, *57*, 325–328.
74. Rutley, F. On Fulgurite from Mont Blanc; with a Note on the Bouteillenstein, or Pseudo-chrysolite of Moldauthein, in Bohemia. *Q. J. Geol. Soc.* **1885**, *41*, 152–156. https://doi.org/10.1144/gsl.jgs.1885.041.01-04.21.
75. Rutley, F. On Fulgurites from Monte Viso. *Q. J. Geol. Soc.* **1889**, *45*, 60–66. https://doi.org/10.1144/gsl.jgs.1889.045.01-04.05.
76. Aston, E.; Bonney, T.G. On an Alpine Nickel-bearing Serpentine, with Fulgurites. *Q. J. Geol. Soc.* **1896**, *52*, 452–460. https://doi.org/10.1144/gsl.jgs.1896.052.01-04.24.
77. Wimmenauer, W.; Himstedt, F. *Dokumentation zum Thema: Fulgurite auf Felsen und Mauerwerk in Südwestdeutschland und Weiteren Fundgebieten: Geländebefunde und Lichtmikroskopische Untersuchungen: Further Findings of Fulgurites in the Black Forest and Other Regions*; Universität Freiburg: Freiburg, Germany, 2012.
78. Pasek, M.A.; Block, K.; Pasek, V. Fulgurite morphology: A classification scheme and clues to formation. *Contrib. Miner. Pet.* **2012**, *164*, 477–492. https://doi.org/10.1007/s00410-012-0753-5.
79. Pasek, M.A.; Pasek, V.D. The forensics of fulgurite formation. *Miner. Pet.* **2017**, *112*, 185–198. https://doi.org/10.1007/s00710-017-0527-x.
80. Block, K.M. Fulgurite Classification, Petrology, and Implications for Planetary Processes. Master's Thesis. The University of Arizona, Tucson, AZ, USA, 2011.
81. Roberts, S.; Sheffer, A.; McCanta, M.; Dyar, M.; Sklute, E. Oxidation state of iron in fulgurites and Trinitite: Implications for redox changes during abrupt high-temperature and pressure events. *Geochim. Cosmochim. Acta* **2019**, *266*, 332–350. https://doi.org/10.1016/j.gca.2019.08.021.
82. Ballhaus, C.; Wirth, R.; Fonseca, R.O.C.; Blanchard, H.; Pröll, W.; Bragagni, A.; Nagel, T.; Schreiber, A.; Dittrich, S.; Thome, V.; et al. Ultra-high pressure and ultra-reduced minerals in ophiolites may form by lightning strikes. *Geochem. Perspect. Lett.* **2017**, 42–46. https://doi.org/10.7185/geochemlet.1744.
83. Ballhaus, C.; Helmy, H.M.; Fonseca, R.O.; Wirth, R.; Schreiber, A.; Jöns, N. Ultra-reduced phases in ophiolites cannot come from Earth's mantle. *Am. Miner.* **2021**, *106*, 1053–1063. https://doi.org/10.2138/am-2021-7612.
84. Gieré, R.; Wimmenauer, W.; Müller-Sigmund, H.; Wirth, R.; Lumpkin, G.R.; Smith, K.L. Lightning-induced shock lamellae in quartz. *Am. Miner.* **2015**, *100*, 1645–1648. https://doi.org/10.2138/am-2015-5218.

85. Pasek, M.A.; Collins, G.S.; Carter, E.A.; Melosh, H.J.; Atlas, Z. Shocked Quartz in a Fulgurite. In *Proceedings of the 73rd Annual Meteoritical Society Meeting,* New York, NY, USA, 26–30 July 2010.
86. Maki, D. Lightning strikes and prehistoric ovens: Determining the source of magnetic anomalies using techniques of environmental magnetism. *Geoarchaeology* **2005**, *20*, 449–459. https://doi.org/10.1002/gea.20059.
87. Jones, G.; Maki, D.L. Lightning-induced magnetic anomalies on archaeological sites. *Archaeol. Prospect.* **2005**, *12*, 191–197. https://doi.org/10.1002/arp.257.
88. Burks, J.; Viberg, A.; Bevan, B. Lightning strikes in archaeological magnetometry data. A case study from the High Bank Works site, Ohio, USA. *Archaeol. Pol.* **2015**, *53*, 256–260.
89. Sheffer, A.A.; Melosh, H.; Jarnot, B.; Lauretta, D. *Reduction of Silicates at High Temperature: Fulgurites and Thermodynamic Modeling*; Northern Trust: Chicago, IL, USA, 2003.
90. Parnell, J.; Thackrey, S.; Muirhead, D.; Wright, A. Transient high-temperature processing of silicates in fulgurites as analogues for meteorite and impact melts. In *Proceedings of the 39th Lunar and Planetary Science Conference,* League City, TX, USA, 10–14 March 2008; Abstract # 1286
91. Stefano, C.J.; Hackney, S.A.; Kampf, A.R. The occurrence of iron silicides in a fulgurite: Implications for fulgurite genesis. *Can. Miner.* **2020**, *58*, 115–123. https://doi.org/10.3749/canmin.1900019.
92. Ramírez Cardona, M.; Castro, K.F.; Cortès Garcia, P.P. Mineralogical study of binary iron silicides (Fe-Si systeM) in a fulgurite from Hidalgo, Mexico. *Boletín Mineral.* **2006**, *17*, 69–76.
93. Sheffer, A.A. Chemical Reduction of Silicates by Meteorite Impacts and Lightning Strikes. Ph.D. Dissertation, The University of Arizona, Tucson, AZ, USA, 2007.
94. Garcia-Guinea, J.; Furio, M.; Fernandez-Hernan, M.; Bustillo, M.A.; Crespo-Feo, E.; Correcher, V.; Sanchez-Muñoz, L.; Matesanz, E.; Gucsik, A. The Quartzofeldspathic Fulgurite of Bustaviejo (Madrid): Cathodoluminescence and Raman Emission. In *AIP Conference Proceedings. Micro-Raman Spectroscopy and Luminiscence Studies in the Earth and Planetary Sciences Micro-raman Spectroscopy and Luminescence Studies in the Earth and Planetary Sciences: Proceedings of the International Conference Spectroscopy 2009, Mainz, Germany, 2–4 April 2009*; AIP: University Park, ML, USA, 2009; pp. 128–134.
95. Ballhaus, C.; Fonseca, R.; Bragagni, A. Reply to Comment on "Ultra-high pressure and ultra-reduced minerals in ophiolites may form by lightning strikes" by Griffin et al., 2018: No evidence for transition zone metamorphism in the Luobusa ophiolite. *Geochem. Perspect. Lett.* **2018**, 3–4. https://doi.org/10.7185/geochemlet.1810.
96. Essene, E.J.; Fisher, D.C. Lightning Strike Fusion: Extreme Reduction and Metal-Silicate Liquid Immiscibility. *Science* **1986**, *234*, 189–193. https://doi.org/10.1126/science.234.4773.189.
97. Miyahara, M.; Tomioka, N.; Bindi, L. Natural and experimental high-pressure, shock-produced terrestrial and extraterrestrial materials. *Prog. Earth Planet. Sci.* **2021**, *8*, 1–26. https://doi.org/10.1186/s40645-021-00451-6.
98. MacDonald, F.A.; Mitchel, K.; Cina, S.E. Evidence for a Lightning-Strike Origin if the Edeowie Glass. In *Proceedings of the Lunar and Planetary Science XXXV,* Houston, TX; USA, 15–19 March 2004.
99. Sheffer, A.A.; Dyar, M.D.; Sklute, E.C. Lightning Strike Glas as an Analog for Impact Glasses: 57Fe Mössbauer Spectroscopy of Fulgurites. In *Proceedings of the Lunar and Planetary Science XXXVII,* Houston, TX; USA, 13–17 March 2006.
100. French, B.M. *Traces of Catastrophe: A Handbook of Shock-Metamorphic Effects in Terrestrial Meteorite Impact Structures*; Lunar and Planetary Institute: Houston, TX, USA, 1998.
101. Eby, G.N.; Charnley, N.; Pirrie, D.; Hermes, R.; Smoliga, J.; Rollinson, G. Trinitite redux: Mineralogy and petrology. *Am. Miner.* **2015**, *100*, 427–441. https://doi.org/10.2138/am-2015-4921.
102. Foley, S.F. A Reappraisal of Redox Melting in the Earth's Mantle as a Function of Tectonic Setting and Time. *J. Pet.* **2010**, *52*, 1363–1391. https://doi.org/10.1093/petrology/egq061.
103. Trønnes, R.; Baron, M.; Eigenmann, K.; Guren, M.; Heyn, B.; Løken, A.; Mohn, C. Core formation, mantle differentiation and core-mantle interaction within Earth and the terrestrial planets. *Tectonophysics* **2018**, *760*, 165–198. https://doi.org/10.1016/j.tecto.2018.10.021.
104. Lin, Y.; van Westrenen, W. Oxygen as a catalyst in the Earth's interior? *Natl. Sci. Rev.* **2021**, *8*, nwab009. https://doi.org/10.1093/nsr/nwab009.
105. Mao, H.-K.; Hu, Q.; Yang, L.; Liu, J.; Kim, D.Y.; Meng, Y.; Zhang, L.; Prakapenka, V.B.; Yang, W.; Mao, W.L. When water meets iron at Earth's core–mantle boundary. *Natl. Sci. Rev.* **2017**, *4*, 870–878. https://doi.org/10.1093/nsr/nwx109.
106. Rohrbach, A.; Ballhaus, C.; Golla–Schindler, U.; Ulmer, P.; Kamenetsky, V.S.; Kuzmin, D.V. Metal saturation in the upper mantle. *Nature* **2007**, *449*, 456–458. https://doi.org/10.1038/nature06183.
107. Ballhaus, C.; Berry, R.; Green, D.H. Oxygen fugacity controls in the Earth's upper mantle. *Nature* **1990**, *348*, 437–440. https://doi.org/10.1038/348437a0.
108. Armstrong, K. *Redox Evolution of the Early Earth's Mantle*; University of Bayreuth: Bayreuth, Germany, 2018.
109. Williams, H.M.; McCammon, C.A.; Peslier, A.H.; Halliday, A.N.; Teutsch, N.; Levasseur, S.; Burg, J.-P. Iron Isotope Fractionation and the Oxygen Fugacity of the Mantle. *Science* **2004**, *304*, 1656–1659. https://doi.org/10.1126/science.1095679.
110. Lukin, A.; Shestopalov, V. Ferrosilicide as indicator of mineral composition of the Earth mantle? *Geofiz. Zhurnal* **2020**, *42*, 3–15. https://doi.org/10.24028/gzh.0203-3100.v42i5.2020.215069.
111. Mergner, V.; Kupenko, I.; Spiekermann, G.; Petitgirard, S.; Libon, L.; Chariton, S.; Krug, M.; Steinbrügge, R.; Sergueev, I.; Sanchez-Valle, C. Sound Velocities in FeSi at Lower Mantle Conditions and the Origin of Ultralow-Velocity Zones. *Geophys. Res. Lett.* **2021**, *48*. https://doi.org/10.1029/2020gl092257.

112. Dobrzhinetskaya, L.; Mukhin, P.; Wang, Q.; Wirth, R.; O'Bannon, E.; Zhao, W.; Eppelbaum, L.; Sokhonchuk, T. Moissanite (SiC) with metal-silicide and silicon inclusions from tuff of Israel: Raman spectroscopy and electron microscope studies. *Lithos* **2018**, *310-311*, 355–368. https://doi.org/10.1016/j.lithos.2017.04.001.
113. Doglioni, C.; Tonarini, S.; Innocenti, F. Mantle wedge asymmetries and geochemical signatures along W- and E–NE-directed subduction zones. *Lithos* **2009**, *113*, 179–189. https://doi.org/10.1016/j.lithos.2009.01.012.
114. Xiong, Q.; Griffin, W.L.; Huang, J.; Gain, S.; Toledo, V.; Pearson, N.J.; O'Reilly, S.Y. Super-reduced mineral assemblages in "ophiolitic" chromitites and peridotites: The view from Mount Carmel. *Eur. J. Miner.* **2017**, *29*, 557–570. https://doi.org/10.1127/ejm/2017/0029-2646.
115. Griffin, W.L.; Gain, S.E.M.; Saunders, M.J.; Huang, J.-X.; Alard, O.; Toledo, V.; O'Reilly, S.Y. Immiscible metallic melts in the upper mantle beneath Mount Carmel, Israel: Silicides, phosphides and carbides. *Am. Miner.* **2021**. https://doi.org/10.2138/am-2021-7934.
116. Griffin, W.; Gain, S.; Adams, D.; Huang, J.-X.; Saunders, M.; Toledo, V.; Pearson, N.; O'Reilly, S. First terrestrial occurrence of tistarite (Ti_2O_3): Ultra-low oxygen fugacity in the upper mantle beneath Mount Carmel, Israel. *Geology* **2016**, *44*, 815–818. https://doi.org/10.1130/g37910.1.
117. Mathez , E.; Fogel, R.; Hutcheon, I.; Marshintsev, V. Carbon isotopic composition and origin of SiC from kimberlites of Yakutia, Russia. *Geochim. Cosmochim. Acta* **1995**, *59*, 781–791. https://doi.org/10.1016/0016-7037(95)00002-h.
118. Nazzareni, S.; Nestola, F.; Zanon, V.; Bindi, L.; Scricciolo, E.; Petrelli, M.; Zanatta, M.; Mariotto, G.; Giuli, G. Discovery of moissanite in a peralkaline syenite from the Azores Islands. *Lithos* **2018**, *324–325*, 68–73. https://doi.org/10.1016/j.lithos.2018.10.036.
119. Di Pierro, S.; Grobety, B.H.; Bernasconi, S.M.; Gnos, E.; Armbruster, T.; Ulmer, P. Rock-forming moissanite (natural α-silicon carbide). *Am. Miner.* **2003**, *88*, 1817–1821. https://doi.org/10.2138/am-2003-11-1223.
120. Shiryaev, A.; Griffin, W.L.; Stoyanov, E. Moissanite (SiC) from kimberlites: Polytypes, trace elements, inclusions and speculations on origin. *Lithos* **2011**, *122*, 152–164. https://doi.org/10.1016/j.lithos.2010.12.011.
121. Gnoevaja, N.; Grozdanov, L. Moissanite from Triassic rocks, NW Bulgaria. *Proc. Bulg. Geol. Soc.* **1965**, *26*, 89–95.
122. Pankov, V.Y.; Spetsius, Z.V. Inclusions of iron silicides and native silicon in moissanite from the Sytykan kimberlite pipe. *Doklady Akademii Nauk SSSR* **1989,** *305*, 704–708.
123. Marshintsev, V.K. Nature of silicon carbide in kimberlite rocks of Yakutia. *Mineral. Zhurnal* **1990**, *12*, 17–26. (In Russian).
124. Jambor, J.L.; Grew, E.S. New mineral names. *Am. Mineral.* **1992**, *77*, 207–2013.
125. Ashchepkov, I.; Logvinova, A.; Reimers, L.; Ntaflos, T.; Spetsius, Z.; Vladykin, N.; Downes, H.; Yudin, D.; Travin, A.; Makovchuk, I.; et al. The Sytykanskaya kimberlite pipe: Evidence from deep-seated xenoliths and xenocrysts for the evolution of the mantle beneath Alakit, Yakutia, Russia. *Geosci. Front.* **2015**, *6*, 687–714. https://doi.org/10.1016/j.gsf.2014.08.005.
126. Ishimaru, S.; Arai, S.; Shukuno, H. Metal-saturated peridotite in the mantle wedge inferred from metal-bearing peridotite xenoliths from Avacha volcano, Kamchatka. *Earth Planet. Sci. Lett.* **2009**, *284*, 352–360. https://doi.org/10.1016/j.epsl.2009.04.042.
127. Griffin, W.L.; Gain, S.; Huang, J.; Saunders, M.; Shaw, J.; Toledo, V.; O'Reilly, S.Y. A terrestrial magmatic hibonite-grossite-vanadium assemblage: Desilication and extreme reduction in a volcanic plumbing system, Mount Carmel, Israel. *Am. Miner.* **2019**, *104*, 207–219. https://doi.org/10.2138/am-2019-6733.
128. Griffin, W.L.; Gain, S.E.; Saunders, M.; Bindi, L.; Alard, O.; Toledo, V.; O'Reilly, S.Y. Parageneses of TiB2 in corundum xenoliths from Mt. Carmel, Israel: Siderophile behavior of boron under reducing conditions. *Am. Miner.* **2020**, *105*, 1609–1621. https://doi.org/10.2138/am-2020-7375.
129. Litasov, K.D.; Kagi, H.; Bekker, T.B. Enigmatic super-reduced phases in corundum from natural rocks: Possible contamination from artificial abrasive materials or metallurgical slags. *Lithos* **2019**, *340–341*, 181–190. https://doi.org/10.1016/j.lithos.2019.05.013.
130. Litasov, K.; Bekker, T.; Kagi, H. Reply to the discussion of "Enigmatic super-reduced phases in corundum from natural rocks: Possible contamination from artificial abrasive materials or metallurgical slags" by Litasov et al. (Lithos, 340–341, pp. 181–190) by W.L. Griffin, V. Toledo and S.Y. O'Reilly. *Lithos* **2019**, *348–349*, 105170. https://doi.org/10.1016/j.lithos.2019.105170.
131. Griffin, W.L.; Toledo, V.; O'Reilly, S.Y. Discussion of "Enigmatic super-reduced phases in corundum from natural rocks: Possible contamination from artificial abrasive materials or metallurgical slags" by Litasov et al. (Lithos, 340–341, pp. 181–190). *Lithos* **2019**, *348–349*, 105122. https://doi.org/10.1016/j.lithos.2019.06.024.
132. Xiong, F.; Xu, X.; Mugnaioli, E.; Gemmi, M.; Wirth, R.; Grew, E.S.; Robinson, P.T.; Yang, J. Two new minerals, badengzhuite, TiP, and zhiqinite, TiSi2, from the Cr-11 chromitite orebody, Luobusa ophiolite, Tibet, China: Is this evidence for super-reduced mantle-derived fluids? *Eur. J. Miner.* **2020**, *32*, 557–574. https://doi.org/10.5194/ejm-32-557-2020.
133. Griffin, W.L.; Gain, S.E.M.; Bindi, L.; Toledo, V.; Cámara, F.; Saunders, M.; O'Reilly, S.Y. Carmeltazite, ZrAl2Ti4O11, a New Mineral Trapped in Corundum from Volcanic Rocks of Mt Carmel, Northern Israel. *Minerals* **2018**, *8*, 601. https://doi.org/10.3390/min8120601.
134. Generalov, M.E.; Naumov, V.; Mokhov, A.V.; Trubkin, N.V. Isovite (Cr,Fe)23C6—A new mineral from the gold-platinum—Bearing placiers of the Urals. *Zap. Vserossiskogo Mineral. Obs.* **1998**, *127*, 26–37. (In Russian)
135. Yang, J.; Wu, W.; Lian, D.; Rui, H. Peridotites, chromitites and diamonds in ophiolites. *Nat. Rev. Earth Environ.* **2021**, *2*, 198–212. https://doi.org/10.1038/s43017-020-00138-4.

136. Zhou, M.-F.; Robinson, P.T.; Malpas, J.; Li, Z. Podiform Chromitites in the Luobusa Ophiolite (Southern Tibet): Implications for Melt-Rock Interaction and Chromite Segregation in the Upper Mantle. *J. Pet.* **1996**, *37*, 3–21. https://doi.org/10.1093/petrology/37.1.3.
137. Trumbull, R.B.; Yang, J.-S.; Robinson, P.T.; Di Pierro, S.; Vennemann, T.; Wiedenbeck, M. The carbon isotope composition of natural SiC (moissanite) from the Earth's mantle: New discoveries from ophiolites. *Lithos* **2009**, *113*, 612–620. https://doi.org/10.1016/j.lithos.2009.06.033.
138. Shi, N.; Bai, W.; Li, G.; Siong, M.; Yang, J.; Ma, Z.; Rong, H. Naquite, FeSi, a New Mineral Species from Luobusha, Tibet, Western China. *Actsa Geol. Sin.* **2012**, *86*, 533–538.
139. Li, G.; Shi, N.; Xiong, M.; Ma, Z.; Bai, W.; Fang, Q. X-ray diffraction investigation of native Si-Fe alloy minerals from Luobusha, Tibet. *Front. Earth Sci. China* **2007**, *1*, 21–25. https://doi.org/10.1007/s11707-007-0003-8.
140. Li, G.; Bai, W.; Shi, N.; Fang, Q.; Xiong, M.; Yang, J.; Ma, Z.; Rong, H. Linzhiite, FeSi2, a redefined and revalidated new mineral species from Luobusha, Tibet, China. *Eur. J. Miner.* **2012**, *24*, 1047–1052. https://doi.org/10.1127/0935-1221/2012/0024-2237.
141. Tishchenko, A.I.; Kasatkin, A.V.; Shkoda, R. *Silicides (naquite, linzhiite, luobusaite and zangboite) in Sarmatian limestones of Crimea*. Noviye Danniye o Mineralakh (New Data on Minerals), **2016**, *51*, 30–37 (In Russia).
142. Bai, W.; Robinson, P.T.; Fang, Q.; Yang, J.; Yan, B.; Zhang, Z.; Hu, X.-F.; Zhou, M.-F.; Malpas, J. The pge and base-metal alloys in the podiform chromitites of the luobusa ophiolite, Southern Tibet. *Can. Miner.* **2000**, *38*, 585–598. https://doi.org/10.2113/gscanmin.38.3.585.
143. Bai, W.J.; Yang, J.S.; Tao, Shi, L.C; .Fng, Q.S.; Ma, Z.S.; Yan, B.G.; Xiong, M.; Dai, M.Q. Si-Fe alloy assemblage in ophiolite of Tibet and their genesis. *Acta Petrol. Mineral.* **2003**, *22*, 279–284. (In Chinese with English abstract).
144. Bai, W.; Shi, N.; Fang, Q.; Li, G.; Xiong, M.; Yang, J.; Rong, H. Luobusaite: A new mineral. *Acta Geol. Sin. (Engl. Ed.)* **2006**, *80*, 656–659.
145. Li Guowu; Fang Qingsong; Shi Nicheng; Bai Wenji; Yang Jingsui; Xiong Ming; Ma Zhesheng; Rong He. Zangboite, TiFeSi2, a new mineral species from Luobusha, Tibet, China, and its crystal structure. *Can. Mineral.* **2009**, *47*, 1265–1274.
146. Miyawaki, R.; Hatert, F.; Pasero, M.; Mills, S.J. New minerals and nomenclature modifications approved in 2019. *Mineral. Mag.* **2019**, *83*, 887–893. https://doi.org/10.1180/mgm.2019.73.
147. Xu, X.; Yang, J.; Robinson, P.T.; Xiong, F.; Ba, D.; Guo, G. Origin of ultrahigh pressure and highly reduced minerals in podiform chromitites and associated mantle peridotites of the Luobusa ophiolite, Tibet. *Gondwana Res.* **2015**, *27*, 686–700. https://doi.org/10.1016/j.gr.2014.05.010.
148. Dobrzhinetskaya, L.F.; Wirth, R.; Yang, J.; Hutcheon, I.D.; Weber, P.K.; Green, H.W. High-pressure highly reduced nitrides and oxides from chromitite of a Tibetan ophiolite. *Proc. Natl. Acad. Sci. USA* **2009**, *106*, 19233–19238. https://doi.org/10.1073/pnas.0905514106.
149. Yang, J.-S.; Robinson, P.T.; Dilek, Y. Diamonds in Ophiolites. *Elements* **2014**, *10*, 127–130. https://doi.org/10.2113/gselements.10.2.127.
150. Griffin, W.L.; Howell, D.; Gonzalez-Jimenez, J.M.; Xiong, Q.; O'Reilly, S.Y. Comment on "Ultra-high pressure and ultra-reduced minerals in ophiolites may form by lightning strikes" by Ballhaus et al., 2017: Ultra-high pressure and super-reduced minerals in ophiolites do not form by lightning strikes. *Geochem. Perspect. Lett.* **2018**, *8*, 6–7.
151. Hu Xiangjian. Native fersilicite of China. *Acta Petrol. Mineral.* **1995**, *14*, 71–77. (In Chinese)
152. He, D.; Gao, C.; Chen, C.; Liu, Y.; Hu, Z. SiC-dominated ultra-reduced mineral assemblage in carbonatitic xenoliths from the Dalihu basalt, Inner Mongolia, China. *Am. Miner.* **2017**, *102*, 312–320. https://doi.org/10.2138/am-2017-5721.
153. Liu, Y.; He, D.; Gao, C.; Foley, S.; Gao, S.; Hu, Z.; Zong, K.; Chen, H. First direct evidence of sedimentary carbonate recycling in subduction-related xenoliths. *Sci. Rep.* **2015**, *5*, 11547. https://doi.org/10.1038/srep11547.
154. Yang, J.; Meng, F.; Xu, X.; Robinson, P.T.; Dilek, Y.; Makeyev, A.B.; Wirth, R.; Wiedenbeck, M.; Cliff, J. Diamonds, native elements and metal alloys from chromitites of the Ray-Iz ophiolite of the Polar Urals. *Gondwana Res.* **2014**, *27*, 459–485. https://doi.org/10.1016/j.gr.2014.07.004.
155. Nikulova, N.Y.; Kozyreva, Irina, Vladimirovna. Moissanite, Native Si and Iron Silicide from the Lower Paleozoic sandstones of the Polar Urals. *Vestn. Inst. Geol. Komi* **2015**, *193*, 17–18.
156. Batovrin, S.; Lipovsky, B.; Gulbin, Y.; Pushkarev, Y.; Shukolyukov, Y.A.; Brownlee, D. Constraints on the origins of iron silicide spherules in ultrahigh-temperature distal impact ejecta. *Meteorit. Planet. Sci.* **2021**, *56*, 1369–1405. https://doi.org/10.1111/maps.13662.
157. Lei Zhao. Ti-rich Minerals and a New Variety—Chromian Kennedyite from Kimberlites in Eastern China. *Geol. Sci. Technol. Inf.* **1991**, *10*, 71–76.
158. Hu Xiongjian. Natural silica-iron ore in China. Journal of Rock Mineralogy. *J. Rock Mineral.* **1995**, *14*, 71–78.
159. Jinsheng Wei; Zili Zheng; Sisong Chen. A study on ferdisilicite and its geological implications. *Acta Mineral. Sin.* **1985**, *2*, 184–186.
160. Zhang, R.; Wang, Z.; Wang, Y. The discovery of ferdisilicite in Anhui, China. *J. Chengdu Coll. Geol*. **1985,** *4*, 48–52.
161. Qirong Liu; Qixin Tan; Yuchi Jiang; Chunrui Han; Yan Sun; Chengwen Zhu. First discovery of ferdisilicite-silicon interlocking mineral gneiss of Jiaodong group of China. *Mar. Geol. Quart. Geol.* **1995**, *4*, 107–112. (In Chinese with English abstract).
162. Hu, X. A preliminary study on ferrosilicium from the Proterozoic, southwestern Zhejiang Province. *Acta Mineral. Sin.* **1991**, *11*, 285–289. (In Chinese with English abstract).

163. Marchi, S.; Drabon, N.; Schulz, T.; Schaefer, L.; Nesvorny, D.; Bottke, W.F.; Koeberl, C.; Lyons, T. Delayed and variable late Archaean atmospheric oxidation due to high collision rates on Earth. *Nat. Geosci.* **2021**, *14*, 827–831. https://doi.org/10.1038/s41561-021-00835-9.
164. Bottke, W.F.; Vokrouhlický, D.; A Minton, D.; Nesvorný, D.; Morbidelli, A.; Brasser, R.; Simonson, B.; Levison, H.F. An Archaean heavy bombardment from a destabilized extension of the asteroid belt. *Nature* **2012**, *485*, 78–81. https://doi.org/10.1038/nature10967.
165. Lehmer, O.R.; Catling, D.C.; Buick, R.; Brownlee, D.E.; Newport, S. Atmospheric CO_2 levels from 2.7 billion years ago inferred from micrometeorite oxidation. *Sci. Adv.* **2020**, *6*, eaay4644. https://doi.org/10.1126/sciadv.aay4644.
166. Yakymchuk, C.; Kirkland, C.L.; Cavosie, A.J.; Szilas, K.; Hollis, J.; Gardiner, N.J.; Waterton, P.; Steenfelt, A.; Martin, L. Stirred not shaken; critical evaluation of a proposed Archean meteorite impact in West Greenland. *Earth Planet. Sci. Lett.* **2021**, *557*, 116730. https://doi.org/10.1016/j.epsl.2020.116730.
167. Novgorodova, M.I.; Yusupov, R.G.; Dmitrieva, M.T.; Tsepin, A.I.; Sivtsov, A.V.; Gorshkov, A.I. Khamrabaevite, (Ti,V,Fe)C, a new mineral. *Zap. Vserossiyskogo Mineral. Obs.* **1984**, *133*, 697–703.
168. Novgorodova, M.I.; Yusupov, R.G.; Dmitrieva, M.T.; Tsepin, A.I.; Sivtsov, A.V.; Gorshkov, A.I.; Korovushkin, V.V.; Yakubovskaya, N.Y. First Occurrence of Suessite on the Earth. *Int. Geol. Rev.* **1984**, *26*, 98–101. https://doi.org/10.1080/00206818409452999.
169. Yusupov, R.G.; Dzhenchuraev, D.D.; and Radzhabov, F.F. Accessory native chromium and a natural compound of the series Fe-Cr-Si in rocks of the Gavasai ore field. *Izvest. Akad. Nauk Kirgiz SSR* **1982**, *5*, 25–26. (In Russian)
170. Dunn, P.L.; Grice, J.D.; Fleischer, M.; Pabst, A. New Mineral Names. *Am. Mineral.* **1984**, *69*, 210–215.
171. Novoseleva, L.N. Iron silicides in Lower Cambrian limestones on the Bazaikha River (tributary of the Yenisei), Krasnoyarsk region. *Zap. Vsesoyuznogo Mineral.-Kogo Obs.* **1975**, *104*, 228–234.
172. Novoselova, L.N.; Bagdasarov, E.A. New data on iron silicides. *Int. Geol. Rev.* **1980**, *22*, 691–696. https://doi.org/10.1080/00206818209466929.
173. Novoselova, L.N.; Lyul', A.Y. Geochemical characteristics of iron silicides from lower cambrian reefal limestones, krasnoyarsk. *Int. Geol. Rev.* **1986**, *28*, 114–118. https://doi.org/10.1080/00206818609466257.
174. Novoselova, L.N.; Bagdasarov, E.A. Novye dannye o silitsidakh zheleza: New data on iron silicides. *Zap. Vsesoyuznogo Mineral. Obs.* **1979**, *108*, 326–333.
175. Novoselova, L.N.; Sokhor, M.I. Moissanite and iron silicides from Lower Cambrian carbonate rocks in the Altai-Sayan region. *Zap. Vses. Min. Obshch.* **1983**, *5*, 582–588.
176. Eremenko, G.K.; Polkanov, Y.A.; Gevork'yan, V.K. Cosmogenic minerals in the Poltava deposits of the Konka–Yalynsk depression in northern Azov Region. *Mineral. Osadochnih Obraz.* **1974**, *1*, 66–75. (In Russian)
177. Tishchenko, A.I.; Kasatkin, A.V.; Shkoda, R. Silicides (naguite, linjia, lobusaite, and cangpoite in Crimean Sarmatian limestone. *Novye Dannye O Miner.* **2016**, *51*, 30–37.
178. Muszer, A. Silicide spherules from Permian sediments of the Fore-Sudetic Monocline (SW Poland). *Physicochem. Probl. Miner. Process.* **2014**, *50*, 107–118. https://doi.org/10.5277/ppmp140110.
179. Khabibullaeva, G.; Dunin-Barkovskaya, E. Rare Accessory Mineral Seussite—Fe3Si From Tien Shan and Conditions of its Formation. *Int. J. Geol. Earth Environ. Sci.* **2017**, *7*, 42–44.
180. Makarova, N.N. O nakhodke redkogo minerala ferdisilitsita v Karpatakh.: The finding of the mineral ferdisilicite in the Carpathians. *Zap. Vsesoyuznogo Mineral. Obs.* **1977**, *2*, 236–237.
181. Jakabská, K. Sférolity z ryolitu z oblasti Banská Štiavnica. *Acta Montan. Slovaca* **1998**, *3*, 71–74.
182. Demko, R.; Kubiš, M.; Bazarnik, J. Petrológia a geochémia acidného aplitu z hodrušsko-štiavnického intruzívneho komplexu z okolia Rumplovskej: Petrology and geochemistry of acid aplites from the Hodruša-Štiavnica intrusive complex in the Rumplovská area. *Miner. Slovaca* **2011**, *43*, 215–226.
183. Elekes, Z. Ion Beam Based Nuclear Microanalysis of Geological and Archaeological Objects. Ph.D. Thesis, University of Debrecen, Debrecen, Hungary, 2001.
184. Jakabská, K.; Rozložník, L. Spherical accessories "spherules" in Gemeric Granites (West Carpathians—Czechoslovakia). *Geol. Zborník—Geol. Carpathica* **1989**, *40*, 305–322.
185. Tchaikovsky, I.; Korotchenkova, O.V. Explosive mineral phases diamondiferous visherites of the Western Urals. *Lithosphäre* 2012, 125–140.
186. Glavatskikh, S.F. Metal formation in the exhalation products of the Great Fissure Tolbachik Eruption, Kamchatka. *Vulkanol. Seismol.* **1995**, *4–5*, 193–214.
187. Karpov, G.A.; Silaev, V.I.; Anikin, L.P.; Rakin, V.I.; Vasilev, E.; Filatov, S.K.; Petrovskii, V.A.; Flerov, G.B. Diamonds and accessory minerals in products of the 2012–2013 Tolbachik Fissure Eruption. *J. Volcanol. Seism.* **2014**, *8*, 323–339. https://doi.org/10.1134/s0742046314060049.
188. Litasov, K.D.; Kagi, H.; Bekker, T.B.; Makino, Y.; Hirata, T.; Brazhkin, V.V. Why Tolbachik Diamonds Cannot be Natural. *Am. Miner.* **2021**, *106*, 44–53. https://doi.org/10.2138/am-2020-7562.
189. Howell, D.; Griffin, W.L.; Yang, J.; Gain, S.; Stern, R.; Huang, J.; Jacob, D.; Xu, X.; Stokes, A.; O'Reilly, S.Y.; et al. Diamonds in ophiolites: Contamination or a new diamond growth environment? *Earth Planet. Sci. Lett.* **2015**, *430*, 284–295. https://doi.org/10.1016/j.epsl.2015.08.023.

190. Levitskiy, V. I.; Solodilova, V. V.; Zavadich, N. S.; Pavlova, L. A.; Spetsius, Z.V.; I. V. Levitskiy. Genetic Nature of Mineralization with Native and Intermetallic Compounds in the Bobruisk Ring Structure (Republic of Belarus). Dokl. Akad. Nauk. *SSSR* 2018, *481*,857–861
191. Lukin, A.E.; Novgorodova, M.I. On finds of ferro-silicide of extraterrestrial origin. *Dokl. Akad. Nauk SSSR* **1994**, *334*, 73–76. (In Russian).
192. Lukin, A.E. On the origin of the Shungite. *Geol. Zhurn.* 2005, 28–47. (In Russian)
193. Safonov, Y.; Belov, A.N.; Galyamov, A.L.; Genkin, A.D.; Podlesski, K.V. *Native Metals, Carbides and Nitrides in Magmatic Breccias of the Voronezh Massif, Their Nature and Metallogenic Significance*; Informations bulletin RFBR; Russian Foundation for Basic Information: Moscow, Russia, 1995. (In Russian)
194. Nakamura-Messenger, K.; Keller, L.P.; Clemett, S.J.; Messenger, S.; Jones, J.H.; Palma, R.L.; Pepin, R.O.; Klöck, W.; Zolensky, M.; Tatsuoka, H. Brownleeite: A new manganese silicide mineral in an interplanetary dust particle. *Am. Miner.* **2010**, *95*, 221–228. https://doi.org/10.2138/am.2010.3263.
195. mindat.org. Brownleeite Mineral Data: Brownleeite. Available online: https://www.mindat.org/min-36014.html (accessed on 11 May 2021).
196. Tatarintsev, V.I.; Tsymbal, S.N.; Sandamirskaya, S.M.; Egorova, L.N.; Vashchenko, A.N; Khnyazkov, A.P. Iron-bearing manganese silicides from the Priazovye (USSR). *Mineral. Zhurnal.* **1990**, *12*, 35–43. (In Russian)
197. Mineralogy Database. Brownleeite Mineral Data. Available online: http://webmineral.com/data/Brownleeite.shtml (accessed on 11 May 2021).
198. Yusupov, R.G.; Stanley, C.J.; Welch, M.D.; Spratt, J.; Cressey, G.; Rumsey, M.S.; Seltmann, R.; Igamberdiev, E. Mavlyanovite, Mn5Si3: A new mineral species from a lamproite diatreme, Chatkal Ridge, Uzbekistan. *Miner. Mag.* **2009**, *73*, 43–50. https://doi.org/10.1180/minmag.2009.073.1.43.
199. mindat.org. UM1990-56-Si:FeMn. Available online: https://www.mindat.org/min-51742.html (accessed on 28 November 2021).
200. mindat.org. Perryite. Available online: https://www.mindat.org/min-3170.html (accessed on 28 November 2021).
201. Buchwald, V. *Handbook of Iron Meteorites*; Center for Meteorite Studies: Tempe, AZ, USA, 1975.
202. Cabri, L.J.; McDonald, A.M.; Stanley, C.J.; Rudashevsky, N.S.; Poirier, G.; Wilhelmij, H.R.; Zhe, W.; Rudashevsky, V.N. Palladosilicide, Pd2Si, a new mineral from the Kapalagulu Intrusion, Western Tanzania and the Bushveld Complex, South Africa. *Miner. Mag.* **2015**, *79*, 295–307. https://doi.org/10.1180/minmag.2015.079.2.08.
203. Fischer, R.A.; Campbell, A.J.; Caracas, R. Equations of state in the Fe-FeSi system at high pressures and temperatures. *J. Geophys. Res. Solid Earth* **2014**, *119*, 2810–2827.
204. Shahar, A.; Ziegler, K.; Young, E.; Ricolleau, A.; Schauble, E.A.; Fei, Y. Experimentally determined Si isotope fractionation between silicate and Fe metal and implications for Earth's core formation. *Earth Planet. Sci. Lett.* **2009**, *288*, 228–234. https://doi.org/10.1016/j.epsl.2009.09.025.
205. Fischer, R.A.; Campbell, A.J.; Caracas, R.; Reaman, D.M.; Dera, P.; Prakapenka, V.B. Equation of state and phase diagram of Fe–16Si alloy as a candidate component of Earth's core. *Earth Planet. Sci. Lett.* **2012**, *357-358*, 268–276. https://doi.org/10.1016/j.epsl.2012.09.022.
206. Morard, G.; Andrault, D.; Guignot, N.; Siebert, J.; Garbarino, G.; Antonangeli, D. Melting of Fe–Ni–Si and Fe–Ni–S alloys at megabar pressures: Implications for the core–mantle boundary temperature. *Phys. Chem. Miner.* **2011**, *38*, 767–776. https://doi.org/10.1007/s00269-011-0449-9.
207. Tagawa, S.; Ohta, K.; Hirose, K.; Kato, C.; Ohishi, Y. Compression of Fe-Si-H alloys to core pressures. *Geophys. Res. Lett.* **2016**, *43*, 3686–3692. https://doi.org/10.1002/2016gl068848.
208. Komabayashi, T.; Pesce, G.; Sinmyo, R.; Kawazoe, T.; Breton, H.; Shimoyama, Y.; Glazyrin, K.; Konôpková, Z.; Mezouar, M. Phase relations in the system Fe–Ni–Si to 200 GPa and 3900 K and implications for Earth's core. *Earth Planet. Sci. Lett.* **2019**, *512*, 83–88. https://doi.org/10.1016/j.epsl.2019.01.056.
209. Morard, G.; Katsura, T. Pressure–temperature cartography of Fe–S–Si immiscible system. *Geochim. Cosmochim. Acta* **2010**, *74*, 3659–3667. https://doi.org/10.1016/j.gca.2010.03.025.
210. Ozawa, H.; Hirose, K.; Yonemitsu, K.; Ohishi, Y. High-pressure melting experiments on Fe–Si alloys and implications for silicon as a light element in the core. *Earth Planet. Sci. Lett.* **2016**, *456*, 47–54. https://doi.org/10.1016/j.epsl.2016.08.042.
211. Brosh, E.; Makov, G.; Shneck, R.Z. Thermodynamic analysis of high-pressure phase equilibria in Fe–Si alloys, implications for the inner-core. *Phys. Earth Planet. Inter.* **2009**, *172*, 289–298. https://doi.org/10.1016/j.pepi.2008.10.012.
212. Lin, J.-F.; Scott, H.P.; Fischer, R.A.; Chang, Y.-Y.; Kantor, I.; Prakapenka, V.B. Phase relations of Fe-Si alloy in Earth's core. *Geophys. Res. Lett.* **2009**, *36*. https://doi.org/10.1029/2008gl036990.
213. Santamaria-Perez, D.; Errandonea, D.; Vegas, A.; Nuss, J.; Jansen, M.; Rodríguez-Hernández, P.; Munoz, A.; Boehler, R. Phase diagram studies on iron and nickel silicides: High-pressure experiments andab initiocalculations. *J. Phys. Conf. Ser.* **2008**, *121*, 022013. https://doi.org/10.1088/1742-6596/121/2/022013.
214. Ikuta, D.; Ohtani, E.; Hirao, N. Two-phase mixture of iron–nickel–silicon alloys in the Earth's inner core. *Commun. Earth Environ.* **2021**, *126*, 1–14. https://doi.org/10.1038/s43247-021-00298-1.
215. Brennan, M.C.; Fischer, R.A.; Couper, S.; Miyagi, L.; Antonangeli, D.; Morard, G. High-Pressure Deformation of Iron–Nickel–Silicon Alloys and Implications for Earth's Inner Core. *J. Geophys. Res. Solid Earth* **2021**, *126*, 1–21. https://doi.org/10.1029/2020jb021077.

216. Berrada, M.; Secco, R.A. Review of Electrical Resistivity Measurements and Calculations of Fe and Fe-Alloys Relating to Planetary Cores. *Front. Earth Sci.* **2021**, *9*. https://doi.org/10.3389/feart.2021.732289.
217. Errandonea, D.; Santamaría-Perez, D.; Vegas, A.; Nuss, J.; Jansen, M.; Rodríguez-Hernandez, P.; Muñoz, A. Structural stability of Fe5Si3 and Ni2Si studied by high-pressure x-ray diffraction andab initiototal-energy calculations. *Phys. Rev. B* **2008**, *77*, 094113. https://doi.org/10.1103/physrevb.77.094113.
218. Caracas, R.; Wentzcovitch, R. Equation of state and elasticity of FeSi. *Geophys. Res. Lett.* **2004**, *31*. https://doi.org/10.1029/2004gl020601.
219. Lord, O.T.; Walter, M.J.; Dobson, D.; Armstrong, L.; Clark, S.; Kleppe, A. The FeSi phase diagram to 150 GPa. *J. Geophys. Res. Earth Surf.* **2010**, *115*. https://doi.org/10.1029/2009jb006528.
220. Spiekermann, G.; Kupenko, I.; Petitgirard, S.; Harder, M.; Nyrow, A.; Weis, C.; Albers, C.; Biedermann, N.; Libon, L.; Sahle, C.J.; et al. A portable on-axis laser-heating system for near-90° X-ray spectroscopy: Application to ferropericlase and iron silicide. *J. Synchrotron Radiat.* **2020**, *27*, 414–424. https://doi.org/10.1107/s1600577519017041.
221. Edmund, E. The Elasticity of Iron-Alloys at Extreme Conditions. Ph.D. Thesis, Sorbonne Université, Paris, France, 2018.
222. Dobson, D.P.; Vočadlo, L.; Wood, I.G. A new high-pressure phase of FeSi. *Am. Miner.* **2002**, *87*, 784–787. https://doi.org/10.2138/am-2002-5-623.
223. Zhang, F.; Oganov, A.R. Iron silicides at pressures of the Earth's inner core. *Geophys. Res. Lett.* **2010**, *37*. https://doi.org/10.1029/2009gl041224.
224. McGuire, C.P.; Kavner, A.; Santamaria, D. High-pressure high-temperature behavior of iron silicide (Fe5Si3) to 58 GPa and 2400 K. In *Proceedings of the AGU Fall Meeting*, San Francisco, CA, USA, 14–18 December 2015.
225. Badro, J.; Côté, A.; Brodholt, J. A seismologically consistent compositional model of Earth's core. *Proc. Natl. Acad. Sci. USA* **2014**, *111*, 7542–7545. https://doi.org/10.1073/pnas.1316708111.
226. Tateno, S.; Kuwayama, Y.; Hirose, K.; Ohishi, Y. The structure of Fe–Si alloy in Earth's inner core. *Earth Planet. Sci. Lett.* **2015**, *418*, 11–19. https://doi.org/10.1016/j.epsl.2015.02.008.
227. Guyot, F.; Zhang, J.; Martinez, I.; Matas, J.; Ricard, Y.; Javoy, M. P-V-T measurements of iron suicide (ε-FeSi) Implications for silicate-metal interactions in the early Earth. *Eur. J. Miner.* **1997**, *9*, 277–286. https://doi.org/10.1127/ejm/9/2/0277.
228. Wann, E.T.H.; Vočadlo, L.; Wood, I.G. High-temperature ab initio calculations on FeSi and NiSi at conditions relevant to small planetary cores. *Phys. Chem. Miner.* **2017**, *44*, 477–484. https://doi.org/10.1007/s00269-017-0875-4.
229. Wann, E.T.H. The Core Composition of Terrestrial Planets: A Study of the Ternary Fe-Ni-Si System. Ph.D. Thesis, University College London, London, UK, 2015.
230. Terasaki, H.; Shibazaki, Y.; Sakamaki, T.; Tateyama, R.; Ohtani, E.; Funakoshi, K.-I.; Higo, Y. Hydrogenation of FeSi under high pressure. *Am. Miner.* **2010**, *96*, 93–99. https://doi.org/10.2138/am.2011.3628.
231. Dobson, D.; Hunt, S.; Ahmed, J.; Lord, O.; Wann, E.T.; Santangeli, J.; Wood, I.G.; Vočadlo, L.; Walker, A.M.; Thomson, A.; et al. The phase diagram of NiSi under the conditions of small planetary interiors. *Phys. Earth Planet. Inter.* **2016**, *261*, 196–206. https://doi.org/10.1016/j.pepi.2016.10.005.
232. Deng, L.; Kono, Y.; Shen, G. Sound wave velocities of Fe5Si at high-pressure and high-temperature conditions: Implications to lunar and planetary cores. *Am. Miner.* **2019**, *104*, 291–299. https://doi.org/10.2138/am-2019-6564.
233. Berrada, M.; Secco, R.A.; Yong, W. Adiabatic heat flow in Mercury's core from electrical resistivity measurements of liquid Fe-8.5 wt%Si to 24 GPa. *Earth Planet. Sci. Lett.* **2021**, *568*, 117053. https://doi.org/10.1016/j.epsl.2021.117053.
234. Genova, A.; Goossens, S.; Mazarico, E.; Lemoine, F.G.; Neumann, G.A.; Kuang, W.; Sabaka, T.J.; Hauck, I.S.A.; Smith, D.E.; Solomon, S.C.; et al. Geodetic Evidence That Mercury Has A Solid Inner Core. *Geophys. Res. Lett.* **2019**, *46*, 3625–3633. https://doi.org/10.1029/2018gl081135.
235. Tao, R.; Fei, Y. High-pressure experimental constraints of partitioning behavior of Si and S at the Mercury's inner core boundary. *Earth Planet. Sci. Lett.* **2021**, *562*, 116849. https://doi.org/10.1016/j.epsl.2021.116849.
236. Brennan, M.C.; Fischer, R.A.; Irving, J.C. Core formation and geophysical properties of Mars. *Earth Planet. Sci. Lett.* **2019**, *530*, 115923. https://doi.org/10.1016/j.epsl.2019.115923.
237. Dumoulin, C.; Tobie, G.; Verhoeven, O.; Rosenblatt, P.; Rambaux, N. Tidal constraints on the interior of Venus. *J. Geophys. Res. Planets* **2017**, *122*, 1338–1352. https://doi.org/10.1002/2016je005249.
238. Berrada, M.; Secco, R.A.; Yong, W.; Littleton, J.A.H. Electrical Resistivity Measurements of Fe-Si With Implications for the Early Lunar Dynamo. *J. Geophys. Res. Planets* **2020**, *125*, 1–15. https://doi.org/10.1029/2020je006380.
239. Plotnykov, M.; Valencia, D. Chemical fingerprints of formation in rocky super-Earths' data. *Mon. Not. R. Astron. Soc.* **2020**, *499*, 932–947. https://doi.org/10.1093/mnras/staa2615.
240. Fulton, B.J.; Petigura, E.A.; Howard, A.W.; Isaacson, H.; Marcy, G.W.; Cargile, P.A.; Hebb, L.; Weiss, L.M.; Johnson, J.A.; Morton, T.D.; et al. The California-KeplerSurvey. III. A Gap in the Radius Distribution of Small Planets. *Astron. J.* **2017**, *154*, 109. https://doi.org/10.3847/1538-3881/aa80eb.
241. Dorn, C.; Hinkel, N.R.; Venturini, J. Bayesian analysis of interiors of HD 219134b, Kepler-10b, Kepler-93b, CoRoT-7b, 55 Cnc e, and HD 97658b using stellar abundance proxies. *Astron. Astrophys.* **2016**, *597*, A38. https://doi.org/10.1051/0004-6361/201628749.
242. Nakamura-Messenger, K.; Zolensky, M.E.; Keller, L.P. New Manganese Silicide Mineral Phase in an Interplanetary Dust Particle. 39th Lunar and Planetary Science Conference, Abstract #2013, Lunar and Planetary Institute: : Houston, TX, USA, 2008.

243. Rietmeijer, F.J.M.; Nakamura, T.; Tsuchiyama, A.; Uesugi, K.; Nakano, T.; Leroux, H. Origin and formation of iron silicide phases in the aerogel of the Stardust mission. *Meteorit. Planet. Sci.* **2008**, *43*, 121–134. https://doi.org/10.1111/j.1945-5100.2008.tb00613.x.
244. Nakamura, T.; Tsuchiyama, A.; Akaki, T.; Uesugi, K.; Nakano, T.; Takeuchi, A.; Suzuki, Y.; Noguchi, T. Bulk mineralogy and three-dimensional structures of individual Stardust particles deduced from synchrotron X-ray diffraction and microtomography analysis. *Meteorit. Planet. Sci.* **2008**, *43*, 247–259. https://doi.org/10.1111/j.1945-5100.2008.tb00620.x.
245. Morello, S.O.; Anesa, J. Hallazgo de siliciuros de Fe en el meteorito El Aybal, Salta. 5° In the proceeding of Congreso de Mineralogía y Metalogenia, Actas. La Plata, Argentina, 23–25 October 2000, pp. 495–496.
246. Acevedo, R.D. *Catalogue of Meteorites from South America*, 1st ed.; Springer: Cham, Switzerland, 2014, ISBN 3319019252.
247. Hazen, R.M. Paleomineralogy of the Hadean Eon: A preliminary species list. *Am. J. Sci.* **2013**, *313*, 807–843. https://doi.org/10.2475/09.2013.01.
248. Morrison, S.M.; Hazen, R.M. An evolutionary system of mineralogy, Part IV: Planetesimal differentiation and impact mineralization (4566 to 4560 Ma). *Am. Miner.* **2021**, *106*, 730–761. https://doi.org/10.2138/am-2021-7632.
249. Matsuno, J.; Tsuchiyama, A.; Watanabe, T.; Tanaka, M.; Takigawa, A.; Enju, S.; Koike, C.; Chihara, H.; Miyake, A. Condensation of Glass with Multimetal Nanoparticles: Implications for the Formation Process of GEMS Grains. *Astrophys. J. Lett.* **2021**, *911*, 47. https://doi.org/10.3847/1538-4357/abe5a0.
250. Shepard, C.U. Examination of a supposed meteoric iron, found near Rutherfordton, North Carolina. *Am. J. Sci. Arts* **1859**, *XXVIII*, 259–270.
251. Rammelsberg, C.F. XII. Über einige nordamerikanische Meteoriten. *J. Prakt. Chem.* **1862**, *85*, 83–88.
252. Pieters, C.M.; Taylor, L.A.; Noble, S.K.; Keller, L.P.; Hapke, B.; Morris, R.V.; Allen, C.C.; McKAY, D.S.; Wentworth, S. Space weathering on airless bodies: Resolving a mystery with lunar samples. *Meteorit. Planet. Sci.* **2000**, *35*, 1101–1107. https://doi.org/10.1111/j.1945-5100.2000.tb01496.x.
253. Hapke, B. Space weathering from Mercury to the asteroid belt. *J. Geophys. Res. Earth Surf.* **2001**, *106*, 10039–10073. https://doi.org/10.1029/2000je001338.
254. Lucey, P.; Korotev, R.L.; Gillis, J.J.; Taylor, L.A.; Lawrence, D.; Campbell, B.A.; Elphic, R.; Feldman, B.; Hood, L.L.; Hunten, D.; et al. Understanding the Lunar Surface and Space-Moon Interactions. *Rev. Miner. Geochem.* **2006**, *60*, 83–219. https://doi.org/10.2138/rmg.2006.60.2.
255. Chapman, C.R. Space weathering of asteroid surfaces. *Annu. Rev. Earth Planet. Sci.* **2004**, *32*, 539–567. https://doi.org/10.1146/annurev.earth.32.101802.120453.
256. Noble, S.K.; Keller, L.P.; Pieters, C.M. Evidence of space weathering in regolith breccias II: Asteroidal regolith breccias. *Meteorit. Planet. Sci.* **2010**, *45*, 2007–2015. https://doi.org/10.1111/j.1945-5100.2010.01151.x.
257. Noguchi, T.; Nakamura, T.; Kimura, M.; Zolensky, M.E.; Tanaka, M.; Hashimoto, T.; Konno, M.; Nakato, A.; Ogami, T.; Fujimura, A.; et al. Incipient Space Weathering Observed on the Surface of Itokawa Dust Particles. *Science* **2011**, *333*, 1121–1125. https://doi.org/10.1126/science.1207794.
258. Pieters, C.M.; Ammannito, E.; Blewett, D.T.; Denevi, B.W.; De Sanctis, M.C.; Gaffey, M.J.; Le Corre, L.; Li, J.-Y.; Marchi, S.; McCord, T.B.; et al. Distinctive space weathering on Vesta from regolith mixing processes. *Nature* **2012**, *491*, 79–82. https://doi.org/10.1038/nature11534.
259. Thompson, M.S.; Christoffersen, R.; Zega, T.J.; Keller, L.P. Microchemical and structural evidence for space weathering in soils from asteroid Itokawa. *Earth Planets Space* **2014**, *66*, 89. https://doi.org/10.1186/1880-5981-66-89.
260. Hoffmann, H. Space Weathering. In *Encyclopedia of Astrobiology*; Gargaud, M., Amils, R., Quintanilla, J.C., Cleaves, H.J., Irvine, W.M., Pinti, D.L., Viso, M., Eds.; Springer: Berlin/Heidelberg, Germany, 2011; pp. 1543–1544, ISBN 978-3-642-11271-3.
261. Thompson, M.S.; Zega, T.J.; Becerra, P.; Keane, J.T.; Byrne, S. The oxidation state of nanophase Fe particles in lunar soil: Implications for space weathering. *Meteorit. Planet. Sci.* **2016**, *51*, 1082–1095. https://doi.org/10.1111/maps.12646.
262. Wu, Y.-Z.; Wang, Z.-C.; Lu, Y. Space weathering of the Moon from in situ detection. *Res. Astron. Astrophys.* **2019**, *19*, 51. https://doi.org/10.1088/1674-4527/19/4/51.
263. Wang, S.-Z.; Zhang, A.-C.; Pang, R.-L.; Li, Y.; Chen, J.-N. Possible records of space weathering on Vesta: Case study in a brecciated eucrite Northwest Africa 1109. *Meteorit. Planet. Sci.* **2019**, *54*, 836–849. https://doi.org/10.1111/maps.13254.
264. Liu, Y.; Keller, L.P.; Fraeman, A.A.; Christoffersen, R.; Rahman, Z.; Ehlmann, B.L.; Noble, S.K.; Barrat, J.A. Agglutinates in howardite 1769: Space weathering on Vesta (Abstract #1706). In *Proceedings of the 46th Lunar and Planetary Science Conference,* CD-ROM, The Woodlands, TX, USA, 2015.
265. Gopon, P.; Fournelle, J.; Llovet, X. *Soft X-ray EPMA of Submicron Phase Lunar Fe-Si Compounds*; Cambridge University Press: New York, NY, USA, 2012.
266. Nazarov, M.A.; Shornikov, S.I.; Demidova, S.I. Origin of native silicon and iron silicides in the Dhofar 280 lunar meteorite. *Petrology* **2015**, *23*, 168–175. https://doi.org/10.1134/s0869591115020071.
267. Nazarov, M.A.; Demidova, S.; Anosova, M.O.; Kostitsyn, Y.; Ntaflos, T.; Brandstaetter, F. Native silicon and iron silicides in the Dhofar 280 lunar meteorite. *Petrology* **2012**, *20*, 506–519. https://doi.org/10.1134/s0869591112060021.
268. Anand, M.; Taylor, L.A.; Patchen, A.; Cahill, J.; Nazarov, M.A. New Minerals from a New Lunar Meteorite, Dhofar 280 (abstract #1653), In *Proceedings of the Lunar and Planetary Science XXXIII,* League City, TX, USA, 11–15 March 2002.

269. Anand, M.; Taylor, L.A.; Nazarov, M.A.; Shu, J.; Mao, H.-K.; Hemley, R.J. New lunar mineral HAPKEITE*: Product of impact-induced vapor-phase deposition in the regolith? In *Proceedings of the 34th Annual Lunar and Planetary Science Conference,* League City, Texas, USA, 17–21 March 2003.
270. Anand, M.; Taylor, L.A.; Nazarov, M.A.; Shu, J.; Mao, H.-K.; Hemley, R.J. Space weathering on airless planetary bodies: Clues from the lunar mineral hapkeite. *Proc. Natl. Acad. Sci. USA* **2004**, *101*, 6847–6851. https://doi.org/10.1073/pnas.0401565101.
271. Korochantseva, E.V.; Buikin, A.I.; Hopp, J.; Lorenz, C.A.; Korochantsev, A.V.; Ott, U.; Trieloff, M. Thermal and irradiation history of lunar meteorite Dhofar 280. *Meteorit. Planet. Sci.* **2016**, *51*, 2334–2346. https://doi.org/10.1111/maps.12732.
272. Wieczorek, M.A.; Weiss, B.P.; Stewart, S.T. An Impactor Origin for Lunar Magnetic Anomalies. *Science* **2012**, *335*, 1212–1215. https://doi.org/10.1126/science.1214773.
273. Jambor, J.L.; Grew, E.S.; Roberts, A.C. New mineral names: Hapkeite. *Am. Mineral.* **2005**, *90*, 518–522.
274. mindat.org. Samples returned by the Russian Luna-24 Mission from Crater Ejecta Blanket. Available online: https://www.mindat.org/loc-7798.html (accessed on 31 October 2021).
275. Ashikmina, N.A.; Bogatikov, O.A.; Gorshkov, A. Aktsesornye minerali steklovatikh fragmentov Luni 24. *Dokl. Akad. Nauk. SSSR. Earth Sci. Sect.* **1979**, *248*, 953–955.
276. Spicuzza, M.J.; Valley, J.W.; Fournelle, J.; Huberty, J.M.; Treiman, A. Native silicon and Fe-silicides from the Apollo 16 lunar regolith: Extreme reduction, metal-silicate immiscibility, and shock melting (Abstract #2231). In *Proceedings of the 42nd Lunar and Planetary Science Conference,* The Woodlands, TX, USA, 7–11 March 2011.
277. Gopon, P.; Spicuzza, M.J.; Kelly, T.F.; Reinhard, D.; Prosa, T.J.; Fournelle, J. Ultra-reduced phases in Apollo 16 regolith: Combined field emission electron probe microanalysis and atom probe tomography of submicron Fe-Si grains in Apollo 16 sample 61500. *Meteorit. Planet. Sci.* **2017**, *52*, 1941–1962. https://doi.org/10.1111/maps.12899.
278. Gopon, P.; Fournelle, J.; Spicuzza, M.; Valley, J. Survey for Fe-Si in Apollo 16 Regolith Sample 61501,22. *Microsc. Microanal.* **2015**, *21*, 2095–2096. https://doi.org/10.1017/S1431927615011253.
279. Gopon, P.; Spicuzza, M.; Kelly, T.; Reinhard; Prosa, T.; Larson, D.; Fournelle, J. Atom Probe Tomography of Reduced Phases in Apollo 16 Regolith Sample 61501,22. *Microsc. Microanal.* **2017**, *23*, 720–721. https://doi.org/10.1017/s1431927617004263.
280. Gopon, P.; Fournelle, J.; Valley, J.; Horn, W.; Pinard, P.; Sobol, P.; Spicuzza, M.; Llovet, X. Soft X-ray EPMA analyses of nanophase lunar Fe-Si compounds. In *Proceedings of the Wisconsin Space Conference,* Marquette University, Milwaukee, WI, USA, 15–16 August 2013. https://doi.org/10.17307/wsc.v0i0.18.
281. Ross, A.J.; Downes, H.; Smith, C.L.; Jones, A.P. Highly reduced metals and sulfides in ureilites: Remnants of the UPB core? In *Proceedings of the 72nd Annual Meteoritical Society Meeting Meteoritics & Planetary Science,* Nancy, France, 13–18 July, 2009, p. 44.
282. Smith. Iron silicide in polymict ureilites—Recording the complex history of the ureilite parent body. Abstract #5221. In *Proceedings of the 73rd Meeting of Meteoritical Society,* New York City, NY, USA, 26–30 July, 2010.
283. Downes, H.; Mittlefehldt, D.W.; Kita, N.T.; Valley, J.W. Evidence from polymict ureilite meteorites for a disrupted and re-accreted single ureilite parent asteroid gardened by several distinct impactors. *Geochim. Cosmochim. Acta* **2008**, *72*, 4825–4844. https://doi.org/10.1016/j.gca.2008.06.028.
284. Broadley, M.W.; Bekaert, D.V.; Marty, B.; Yamaguchi, A.; Barrat, J.A. Noble gas variations in ureilites and their implications for ureilite parent body formation. *Geochim. Cosmochim. Acta* **2019**, *270*, 325–337. https://doi.org/10.1016/j.gca.2019.11.032.
285. Cohen, B.A.; Goodrich, C.A.; Keil, K. Feldspathic clast populations in polymict ureilites: Stalking the missing basalts from the ureilite parent body. *Geochim. Cosmochim. Acta* **2004**, *68*, 4249–4266. https://doi.org/10.1016/j.gca.2004.01.027.
286. Goodrich, C.A.; Van Orman, J.; Wilson, L. Fractional melting and smelting on the ureilite parent body. *Geochim. Cosmochim. Acta* **2007**, *71*, 2876–2895. https://doi.org/10.1016/j.gca.2007.03.023.
287. Goodrich, C.A.; Wilson, L.; Van Orman, J.; Michel, P. Comment on “Parent body depth-pressure-temperature relationships and the style of the ureilite anatexis” by P. H. Warren (MAPS 47:209-227). *Meteorit. Planet. Sci.* **2013**, *48*, 1096–1106. https://doi.org/10.1111/maps.12131.
288. Hoffmann, V.H.; Hochleitner, R.; Torii, M.; Funaki, M.; Mikouchi, T.; Kaliwoda, M.; Jenniskens, P.; Shaddad, M.H. Magnetism and mineralogy of Almahata Sitta polymict ureilite (= asteroid 2008 TC3): Implications for the ureilite parent body magnetic field. *Meteorit. Planet. Sci.* **2011**, *46*, 1551–1564. https://doi.org/10.1111/j.1945-5100.2011.01248.x.
289. Nabiei, F.; Badro, J.; Dennenwaldt, T.; Oveisi, E.; Cantoni, M.; Hébert, C.; El Goresy, A.; Barrat, J.A.; Gillet, P. A large planetary body inferred from diamond inclusions in a ureilite meteorite.. *Nat. Commun.* **2018**, *9*, 1327. https://doi.org/10.1038/s41467-018-03808-6.
290. Singletary, S.J.; Grove, T.L. Early petrologic processes on the ureilite parent body. *Meteorit. Planet. Sci.* **2003**, *38*, 95–108. https://doi.org/10.1111/j.1945-5100.2003.tb01048.x.
291. Smith. Metal and sulphide phases in interstitial veins in “dimict” ureilites—Insights into the history and petrogenesis of the ureilite parent body. In *Proceeding of 39th LPSC.* League City, TX, USA, 10–14 March 2008, Abstract #1669
292. van Kooten, E.M.; Schiller, M.; Bizzarro, M. Magnesium and chromium isotope evidence for initial melting by radioactive decay of 26Al and late stage impact-melting of the ureilite parent body. *Geochim. Cosmochim. Acta* **2017**, *208*, 1–23. https://doi.org/10.1016/j.gca.2017.03.033.
293. Warren, P.H. Parent body depth-pressure-temperature relationships and the style of the ureilite anatexis. *Meteorit. Planet. Sci.* **2012**, *47*, 209–227. https://doi.org/10.1111/j.1945-5100.2011.01320.x.
294. Gabriel, A.D. Origin and Evolution of Ureilite vein Metal—Fe, Ni, Co and Ni Isotope Systematics of Ureilite Vein Metal and Ureilite Silicates. Ph.D. Thesis, Georg-August-Universität, Göttngen, Germany, 2009.

295. Young, E.D.; Yin, Q.-Z.; Sanborn, M.E.; Shaddad, M.H. Carbonaceous Chondrite-Like Xenoliths in Polymict Ureilites: A Large Variety of Uniue Outer Solar System Materials. LPI Contrib. No. 2132. In *Proceedings of the 50th Lunar and Planetary Science Conference,* The Woodlands, Texas, USA, 18–22 March, 2019.
296. Russell, S.S.; Zipfel, J.; Folco, L.; Jones, R.; Grady, M.M.; McCoy, T.; Grossman, J.N. The Meteoritical Bulletin, No. 87, 2003 July. *Meteorit. Planet. Sci.* **2003**, *38*, A189–A248. https://doi.org/10.1111/j.1945-5100.2003.tb00328.x.
297. Herrin, J.S.; Mittlefehldt, D.W.; Downes, H.; Humayum, M. Diverse metals and sulfides in polymict ureilites EET 83309 and EET 87720. In *Proceedings of the 38th LPSC,* League City , TX, USA, 12–16 March, 2007.
298. Ross. DaG 1047: A polymict ureilite containing exotic clasts including a chondrite. Abstract #2361. In *Proceedings of the 41st LPSC,* The Woodlands, TX, USA, 1–5 March, 2010.
299. Grossman, J.N. The Meteoritical Bulletin, No. 82, 1998 July. *Meteorit. Planet. Sci.* **1998**, *33*, A221–A239. https://doi.org/10.1111/j.1945-5100.1998.tb01336.x.
300. Ikeda. Lithic and mineral clasts in the Dar al Gani (DaG) 319 polymict ureilite. *Antarct. Meteor. Res.* **2000**, *13*, 177–221.
301. Garvie, L.A.J. The Meteoritical Bulletin, No. 99, April 2012. *Meteorit. Planet. Sci.* **2012**, *99*, E1–E52.
302. The Meteoritical Society. Dar al Gani 1066: Meteoritical Bulletin Database. Available online: https://www.lpi.usra.edu/meteor/metbull.php?code=61777 (accessed on 31 October 2021).
303. Bouvier, A.; Gattacceca, J.; Agee, C.; Grossman, J.; Metzler, K. The Meteoritical Bulletin, No. 104. *Meteorit. Planet. Sci.* **2017**, *52*, 2284–2284. https://doi.org/10.1111/maps.12930.
304. Moggi Cecchi, V.; Caporali, S.; Pratesi, G. DaG 1066: A newfound anomalous ureilite with chondritic inclusions. In *Proceedings of the 78th Annual Meeting of the Meteoritical Society. Berkeley,* CA, USA, 27-31 July, 2015. Abstract. #5252
305. Prinz, M.; Weisberg, M.K.; Nehru, C.E.; Delaney, J.S. EET 83309, a polymict ureilite: Recognition of a new group. *Lunar Planet. Sci.* **1987**, *18*, 802.
306. Downes, H.; Beard, A.D.; Howard, K. Petrology of a Granitic Clast in Polymict Ureilite EET 83309. In *Proceedings of the 72nd Annual Meteoritical Society Meeting,* Nancy, France, 13–18 July 2009; p. 72.
307. Beard, A.D.; Downes, H.; Howard, K.T. Significance of Opal in Ureilites—Delivery of H_2O to the Inner Solar System? In *Proceedings of the 74th Annual Meteoritical Society Meeting,* London, UK, 8–12 August, 2011; p. 74.
308. Prinz, M.; Weisberg, M.K.; Nehru, C.E.; Delaney, J.S. North Haig and Nilpena: Paired Polymict Ureilites with Angra DOS Reis-Related and other Clasts. In *Proceedings of the Lunar and Planar Science XVII, Houston,* TX, USA, 17–21 March 1986; pp. 681–682.
309. Keil, K.; Berkley, J.L. Suessite, Fe3Si: A new mineral in the North Haig ureilite. *Am. Mineral.* **1982**, *67*, 126–131.
310. Jaques, A.; Fitzgerald, M. The Nilpena ureilite, an unusual polymict breccia: Implications for origin. *Geochim. Cosmochim. Acta* **1982**, *46*, 893–900. https://doi.org/10.1016/0016-7037(82)90045-x.
311. Graham, A.L. The Meteoritical Bulletin No. 59. *Meteoritics* **1981**, *16*, 193–199. https://doi.org/10.1111/j.1945-5100.1981.tb00543.x.
312. Wlotzka, F. The Meteoritical Bulletin, No. 77, 1994 November. *Meteorit. Planet. Sci.* **1994**, *29*, 891–897. https://doi.org/10.1111/j.1945-5100.1994.tb01104.x.
313. Wlotzka, F. The Meteoritical Bulletin, No. 72. *Meteorit. Planet. Sci.* **1992**, *27*, 109–117. https://doi.org/10.1111/j.1945-5100.1992.tb01068.x.
314. The Meteoritical Society. Frontier Mountain 90036: Meteoritical Bulletin Database. Available online: https://www.lpi.usra.edu/meteor/metbull.php?sea=Frontier+Mountain+90036&sfor=names&ants=&nwas=&falls=&valids=&stype=contains&lrec=50&map=ge&browse=&country=All&srt=name&categ=All&mblist=All&rect=&phot=&strewn=&snew=0&pnt=Normal%20table&code=10434 (accessed on 31 October 2021).
315. Wlotzka, F. The Meteoritical Bulletin, No. 73. *Meteorit. Planet. Sci.* **1992**, *27*, 477–483. https://doi.org/10.1111/j.1945-5100.1992.tb00235.x.
316. The Meteoritical Society. Frontier Mountain 90054: Meteoritical Bulletin Database. Available online: https://www.lpi.usra.edu/meteor/metbull.php?sea=Frontier+Mountain+90054&sfor=names&ants=&nwas=&falls=&valids=&stype=contains&lrec=50&map=ge&browse=&country=All&srt=name&categ=All&mblist=All&rect=&phot=&strewn=&snew=0&pnt=Normal%20table&code=10452 (accessed on 31 October 2021).
317. The Meteoritical Society. Frontier Mountain 93008: Meteoritical Bulletin Database. Available online: https://www.lpi.usra.edu/meteor/metbull.php?sea=Frontier+Mountain+93008&sfor=names&ants=&nwas=&falls=&valids=&stype=contains&lrec=50&map=ge&browse=&country=All&srt=name&categ=All&mblist=All&rect=&phot=&strewn=&snew=0&pnt=Normal%20table&code=10639 (accessed on 31 October 2021).
318. Ruzicka, A.; Grossman, J.; Bouvier, A.; Agee, C.B. The Meteoritical Bulletin, No. 103. *Meteorit. Planet. Sci.* **2017**, *52*, 1014. https://doi.org/10.1111/maps.12888.
319. The Meteoritical Society. Frontier Mountain 90233: Meteoritical Bulletin Database. Available online: https://www.lpi.usra.edu/meteor/metbull.php?sea=Frontier+Mountain+90233&sfor=names&ants=&nwas=&falls=&valids=&stype=contains&lrec=50&map=ge&browse=&country=All&srt=name&categ=All&mblist=All&rect=&phot=&strewn=&snew=0&pnt=Normal%20table&code=10621 (accessed on).
320. The Meteoritical Society. Mountain 90228: Meteoritical Bulletin Database. Available online: https://www.lpi.usra.edu/meteor/metbull.php?sea=Frontier+Mountain+90228&sfor=names&ants=&nwas=&falls=&valids=&stype=contains&lrec=50&map=ge&browse=&country=All&srt=name&categ=All&mblist=All&rect=&phot=&strewn=&snew=0&pnt=Normal%20table&code=10617 (accessed on).

321. Ikeda, Y. Petrology of an unusual monomict ureilite, NWA1241. *Polar Sci.* **2007**, *1*, 45–53. https://doi.org/10.1016/j.polar.2007.05.002.
322. Funaki, M.; Mikouchi, T.; Almaha Sitta Consortium. Magnetism and Mineralogy of Almaha Sitta. In *Proceedings of the 41st Lunar and Planetary Science Conference,* The Woodlands, TX, USA, 1–5 March 2010; p. 41.
323. Meteoritical Bulletin Database. The Meteoritical Bulletin, No. 110. 2021, *In preparation*.
324. Meteoritical Bulletin Database. Northeast Africa 027. Available online: https://www.lpi.usra.edu/meteor/metbull.php?sea=NEA+027&sfor=names&ants=&nwas=&falls=&valids=&stype=contains&lrec=50&map=ge&browse=&country=All&srt=name&categ=All&mblist=All&rect=&phot=&strewn=&snew=0&pnt=Normal%20table&code=74844 (accessed on 6 November 2021).
325. Jenniskens, P.; Shaddad, M.H.; Numan, D.; Elsir, S.; Kudoda, A.M.; Zolensky, M.; Le, L.; Robinson, G.A.; Friedrich, J.M.; Rumble, D.; et al. The impact and recovery of asteroid 2008 TC3. *Nature* **2009**, *458*, 485–488. https://doi.org/10.1038/nature07920.
326. Gayon-Markt, J.; Delbo, M.; Morbidelli, A.; Marchi, S. On the origin of the Almahata Sitta meteorite and 2008 TC3 asteroid. *Mon. Not. R. Astron. Soc.* **2012**, *424*, 508–518. https://doi.org/10.1111/j.1365-2966.2012.21220.x.
327. Hamilton, V.E.; Goodrich, C.A.; Treiman, A.H.; Connolly, H.C.; Zolensky, M.E.; Shaddad, M.H. Meteoritic evidence for a Ceres-sized water-rich carbonaceous chondrite parent asteroid. *Nat. Astron.* **2020**, *5*, 350–355. https://doi.org/10.1038/s41550-020-01274-z.
328. Kaliwoda, M.; Hochleitner, R.; Hoffmann, V.H.; Mikouchi, T.; Gigler, A.M.; Schmahl, W.W. New Raman Spectroscopic Data of the Almahata Sitta Meteorite. *Spectrosc. Lett.* **2013**, *46*, 141–146. https://doi.org/10.1080/00387010.2011.610423.
329. Horstmann, M.; Humayun, M.; Fischer-Gödde, M.; Bischoff, A.; Weyrauch, M. Si-bearing metal and niningerite in Almahata Sitta fine-grained ureilites and insights into the diversity of metal on the ureilite parent body. *Meteorit. Planet. Sci.* **2014**, *49*, 1948–1977. https://doi.org/10.1111/maps.12370.
330. Grady, M.M. *Catalogue of Meteorites: With Special Reference to Those Represented in the Collection of the Natural History Museum, London*; 5th ed.; Cambridge University Press: Cambridge, UK, 2000; ISBN 0521663032.
331. Grossman, J.N.; Zipfel, J. The Meteoritical Bulletin, No. 85, 2001 September. *Meteorit. Planet. Sci.* **2001**, *36*, A293–A322. https://doi.org/10.1111/j.1945-5100.2001.tb01542.x.
332. Hoffmann, V.H.; Mikouchi, T.; Torii, M.; Funaki, M.; Kaliwoda, M.; Hochleitner, R.; Horstmann, M.; Bischoff, A.; Gnos, E.; Hofmann, B.; et al. Almahata Sitta Magnetism—A Compilation. Asteroids, Comets, Meteors. In *Proceedings of the Asteroids, Comets,* Meteors 2012, Niigata, Japan, 16–20 May 2012.
333. Kuehner, S.M.; Irving, A.J.; Sipiera, P.P. Diversity Among EH Chondrites: Anomallous EH3 Chondrite Northwest Africa 8789 and Rare EH Melt Rocks Northwest Africa 7324 and Northwest Africa 10237. In *Proceedings of the 79th Annual Meeting of the Meteoritical Society,* Berlin, Germany, 7–12 August 2016, p. 79.
334. Bouvier, A.; Gattacceca, J.; Grossman, J.; Metzler, K. The Meteoritical Bulletin, No. 105. *Meteorit. Planet. Sci.* **2017**. https://doi.org/10.1111/maps.12944.
335. Lin, Y.; El Goresy, A. A comparative study of opaque phases in Qingzhen (EH3) and MacAlpine Hills 88136 (EL3): Representatives of EH and EL parent bodies. *Meteorit. Planet. Sci.* **2002**, *37*, 577–599. https://doi.org/10.1111/j.1945-5100.2002.tb00840.x.
336. Gattacceca, J.; McCubbin, F.M.; Grossman, J.; Bouvier, A.; Bullock, E.; Aoudjehane, H.C.; Debaille, V.; D'Orazio, M.; Komatsu, M.; Miao, B.; et al. The Meteoritical Bulletin, No. 109. *Meteorit. Planet. Sci.* **2021**, *56*, 1626–1630. https://doi.org/10.1111/maps.13714.
337. Vernazza, P.; Brunetto, R.; Binzel, R.; Perron, C.; Fulvio, D.; Strazzulla, G.; Fulchignoni, M. Plausible parent bodies for enstatite chondrites and mesosiderites: Implications for Lutetia's fly-by. *Icarus* **2009**, *202*, 477–486. https://doi.org/10.1016/j.icarus.2009.03.016.
338. Sierks, H.; Lamy, P.; Barbieri, C.; Koschny, D.; Rickman, H.; Rodrigo, R.; A'Hearn, M.F.; Angrilli, F.; Barucci, M.A.; Bertaux, J.L.; et al. Images of Asteroid 21 Lutetia: A Remnant Planetesimal from the Early Solar System. *Science* **2011**, *334*, 487–490. https://doi.org/10.1126/science.1207325.
339. Coradini, A.; Capaccioni, F.; Erard, S.; Arnold, G.; De Sanctis, M.C.; Filacchione, G.; Tosi, F.; Barucci, M.A.; Capria, M.T.; Ammannito, E.; et al. The Surface Composition and Temperature of Asteroid 21 Lutetia As Observed by Rosetta/VIRTIS. *Science* **2011**, *334*, 492–494. https://doi.org/10.1126/science.1204062.
340. Connolly, H.C.; Smith, C.; Benedix, G.; Folco, L.; Righter, K.; Zipfel, J.; Yamaguchi, A.; Aoudjehane, H.C. The Meteoritical Bulletin, No. 92, 2007 September. *Meteorit. Planet. Sci.* **2007**, *42*, 1647–1694. https://doi.org/10.1111/j.1945-5100.2007.tb00596.x.
341. Kimura, M.; Karube, T.; Weisberg, M.K.; Mikouchi, T.; Noguchi, T. Opaque MInerals in Chi Chondrites: Indicators of Formation Conditions. In *Proceedings of the 74th Annual Meteoritical Society Meeting,* London, UK, 8–12 August 2011; p. 74.
342. Moyano-Cambero, C.E.; Trigo-Rodríguez, J.M.; Llorca, J.; Fornasier, S.; Barucci, M.A.; Rimola, A. A plausible link between the asteroid 21 Lutetia and CH carbonaceous chondrites. *Meteorit. Planet. Sci.* **2016**, *51*, 1795–1812. https://doi.org/10.1111/maps.12703.
343. Lin, C.; Hollister, L.S.; MacPherson, G.J.; Bindi, L.; Ma, C.; Andronicos, C.L.; Steinhardt, P. Evidence of cross-cutting and redox reaction in Khatyrka meteorite reveals metallic-Al minerals formed in outer space. *Sci. Rep.* **2017**, *7*, 1637. https://doi.org/10.1038/s41598-017-01445-5.
344. Ruzicka, A.; Grossman, J.N.; Garvie, L. The Meteoritical Bulletin, No. 100, 2014 June. *Meteorit. Planet. Sci.* **2014**, *49*, E1–E101.

345. Ma, C.; Lin, C.; Bindi, L.; Steinhardt, P.J. Discovery of New Al-Cu-Fe Minerals in the Khatyrka CV3 Meteorite. In *Proceedings of the 79th Annual Meeting of the Meteoritical Society*, Berlin, Germany, 7–12 August 2016; p. 79.
346. MacPherson, G.J.; Andronicos, C.L.; Bindi, L.; Distler, V.V.; Eddy, M.P.; Eiler, J.M.; Guan, Y.; Hollister, L.S.; Kostin, A.; Kryachko, V.; et al. Khatyrka, a new CV3 find from the Koryak Mountains, Eastern Russia. *Meteorit. Planet. Sci.* **2013**, *48*, 1499–1514. https://doi.org/10.1111/maps.12170.
347. Ma, C.; Lin, C.; Bindi, L.; Steinhardt, P. Hollisterite (Al3Fe), kryachkoite (Al,Cu)6(Fe,Cu), and stolperite (AlCu): Three new minerals from the Khatyrka CV3 carbonaceous chondrite. *Am. Miner.* **2017**, *102*, 690–693. https://doi.org/10.2138/am-2017-5991.
348. Khatyrka Meteorite, Iomrautvaam massif, Anadyrsky District, Chukotka Autonomous Okrug, Russia. Available online: https://www.mindat.org/loc-2717.html (accessed on 15 February 2021).
349. Bindi, L.; Yao, N.; Lin, C.; Hollister, L.S.; MacPherson, G.J.; Poirier, G.R.; Andronicos, C.L.; Distler, V.V.; Eddy, M.P.; Kostin, A.; et al. Steinhardtite, a new body-centered-cubic allotropic form of aluminum from the Khatyrka CV3 carbonaceous chondrite. *Am. Miner.* **2014**, *99*, 2433–2436. https://doi.org/10.2138/am-2014-5108.
350. Steinhardt, P.J. Quasicrystals: A brief history of the impossible. *Rend. Lince* **2012**, *24*, 85–91. https://doi.org/10.1007/s12210-012-0203-3.
351. Bindi, L.; Steinhardt, P.; Yao, N.; Lu, P. Icosahedrite, Al63Cu24Fe13, the first natural quasicrystal. *Am. Miner.* **2011**, *96*, 928–931. https://doi.org/10.2138/am.2011.3758.
352. Bindi, L.; Yao, N.; Lin, C.; Hollister, L.S.; Andronicos, C.L.; Distler, V.V.; Eddy, M.P.; Kostin, A.; Kryachko, V.; MacPherson, G.J.; et al. Natural quasicrystal with decagonal symmetry. *Sci. Rep.* **2015**, *5*, srep09111. https://doi.org/10.1038/srep09111.
353. Bindi, L.; Dmitrienko, V.E.; Steinhardt, P.J. Are quasicrystals really so rare in the Universe? *Am. Miner.* **2020**, *105*, 1121–1125. https://doi.org/10.2138/am-2020-7519.
354. mindat.org. Icosahedrite. Available online: https://www.mindat.org/min-40647.html (accessed on 31 October 2021).
355. mindat.org. Decagonite. Available online: https://www.mindat.org/min-46637.html (accessed on 31 October 2021).
356. Asimow, P.D.; Lin, C.; Bindi, L.; Ma, C.; Tschauner, O.; Hollister, L.S.; Steinhardt, P.J. Shock synthesis of quasicrystals with implications for their origin in asteroid collisions. *Proc. Natl. Acad. Sci. USA* **2016**, *113*, 7077–7081. https://doi.org/10.1073/pnas.1600321113.
357. Hollister, L.S.; Bindi, L.; Yao, N.; Poirier, G.R.; Andronicos, C.L.; MacPherson, G.J.; Lin, C.; Distler, V.V.; Eddy, M.P.; Kostin, A.; et al. Impact-induced shock and the formation of natural quasicrystals in the early solar system. *Nat. Commun.* **2014**, *5*, 4040. https://doi.org/10.1038/ncomms5040.
358. McGeoch, M.W.; Dikler, S.; McGeoch, J.E.M. Hemolithin: A Meteoritic Protein containing Iron and Lithium. *arXiv* **2020**, arXiv:2002.11688.
359. Ma, C.; Beckett, J.R. Kaitianite, $Ti^{3+}{}_2Ti^{4+}O_5$, a new titanium oxide mineral from Allende. *Meteorit. Planet. Sci.* **2020**, *56*, 96–107. https://doi.org/10.1111/maps.13576.
360. Savva, N.E.; Minyuk, P.S.; Subbotnikova, T.V. An exotic find of iron silicide in the zone of passage of the Tunguska meteorite and Vitim car. In *Collection of Scientific Papers on Materials International Scientific Conference. Scientific Achievements of the Third Millennium*; Scientific Achievements of the Third Millennium, Ed.; Science Publishing Corporation: New York, NY, USA, 2019; pp. 56–62.
361. Bilyk, N.T.; Makovskyi, J.S.; Poberezhskaya, I.V.; Stepanov, V.B.; Tymoschuk, V.R.; Shevchenko, T.G.; Yatsenko, I.G. New Occurence of Iron Silicide in the Ukraine. Cosmogenic or Telluric Nature? *Geologia* **2014**, *17*, 101–111.
362. Kapišinský, I.; Iždinský, J.; Ivan, K.; Pánek, Z.; Zemánková, M. Reanalysis of the cosmic dust L 2011 S2 and L 2009 I14 NASA samples. *Contrib. Geophys. Geod.* **2006**, *36*, 63–71.
363. Nikolayeva, E.P.; Shabanin, M.A. Muassonit iz osadochnikh otlozheniy Fergani. *Zap. Vsesoyuznogo Mineral. Obs.* **1971**, *100*, 291–296.
364. Gevork'yan, V. The occurrence of natural ferrosilicon in the northern Azov region. *Dokl. Akad. Nauk SSSR* **1969**, *185*, 416–418. (In Russian)
365. Gevork'yan, V.; Litvin, A.L.; Povarennykh, A.S. Occurrence of the new minerals fersilicite and ferdisilicite. *Geol. Zsurnal Akad. Nauk. Ukr. SSR* **1969**, *29*, 62–71. (In Russian)
366. Fleischer, M. Fersilicite, Ferdisilicite. *Am. Mineral.* **1969**, *54*, 1737–1742.
367. Gevork'yan, V. On Natural Ferrosilicon in the Sand Mass of the Poltava Series of the Konsko-Yalynskaya Depression (North Cisasov Area) *Dop. Akad. Nauk. URSR* **1968**, *6*, 513–517. (In Ukrainian)
368. Yeremenko, G.K.; Polkanov, Y.A.; Vitrichenko, E.A. *Cosmogenic Material in Placers. Dverniye i Pogrebennyye Rossypi SSSR;* Naukova Dumka Press: Kiev, SSSR, 1977; pp. 68–75.
369. mindat.org. Barringerite. Available online: https://www.mindat.org/min-537.html (accessed on 17 November 2021).
370. Yu, Z.: Two new minerals gupeiite and xifengite in cosmic dusts from Yanshan. *Acta Petrol. Mineral. Anal.* **1984**, *3*, 231–238. (In Chinese with an English abstract)
371. Dunn, P.J.; Chao, G.Y.; Fitzpatrick, J.J.; Langley, R.H.; Fleischer, M.; Zilczer, J.A. New Mineral Names. *Am. Mineral.* **1986**, *71*, 227–232.
372. Zuxiang, Y. Some new minerals from platinum-bearing rocks in Yanshan and Tibet regions, China. *Bull. Inst. Geol. Chin. Acad. Geol. Sci.* **1986**, *2*, 49–57. (In Chinese)

373. Szöőr, G.; Elekes, Z.; Rózsa, P.; Uzonyi, I.; Simulák, J.; Kiss, Á.Z. Magnetic spherules: Cosmic dust or markers of a meteoritic impact? *Nucl. Instrum. Methods Phys. Res. Sect. B Beam Interactions Mater. Atoms* **2001**, *181*, 557–562. https://doi.org/10.1016/s0168-583x(01)00380-9.
374. Drake, S.M.; Beard, A.D.; Jones, A.P.; Brown, D.J.; Fortes, A.; Millar, I.L.; Carter, A.; Baca, J.; Downes, H. Discovery of a meteoritic ejecta layer containing unmelted impactor fragments at the base of Paleocene lavas, Isle of Skye, Scotland. *Geology* **2017**, *46*, 171–174. https://doi.org/10.1130/g39452.1.
375. Romano, A. Mineralogy of an unusual type of rock of possible meteoritic origin Symposia: MPN-01 General contributions to mineralogy. In *Proceedings of the 33rd IGC, International Geological Congress*, Oslo, Norway, 6–14 August 2008; p. 33.
376. Romano, A. Mineralogy of an Unusual Type of Rock of Possible Meteoritic Origin. In *Proceedings of the 33rd International Geological Congress 2008*, Oslo, Norway, 6–14 August 2008; Norwegian Academy of Science and Letters, Ed.; Curran Associates Inc.: Red Hook, NY, USA, 2013; p. 4475, ISBN 978-1-62748-373-5.
377. Wittke, J.H.; Bunch, T.E.; West, A.; Harris, R.S. Melt Spherules from Peter's Pond, A Carolina Bay, South Carolina. In *Proceedings of the 70th Annual Meteoritical Society Meeting*, Tucson, AZ, USA, 13–17 August 2007.
378. Suttle, M.D.; Genge, M.J. Diagenetically altered fossil micrometeorites suggest cosmic dust is common in the geological record. *Earth Planet. Sci. Lett.* **2017**, *476*, 132–142. https://doi.org/10.1016/j.epsl.2017.07.052.
379. Yanev, Y.; Benderev, A.; Zotov, N.; Ilieva, I.; Iliev, T.; Georgiev, S. Tektite or meteorite from Koshava gypsum mine, NW Bulgaria. In *Proceedings of the Jubilee Scientific Conference "Geosciences 2015"*, Sofia, Bulgaria, https://doi.org/10.13140/rg.2.1.3262.0563.
380. Yanev, Y.; Iliev, T.; Zotov, N.; Benderev, A.; Nihtianova, Diana, Ilieva, Iren. Silicides and alloys from Koshava tektite (or meteorite), NW Bulgaria. In *Proceedings of the GEOSCIENCES 2016: National Conference with International Participation*; Bulgarian Geological Society, Ed.; BGS: Sofia, Bulgaria, 2016; pp. 43–44.
381. Yanev, Y.; Benderev, A.; Zotov, N.; Dubinina, E.; Iliev, T.; Georgiev, S.; Ilieva, I.; Sergeeva, I. Exotic rock block from the Koshava gypsum mine, Northwest Bulgaria: Petrography, geochemistry, mineralogy and melting phenomena. *Geol. Balc.* **2021**, *50*, 45–65. https://doi.org/10.52321/geolbalc.50.1.45.
382. Buchner, E.; Schwarz, W.H.; Schmieder, M.; Trieloff, M. Establishing a 14.6 ± 0.2 Ma age for the Nördlinger Ries impact (Germany)-A prime example for concordant isotopic ages from various dating materials. *Meteorit. Planet. Sci.* **2010**, *45*, 662–674. https://doi.org/10.1111/j.1945-5100.2010.01046.x.
383. Bunch, T.E.; Hermes, R.E.; Moore, A.M.; Kennett, D.J.; Weaver, J.C.; Wittke, J.H.; DeCarli, P.S.; Bischoff, J.L.; Hillman, G.C.; Howard, G.A.; et al. Very high-temperature impact melt products as evidence for cosmic airbursts and impacts 12,900 years ago. *Proc. Natl. Acad. Sci. USA* **2012**, *109*, E1903–E1912. https://doi.org/10.1073/pnas.1204453109.
384. Wu, Y.; Sharma, M.; LeCompte, M.A.; Demitroff, M.N.; Landis, J.D. Origin and provenance of spherules and magnetic grains at the Younger Dryas boundary. *Proc. Natl. Acad. Sci. USA* **2013**, *110*, E3557–E3566. https://doi.org/10.1073/pnas.1304059110.
385. Schrand, C.; Deutsch, A. Formation of Lechatelierite and Impact Melt Glasses in Experimentally Shocked Rocks. Lunar and Planetary Science 1998, 29.
386. Kennett, J.P.; Kennett, D.J.; Culleton, B.J.; Tortosa, J.E.A.; Bischoff, J.L.; Bunch, T.E.; Daniel, I.R., Jr.; Erlandson, J.M.; Ferraro, D.; Firestone, R.B.; et al. Bayesian chronological analyses consistent with synchronous age of 12,835–12,735 Cal B.P. for Younger Dryas boundary on four continents. *Proc. Natl. Acad. Sci. USA* **2015**, *112*, E4344–E4353. https://doi.org/10.1073/pnas.1507146112.
387. Muschitiello, F.; Wohlfarth, B. Time-transgressive environmental shifts across Northern Europe at the onset of the Younger Dryas. *Quat. Sci. Rev.* **2015**, *109*, 49–56. https://doi.org/10.1016/j.quascirev.2014.11.015.
388. Nakagawa, T.; Kitagawa, H.; Yasuda, Y.; Tarasov, P.E.; Nishida, K.; Gotanda, K.; Sawai, Y.; Yangtze River Civilization Program Members. Asynchronous Climate Changes in the North Atlantic and Japan During the Last Termination. *Science* **2003**, *299*, 688–691. https://doi.org/10.1126/science.1078235.
389. Partin, J.; Quinn, T.; Shen, C.-C.; Okumura, Y.; Cardenas, M.; Siringan, F.; Banner, J.; Lin, K.; Hu, H.-M.; Taylor, F. Gradual onset and recovery of the Younger Dryas abrupt climate event in the tropics. *Nat. Commun.* **2015**, *6*, 8061. https://doi.org/10.1038/ncomms9061.
390. Sun, N.; Brandon, A.D.; Forman, S.L.; Waters, M.R.; Befus, K.S. Volcanic origin for Younger Dryas geochemical anomalies ca. 12,900 cal B.P.. *Sci. Adv.* **2020**, *6*, eaax8587. https://doi.org/10.1126/sciadv.aax8587.
391. Mithen, S. *After the Ice: A Global Human History, 20.000–5.000 BC*, 1st ed.; Harvard Univ. Press: Cambridge, MA, USA, 2006; ISBN 0-674-01570-3.
392. Moore, A.M.T.; Kennett, J.P.; Napier, W.M.; Bunch, T.E.; Weaver, J.C.; Lecompte, M.; Adedeji, A.V.; Hackley, P.; Kletetschka, G.; Hermes, R.E.; et al. Evidence of Cosmic Impact at Abu Hureyra, Syria at the Younger Dryas Onset (~12.8 ka): High-temperature melting at >2200 °C. *Sci. Rep.* **2020**, *10*, 4185. https://doi.org/10.1038/s41598-020-60867-w.
393. Brakenridge, G.R. Core-collapse supernovae and the Younger Dryas/terminal Rancholabrean extinctions. *Icarus* **2011**, *215*, 101–106. https://doi.org/10.1016/j.icarus.2011.06.043.
394. Baldini, J.U.L.; Brown, R.J.; Mawdsley, N. Evaluating the link between the sulfur-rich Laacher See volcanic eruption and the Younger Dryas climate anomaly. *Clim. Past* **2018**, *14*, 969–990. https://doi.org/10.5194/cp-14-969-2018.
395. Broecker, W.S. Was the Younger Dryas Triggered by a Flood? *Science* **2006**, *312*, 1146–1148. https://doi.org/10.1126/science.1123253.
396. Murton, J.B.; Bateman, M.; Dallimore, S.R.; Teller, J.T.; Yang, Z. Identification of Younger Dryas outburst flood path from Lake Agassiz to the Arctic Ocean. *Nature* **2010**, *464*, 740–743. https://doi.org/10.1038/nature08954.

397. Wang, L.; Jiang, W.Y.; Jiang, D.B.; Zou, Y.F.; Liu, Y.Y.; Zhang, E.L.; Hao, Q.Z.; Zhang, D.G.; Zhang, D.T.; Peng, Z.Y.; et al. Prolonged Heavy Snowfall During the Younger Dryas. *J. Geophys. Res. Atmos.* **2018**, *123*, 13748–13762. https://doi.org/10.1029/2018jd029271.
398. Keigwin, L.D.; Klotsko, S.; Zhao, N.; Reilly, B.; Giosan, L.; Driscoll, N.W. Deglacial floods in the Beaufort Sea preceded Younger Dryas cooling. *Nat. Geosci.* **2018**, *11*, 599–604. https://doi.org/10.1038/s41561-018-0169-6.
399. A LaViolette, P. Evidence for a Solar Flare Cause of the Pleistocene Mass Extinction. *Radiocarbon* **2011**, *53*, 303–323. https://doi.org/10.1017/s0033822200056575.
400. Basu, S.; Murty, S.; Shukla, P.N.; Shukla, A.D. Origin of Silicides (Unknown Meteorites). *Meteorit. Planet. Sci.* **2000**, *35*, A22–A23.
401. Batovrin, S.; Lipovsky, B. *Previously Unknown Class of Meteorites*; Batovrin-Lipovsky: Holmdel, NJ, USA, 1998.
402. Newman, J.D. Impact-Generated Dykes and Shocked Carbonates from the Tunnunik and Haughton Impact Structures, Canadian High Arctic. Ph.D. Thesis, The University of Western Ontario, London, ON, Canada, 2020.
403. Glass, B.J.; Domville, S.; Sanjanwala, R.; Lee, P. Constrained model interpreation from Haughton crater geophysical datasets. In *Proceedings of the 43rd Lunar and Planetary Science Conference,* The Woodlands, TX, USA, 19–23 March 2012; p. 2021.
404. Rappenglück, M.; Rappenglück, B.; Ernstson, K. Kosmische Kollision in der Frühgeschichte: Der Chiemgau-Impakt: Die Erforschung eines bayerischen Meteoritenkrater-Streufelds. *Z. Anomalistik* **2017**, *17*, 235–260.
405. Ernstson, K.; Mayer, W.; Neumair, A.; Rappenglück, B.; Rappenglück, M.A.; Sudhaus, D.; Zeller, K.W. The Chiemgau Crater Strewn Field: Evidence of a Holocene Large Impact Event in Southeast Bavaria, Germany. *J. Sib. Fed. Univ. Eng. Technol.* **2010**, *1*, 72–103.
406. Hoffmann, V.; Rösler, W.; Partzelt, A.; Raeymaekers, B.; van Espen, P. Characterization of a small crater-like strcuture in SE Bavaria, Germany. In *Proceedings of the 68th Annual Meteoritical Society Meeting,* Gatlinburg, TN, USA, 12–16 September 2005.
407. Rappenglück, B.; Hiltl, M.; Rappenglück, M.; Ernstson, K. The Chiemgau Impact—A meteorite impact in the Bronze¬/Iron Age and its extraordinary appearance in the archaeological record. In *Himmelswelten und Kosmovisionen—Imaginationen, Modelle, Weltanschauungen: Proceedings der Tagung der Gesellschaft für Archäoastronomie in Gilching, 29–31 März 2019*; Wolfschmidt, G., Ed.; Tredion: Hamburg, Germany, 2020; pp. 330–349.
408. Rappenglück, B.; Hiltl, M.; Ernstson, K. The Chiemgau Impact: Evidence of a Latest Bronze Age/Early Iron Age meteorite impact in the archaeological record, and resulting critical considerations of catastrophism. In *Beyond Paradigms in Cultural Astronomy*; González-García, C., Frank, R.M., Sims, L.D., Rappenglück, M.A., Zotti, G., Belmonte, J.A., Šprajc, I., Eds.; BAR: Oxford, UK, 2021; pp. 57–64.
409. Fehr, K.T.; Pohl, J.; Mayer, W.; Hochleitner, R.; Fassbinder, J.; Geiss, E.; Kerscher, H. A meteorite impact crater field in eastern Bavaria? A preliminary report. *Meteorit. Planet. Sci.* **2005**, *40*, 187–194. https://doi.org/10.1111/j.1945-5100.2005.tb00374.x.
410. Fehr, K.T.; Hochleitner, R.; Hölzl, S.; Geiss, E.; Pohl, J.; Fassbinder, J. Ferrosilizium-Pseudometeorite aus dem Raum Burghausen, Bayern. *Aufschluss* **2004**, *55*, 297–303.
411. Doppler, G.; Geiss, E.; Kroemer, E.; Traidl, R. Response to 'The fall of Phaethon: A Greco-Roman geomyth preserves the memory of a meteorite impact in Bavaria (south-east Germany)' by Rappenglück et al. (Antiquity 84). *Antiquity* **2011**, *85*, 274–277. https://doi.org/10.1017/s0003598x00067600.
412. Huber, R.; Darga, R.; Lauterbach, H. Der späteiszeitliche Tüttensee-Komplex als Ergebnis der Abschmelzgeschichte am Ostrand des Chiemsee-Gletschers und sein Bezug zum „Chiemgau Impakt" (Landkreis Traunstein, Oberbayern). *E G Quat. Sci. J.* **2020**, *69*, 93–120. https://doi.org/10.5194/egqsj-69-93-2020.
413. Völkel, J.; Andrew, M.; Matthias, L.; Hürkamp, K. Colluvial filling of a glacial bypass channel near the Chiemsee (Stöttham) and its function as geoarchive. *Z. Geomorphol. NF* **2012**, *56*, 371–386.
414. Hoffmann, V.; Rösler, W.; Schibler, L. Anomalous magnetic signature of top soils in Burghausen area, SE Germany. *Geophys. Res. Abstr.* **2004**, *6*. #05041
415. Hoffmann, V.; Rösler, W.; Patzelt, A.; Raeymaekers, B.; van Espen, P. Characterisation of a small crater-like structure in SE Bavaria, Germany. *Meteor. Planet. Sci* **2005**, *40*, A129.
416. Rösler, W.; Hoffmann, V.; Raeymaekers, B.; Schryvers, D.; Popp, J. Diamonds in carbon spherules—Evidence for a cosmic impact? *Meteorit. Soc.* **2005**, *40,* 5114
417. Schryvers, D.; Raeymakers, B. EM characterisation of a potential meteorite sample. #MS16.P13. In *Proceedings of the 13th European Microscopy Congress, Antwerp, Belgium, 22–27 August 2004: Materials Sciences*; van Tendeloo, G., Ed.; Belgian Society for Microscopy: Liege, Belgium, 2004; pp. 859–860.
418. Yang, Z.; Verbeeck, J.; Schryvers, D.; Tarcea, N.; Popp, J.; Rösler, W. TEM and Raman characterisation of diamond micro- and nanostructures in carbon spherules from upper soils. *Diam. Relat. Mater.* **2008**, *17*, 937–943. https://doi.org/10.1016/j.diamond.2008.01.104.
419. Rappenglück, M.A.; Bauer, F.; Ernstson, K.; Hiltl, M. Meteorite impact on a micrometer scale: iron silicide, carbide and CAI minerals from the Chiemgau impact event (Germany). *Problems and perspectives of modern mineralogy (Yushkin Memorial Seminar–2014) Proceedings, Syktyvkar, Komi Republic, Russia 19–22 May 2014, Syktyvkar*; IG Komi SC UB RAS, Ed.; Geoprint: Syktyvar, Russia, 2014.
420. Raeymaekers, B. A Prospective Biomonitoring Campaign with Honey Bees in a District of Upper-Bavaria (Germany). *Environ. Monit. Assess.* **2006**, *116*, 233–243. https://doi.org/10.1007/s10661-006-7389-8.

421. Rappenglück, B.; Rappenglück, M.A.; Ernstson, K.; Mayer, W.; Neumair, A.; Sudhaus, D.; Liritzis, I. Reply to Doppler et al. 'Response to "The fall of Phaethon: A Greco-Roman geomyth preserves the memory of a meteorite impact in Bavaria (south-east Germany) (Antiquity 84)"'. *Antiquity* **2011**, *85*, 278–280. https://doi.org/10.1017/s0003598x00067612.
422. Rappenglück, B.; Rappenglück, M.A.; Ernstson, K.; Mayer, W.; Neumair, A.; Sudhaus, D.; Liritzis, I. The fall of Phaethon: A Greco-Roman geomyth preserves the memory of a meteorite impact in Bavaria (south-east Germany). *Antiquity* **2010**, *84*, 428–439. https://doi.org/10.1017/s0003598x00066680.
423. Hoffmann, V.; Torii, M.; Funaki, M. Peculiar magnetic signature of Fe-Silicide phases and diamond/Fullerence containing carbon spherules. *Travaux Géophysiques* **2006**, *XXVII*, 52–53.
424. Bauer, F.; Hiltl, M.; Rappenglück, M.A.; Ernstson, K. Trigonal and cubic Fe2Si polymorphs (hapkeite) in the eight kilograms find of natural iron silicide from Grabenstätt (Chiemgau, Southeast Germany). In *Proceedings of the 50th Lunar and Planetary Science Conference,* The Woodlands, Texas, USA, 18–22 March 2019; LPI Contrib. No. 2132.
425. Bauer, F.; Hiltl, M.; Rappenglück, M.A.; Neumaier, A.; Ernstson, K. Fe2Si (hapkeite) from the subsoil in the Alpine forland (Southeast Germany): Is it associated with an impact? In *Proceedings of the 76th Annual Meteoritical Society Meeting,* Alberta, Canada, 29 July–2 August 2013.
426. Rappenglück, M.A.; Bauer, F.; Hiltl, M.; Neumair, A.; Ernstson, K. Calcium-aluminium-rich inclusions (CAIs) In Iron silicide (xifengite, gupeiite, hapkeite) matter: Evidence of a cosmic origin. In *Proceedings of the 76th Annual Meteoritical Society Meeting,* Alberta, Canada, 29 July–2 August 2013.
427. Hiltl, M.; Bauer, F.; Ernstson, K. SEM and TEM analyses of minerals Xifengite, Gupeiite, Fe2Si (Hapkeite?), titanium carbide (TiC) and cubic moissanite (SiC) from the subsoil in the alpine foreland: Are they cosmochemical? In *Proceedings of the 42nd Lunar and Planetary Science Conference,* The Woodlands, TX, USA, 7–11 March 2011.
428. Ma, C.; Kampf, A.R.; Connolly, H.C.; Beckett, J.R.; Rossman, G.R.; Smith, S.A.S.; Schrader, D.L. Krotite, CaAl2O4, a new refractory mineral from the NWA 1934 meteorite. *Am. Miner.* **2011**, *96*, 709–715. https://doi.org/10.2138/am.2011.3693.
429. Cámara, F.; Bindi, L.; Pagano, A.; Pagano, R.; Gain, S.E.M.; Griffin, W.L. Dellagiustaite: A Novel Natural Spinel Containing V2+. *Minerals* **2018**, *9*, 4. https://doi.org/10.3390/min9010004.
430. Smith, D.G.W.; Nickel, E.H. A system of codification for unnamed minerals: report of the subcommittee for unnamed minerals of the ima commission on new minerals, nomenclature and classification. *Can. Miner.* **2007**, *45*, 983–990. https://doi.org/10.2113/gscanmin.45.4.983.
431. Mitchell, R.H.; Welch, M.D.; Chakhmouradian, A.R. Nomenclature of the perovskite supergroup: A hierarchical system of classification based on crystal structure and composition. *Miner. Mag.* **2017**, *81*, 411–461. https://doi.org/10.1180/minmag.2016.080.156.
432. Mineralogy Database. *Hatrurim Formation, Middle East*; Mineralogy Database, Emerald Group Publishing: Bingley, West Yorkshire, UK, 2004. Avalialble online: https://www.mindat.org/loc-2063.html (accessed on 31 October 2021)
433. Gross, S. The mineralogy of the Hatrurim Formation, Israel. *Geol. Surv. Isr. Bull.* **1977**, *70*, 1–80.
434. Mineralogy Database. *Bellerberg volcano, Vordereifel, Mayen-Koblenz District, Rhineland-Palatinate, Germany*; Mineralogy Database, Emerald Group Publishing: Bingley, West Yorkshire, UK, 2004. Avaliable online: https://www.mindat.org/loc-204826.html (accessed on 31 October 2021)
435. Rösler, W.; Patzelt, A.; Hoffmann, V.; Raeymaekers, B. Characterisation of a small crater-like structure in SE Bavaria, Germany: Abstract, European Space Agency. In *Proceedings of the First International Conference on Impact Cratering in the Solar System, ESTEC,* Noordwijk, The Netherlands, 8–12 May 2006.
436. De Lange, G.; Rispens, F. Indication of a diagenetically induced precipitate of an Fe-Si mineral in sediment from the Nares Abyssal Plain, western North Atlantic. *Mar. Geol.* **1986**, *73*, 85–97. https://doi.org/10.1016/0025-3227(86)90112-x.
437. Rudashevskii, N.S.; Kretser, Y.; Anikeeva, L.I.; Andreev, S.I.; Torokhov, M.P.; Kazakova, V.E. Platinum minerals in oceanic ferromanganese crusts. *Dokl. Earth Sci. (Engl. Transl.)* **2001**, *378*, 464–467.
438. Jambor, J.L.; Grew, E.S.; Roberts, A.C. New mineral names. *Am. Mineral.* **2002**, *87*, 181–184.
439. Kruszewski, Ł.; Ciesielczuk, J. The Behaviour of Siderite Rocks in an Experimental Imitation of Pyrometamorphic Processes in Coal-Waste Fires: Upper and Lower Silesian Case, Poland. *Minerals* **2020**, *10*, 586. https://doi.org/10.3390/min10070586.
440. Kruszewski, Ł.; Ciesielczuk, J.; Misz-Kennan, M.; Fabiańska, M. Chemical composition of glasses and associating mineral species in various pyrometamorphic rocks from coal-mining dumps of the Lower Silesia. *Mineral. Spec. Pap.* **2014**, *42*, 70–71.
441. mindat.org. Oldhamite. Available online: https://www.mindat.org/min-2970.html (accessed on 18 November 2021).
442. Kruszewski, Ł.; Ciesielczuk, J.; Misz-Kennan, M. What have meteorites to do with coal fires? A case of Upper and Lower Silesian Basins. *Mineral. Spec. Pap.* **2012**, *40*, 28–30.
443. Goderis, S.; Chakrabarti, R.; Debaille, V.; Kodolányi, J. Isotopes in cosmochemistry: Recipe for a Solar System. *J. Anal. At. Spectrom.* **2016**, *31*, 841–862. https://doi.org/10.1039/c5ja00411j.
444. Ferrarotti, A.; Gail, H.-P.; Degiorgi, L.; Ott, H.R. FeSi as a possible new circumstellar dust component. *Astron. Astrophys.* **2000**, *357*, L13–L16.
445. Ferrarotti, A.S.; Gail, H.-P. Mineral formation in stellar winds. II. Effects of Mg/Si abundance variations on dust composition in AGB stars. *Astron. Astrophys.* **2001**, *371*, 133–151. https://doi.org/10.1051/0004-6361:20010316.
446. Ferrarotti, A.S.; Gail, H.-P. Mineral formation in stellar winds. III. Dust formation in S-stars. Astron. Astrophys. 2002, *382*, 256–281. https://doi.org/10.1051/0004-6361:20011580.

447. Ferrarotti, A.S. Staubbildung in Sternwinden: Inaugural-Dissertation zur Erlangung der Doktorwürde der Naturwissenschaftlich-Mathematischen Gesamtfakultät der Ruprecht-Karls-Universität Heidelberg. Ph.D. Thesis, Ruprecht-Karls-Universität Heidelberg, Heidelberg, Germany, 2003.
448. Humphreys, R.M.; Stanek, K.Z. (Eds.) *The Fate of the Most Massive Stars*; Astronomical Society of the Pacific: San Francisco, CA, USA. 2005.
449. Keenan, P.C.; Boeshaar, P.C. Spectral types of S and SC stars on the revised MK system. *Astrophys. J. Suppl. Ser.* **1980**, *43*, 379–391. https://doi.org/10.1086/190673.
450. Ramstedt, S.; Schoeier, F.L.; Olofsson, H. Circumstellar molecular line emission from S-type AGB stars: Mass-loss rates and SiO abundances. *Astron. Astrophys.* **2009**, *499*, 515–527. https://doi.org/10.1051/0004-6361/200911730.
451. Vink, J.S. *Eta Carinae and the Luminous Blue Variables. In Eta Carinae and the Supernova Impostors*; Davidson, K., Humphreys, R.M., Eds.; Springer: Boston, MA, USA, 2012; pp. 221–247, ISBN 978-1-4614-2274-7.
452. Weis, K.; Bomans, D.J. Luminous Blue Variables. *Galaxies* **2020**, *8*, 20. https://doi.org/10.3390/galaxies8010020.
453. Smith, T.L.; Gordon, K.D.; Clayton, G.C. The Newly Discovered NIR Features in NGC 7023 and Other Reflection Nebulae. In *Proceedings of the 199th American Astronomical Society Meeting,* Washington DC, WA, USA, 7–10 January 2002
454. Gordon, K.D.; Witt, A.N.; Rudy, R.J.; Puetter, R.C.; Lynch, D.K.; Mazuk, S.; Misselt, K.A.; Clayton, G.C.; Smith, T.L. Dust Emission Features in NGC 7023 between 0.35 and 2.5 Microns: Extended Red Emission (0.7 Microns) and Two New Emission Features (1.15 and 1.5 Microns). *Astrophys. J. Lett.* **2000**, *544*, 859–866. https://doi.org/10.1086/317245.
455. Bobrowsky, M.; Ueta, T.; Meixner, M. NICMOS Imaging of HD 179821 and AFGL 4106. *Proc. Int. Astron. Union* **2006**, *2*, 371–372. https://doi.org/10.1017/s1743921306003292.
456. Molster, F.J.; Waters, N.R.; vanTrams, H.; Decin, L.; van Loon, J.T.; Jager, C.; Henning, T.; Kaufl, H.-U.; de Koetr, A.; Bouwman, J. The composition and nature of the dust shell surrounding the binary AFGL 4106. *Astron. Astrophys.* **1999**, *350*, 163–180.
457. van Loon, J.T.; Molster, F.J.; van Winckel, H.; Waters, L. The circumstellar envelope of AFGL 4106. *Astron. Astrophys.* **1999**, *350* 120–128.
458. Prialnik, D. Novae. In *Encyclopedia of Astronomy and Astrophysics*; Murdin, P., Ed.; IOP Publishing: Bristol, UK, 2001; pp. 1846–1856, ISBN 978-1-56159-268-5.
459. Martin, P.; Dubus, G.; Jean, P.; Tatischeff, V.; Dosne, C. Gamma-ray emission from internal shocks in novae. *Astron. Astrophys.* **2018**, *612*, A38. https://doi.org/10.1051/0004-6361/201731692.
460. Lodders, K. They Came from the Deep in the Supernova: The Origin of TiC and Metal Subgrains in Presolar Graphite Grains. *Astrophys. J. Lett.* **2006**, *647*, L37–L40. https://doi.org/10.1086/507181.
461. Fedkin, A.; Meyer, B.; Grossman, L. Condensation and mixing in supernova ejecta. *Geochim. Cosmochim. Acta* **2010**, *74*, 3642–3658. https://doi.org/10.1016/j.gca.2010.03.021.
462. Ebel, D.; Grossman, L. Condensation from supernova gas made of free atoms. *Geochim. Cosmochim. Acta* **2001**, *65*, 469–477. https://doi.org/10.1016/s0016-7037(00)00550-0.
463. Meyer, B.S.; Weaver, T.A.; Woosley, S.E. Isotope source table for a 25 $M_\odot$ supernova. *Meteoritics* **1995**, *30*, 325–334. https://doi.org/10.1111/j.1945-5100.1995.tb01131.x.
464. Singerling, S.A.; Liu, N.; Nittler, L.R.; Alexander, C.M.O.; Stroud, R.M. TEM Analyses of Unusual Presolar Silicon Carbide: Insights into the Range of Circumstellar Dust Condensation Conditions. *Astrophys. J. Lett.* **2021**, *913*, 90. https://doi.org/10.3847/1538-4357/abece2.
465. Hynes, K.M.; Croat, T.K.; Amari, S.; Mertz, A.F.; Bernatowicz, T.J. Structural and isotopic microanalysis of presolar SiC from supernovae. *Meteorit. Planet. Sci.* **2010**, *45*, 596–614. https://doi.org/10.1111/j.1945-5100.2010.01045.x.
466. Hynes, K. Microanalytical Investigations of Presolar SiC Grains as Probes of Condensation Conditions in Astrophysical Environments.. https://doi.org/10.7936/k7bz6455.
467. Hazen, R.M.; Morrison, S.M. An evolutionary system of mineralogy. Part I: Stellar mineralogy (>13 to 4.6 Ga). *Am. Miner.* **2020**, *105*, 627–651. https://doi.org/10.2138/am-2020-7173.
468. Heck, P.R.; Greer, J.; Kööp, L.; Trappitsch, R.; Gyngard, F.; Busemann, H.; Maden, C.; Avila, J.N.; Davis, A.M.; Wieler, R. Lifetimes of interstellar dust from cosmic ray exposure ages of presolar silicon carbide. *Proc. Natl. Acad. Sci. USA* **2020**, *117*, 1884–1889. https://doi.org/10.1073/pnas.1904573117.
469. Croat, T.K.; Jadhav, M.; Lebsack, E.; Bernatowic, T.J. A Unique Supernova Graphite: Contemporaneous Condensation of All Things Carbonaceous. In *Proceedings of the 42nd Lunar and Planetary Science Conference,* The Woodlands, TX, USA, 7–11 March 2011; Abstract. #1533.
470. Rowan, L.R. I. Equation of State of Molten Mid-Ocean Ridge Basalt. Structure of Kilauea Volcano. Ph.D. Thesis, California Institute of Technology, Pasadena, CA, USA, 1993.
471. Suttle, M.D. The Parent Bodies of Fine-grained Micrometeorites: A Petrologic & Spectroscopic Perspective. Ph.D. Thesis, Imperial College London, London, UK, 2018.
472. Ross, A.J.; Downes, H.; Herrin, J.S.; Mittlefehldt, D.W.; Humayun, M.; Smith, C. The origin of iron silicides in ureilite meteorites. *Geochemistry* **2019**, *79*, 125539. https://doi.org/10.1016/j.chemer.2019.125539.
473. Schmidt, M.W.; Gao, C.; Golubkova, A.; Rohrbach, A.; Connolly, J.A. Natural moissanite (SiC)—A low temperature mineral formed from highly fractionated ultra-reducing COH-fluids. *Prog. Earth Planet. Sci.* **2014**, *1*, 27. https://doi.org/10.1186/s40645-014-0027-0.